

ABSTRACT

Title of dissertation: AN OPTIMAL CONTROL MODEL
FOR HUMAN POSTURAL REGULATION

Yao Li, Doctor of Philosophy, 2010

Dissertation directed by: Professor William S. Levine
Department of Electrical and Computer Engineering

Human upright stance is inherently unstable without a balance control scheme. Many biological behaviors are likely to be optimal with respect to some performance measure that involves energy. It is reasonable to believe that the human is (unconsciously) optimizing some performance measure as he regulates his balance posture. In experimental studies, a notable feature of postural control is a small constant sway. Specifically, there is greater sway than would occur with a linear feedback control without delay. A second notable feature of the human postural control is that the response to perturbations varies with their amplitude. Small disturbances produce motion only at the ankles with the hip and knee angles unchanging. Large perturbation evoke ankle and hip angular movement only. Still larger perturbation result in movement of all three joint angles.

Inspired by these features, we propose a biomechanical model resembling human balance control. The proposed model consists of three main components which are the body dynamics, a sensory estimator for delay and disturbance, and an optimal

nonlinear control scheme providing minimum required corrective response. The human body is modeled as a multiple segment inverted pendulum in the sagittal plane and controlled by ankle and hip joint torques. A series of nonlinear optimal control problems are devised as mathematical models of human postural control during quiet standing. Several performance criteria that are high even orders in the body state (or functions of these states) and quadratic in the joint control are utilized. For example,

$$J = \int_0^{\infty} \left[ql_x^{2m}(t) + \sum_{j=1}^L r_j u_j^{2n}(t) \right] dt$$

where q and r_j are cost coefficients, L , m , n are integers, and l_x represents deviations from the nominal equilibrium values of body states and functions of these states (such as joint angle, Center of Pressure *COP* or Center of Mass *COM*) in the sagittal plane. The u_j are control torques at each joint.

This objective function provides a trade-off between the allowed deviations of the position from its nominal value and the neuromuscular energy required to correct for these deviations. Note that this performance measure reduces the actuator energy used by penalizing small postural errors very lightly. By using the Model Predictive Control (MPC) technique, the discrete-time approximation to each of these problems can be converted into a nonlinear programming problem and then solved by optimization methods. The solution gives a control scheme that agrees with the main features of the joint kinematics and its coordination process. The derived model is simulated for different scenarios to validate and test the performance of the proposed postural control architecture.

AN OPTIMAL CONTROL MODEL
FOR HUMAN POSTURAL REGULATION

by

Yao Li

Dissertation submitted to the Faculty of the Graduate School of the
University of Maryland, College Park in partial fulfillment
of the requirements for the degree of
Doctor of Philosophy
2010

Advisory Committee:

Dr. William S. Levine, Chair/Advisor

Dr. André Tits

Dr. Nuno Martins

Dr. Shuvra S. Bhattacharyya

Dr. Jane Clark

ACKNOWLEDGEMENT

I would like to thank my advisor Dr. Levine whose wisdom, encouragement and patience helped me take this work from impossible to possible.

I would like to thank my committee members, Dr. André Tits, Dr. Nuno Martins, Dr. Shuvra Bhattacharyya and Dr. Jane Clark, for their time, comments and feedback.

I thank my parents, who had given their love and faith to let me pursue my career and life.

TABLE OF CONTENTS

LIST OF FIGURES	v
1 Introduction	1
1.1 Motivation	1
1.2 Hypothesis	2
1.3 Thesis Outline	4
2 Background	6
2.1 The Central Nervous System (CNS)	8
2.2 The Peripheral Nervous System (PNS)	10
2.3 The Musculoskeletal System	13
2.3.1 Bones, Joints and Ligament	13
2.3.2 Muscles	14
2.4 Neurophysiology of Balance Control	14
3 Balance Control of Upright Posture	17
3.1 Experimental Studies	18
3.2 Biomechanic Models	20
3.2.1 Linear Feedback Control Strategies	21
3.2.2 Nonlinear Control Strategies	23
3.2.3 Optimal Control Strategies	24
3.3 Proposed Nonlinear Optimal Control Model	25
4 Single Joint Balance Control	27
4.1 Single Inverted Pendulum Model	27
4.2 The Optimal Control Problem	32
4.3 LQR Case	35
4.4 Model Predictive Control	36
4.5 The Optimization Problem	38
4.6 The MPC Solution	41
4.6.1 Newton-KKT Methods	42
4.7 Results	44
4.7.1 The Nonlinear Full-State Feedback Solution	44
4.7.2 The Performance of the Full-State Feedback Solution	47
4.8 Summary	53

5	Model with Delay and Noise	54
5.1	Neurophysiology of Neural Delay	54
5.2	Model with Delay	55
5.2.1	Example - Single Unit Delay Model	59
5.3	Optimal State Estimator	66
5.3.1	<i>LQG Case</i>	67
5.3.2	SEHOC Case	69
5.4	Summary	77
6	Coordinated Control	78
6.1	Double Inverted Pendulum Model	78
6.2	Optimal Coordinated Control	84
6.3	The Results	87
6.3.1	Ankle strategy	87
6.3.2	Hip Strategy	89
6.3.3	Ankle and Hip Coordination	91
7	Control of Center of Pressure	96
7.1	Optimal Control of COP	106
7.2	The Results	109
7.2.1	Transient Response	109
7.2.2	<i>Steady State Response</i>	113
7.3	Summary	116
8	Conclusion and Discussion	118
8.1	Conclusion	118
8.2	The Future Work	120
	Bibliography	122

LIST OF FIGURES

2.1	Balance control during quiet standing is a highly integrated task	7
2.2	Central nervous system (CNS) [55]	8
2.3	Diagrammatic presentation of knee jerk reflex action[65]	11
2.4	The static and dynamic receptors in the Labyrinth provide the necessary angle and angular velocity signals to balance the body in the presence of time delays in the auditory neural pathways [29].	12
2.5	Contraction of different groups of muscles and posterior/anterior movement of joints (hip, knee, ankle) during balance control [55]	15
3.1	Spontaneous body sway movement with small magnitude [55].	19
4.1	Single joint inverted pendulum model for postural balance control during quiet standing in the sagittal plane. (Left figure is from [55])	28
4.2	The single joint balance control system	32
4.3	Moving horizon control	37
4.4	Control Torque Map in the Feasible Sway Range	46
4.5	Trajectories of angular state x_1 , angular velocity x_2 and the control input u for different performance criteria with fixed noise level	48
4.6	State trajectories of four different control schemes to maintain the equilibrium state driven by different levels of noise	50
4.7	SDF function of four different control schemes to maintain the equilibrium state driven by different levels of noise	52
5.1	The balance control system with delay	56
5.2	Trajectories of angular state x_1 , angular velocity x_2 and the control input u for SDHOC and LQR	65
5.3	The system diagram of Single inverted pendulum model with state Estimator and Higher order Optimal Control (SEHOC)	66
5.4	The SEHOC control scheme	71
5.5	Trajectories of angular state x_1 , angular velocity x_2 and the control input u during balance restoration for PID (\cdots), LQG ($--$) and SEHOC($—$)	73
5.6	Trajectories of angular state x_1 , angular velocity x_2 and the control input u during balance maintenance for PID (\cdots), LQG ($--$) and SEHOC($—$)	74
5.7	State trajectories of angular state x_1 , angular velocity x_2 during balance maintenance for PID (\cdots), LQG ($--$) and SEHOC($—$)	75

5.8	Stabiligram difussion function (SDF) of angular state x_1 during steady state response for PID (\cdots), LQG ($--$) and SEHOC($—$)	76
6.1	The three link sagittal biped is composed of three rigid links. The term k for $i = 1, 2, 3$ is the distance from the bottom of link i to the center of mass of link i . The term L_i is the length of link i	79
6.2	Body segment length expressed as a fraction of body height [84]	82
6.3	Trajectories of ankle and hip angle under control of ankle strategy	88
6.4	State trajectories of angular state and angular velocity for ankle and hip joint under control of ankle strategy	89
6.5	Trajectories of ankle and hip angle under control of hip strategy	90
6.6	State trajectories of angular state and angular velocity for ankle and hip joint under control of hip strategy	91
6.7	Trajectories of angular state, control torque and COM/COP for ankle and hip joints starting from equilibrium point driven by different noise levels	93
6.8	State trajectories of angular state and angular velocity for ankle and hip joint under control of ankle and hip coordination	93
6.9	Trajectories of COM, COP and SDF starting from equilibrium point driven by different noise level	95
7.1	The three link sagittal biped is composed of three rigid links. The term k_i for $i = 1, 2, 3$ is the distance from the bottom of link i to the center of mass of link i . The term L_i is the length of link i . The torque at toe, ankle and hip joint are u_{toe} , u_{ankle} and u_{hip}	97
7.2	f_v is the horizontal component of the ground reaction force.	100
7.3	Trajectories of COM and COP during transient response	111
7.4	Trajectories of ankle and hip angle during transient response	111
7.5	Control torque of ankle and hip joint during transient response	112
7.6	Trajectories of COM and COP during steady state response	114
7.7	Control torque of ankle and hip joint during steady state response	114
7.8	Trajectories of ankle and hip angle during steady state response	115
7.9	SDF of simulation and experimental data	116

Chapter 1

Introduction

1.1 Motivation

Humans are capable of maintaining postural stability over a wide range of complex scenarios and configurations. There are two scenarios of special interest to clinical and engineering studies: the static posture during standing and the dynamic posture during walking. Different postural control strategies can be selected by the central nervous system depending on the scenario. The two posture regulation scenarios overlap in the necessity for maintaining the balance of the body through a stabilizing postural control process.

Human upright stance is inherently unstable without a balance control scheme. This scheme consists of central nervous system (CNS), musculoskeletal system and sensorimotor processes using the vestibular, joint angle proprioceptive, force sensors, and visual perception [40]. This task will become more difficult due to aging, illness

and disabilities. The neural mechanisms that determine control patterns during quiet standing postural regulation are still not well understood.

The merits of biological control have always been highlighted and discussed from an engineering perspective. A properly designed biomechanics model and its computer implementation could quantitatively reproduce the corresponding human performance and help us understand the core principles of human postural control. At the clinical level, it would be particularly useful for diagnosis and treatment of motor control disorders, and the development of functional electrical stimulation for recovery of lost motor function. In the practical engineering level, this also provides insights and inspiration for humanoid robot design.

1.2 Hypothesis

Balance control during quiet standing is a highly integrated task. The CNS integrates sensory information, makes decisions based on this information, and then directs the ensemble of muscles during the task. The human sensorimotor system is also a system with the capability of learning, developing, and adapting to improve performance. The objective of our work is to develop a model of human upright stance that is descriptive of the experimentally observed postural response, physiologically relevant, and straightforward to interpret.

Many biological behaviors are likely to be optimal with respect to some performance measure that involves energy. It is reasonable to believe that the human is

(unconsciously) optimizing some performance measure as he regulates his balance posture. In engineering, optimal control methods require a performance criterion that describes the goal and then fills in all the control details automatically by finding the control strategy that achieves the best possible performance. Ideally, the cost assumed in a human optimal control model should involve cost terms for body positions and controls and correspond to what the sensorimotor system is trying to achieve.

In experimental studies, a notable feature of postural control is a constant sway phenomenon with small magnitude. Specifically, there is greater sway than would occur with a linear feedback control without delay. A second notable feature of the human postural control is that the response to perturbations varies with their amplitude. Small disturbances produce motion only at the ankles with the hip and knee angles changing. Large perturbation evoke ankle and hip angular movement only. Still larger perturbation result in movement of all these joint angles.

Inspired by these features, we propose a biomechanical model resembling human postural control and devised it for the study of the neurophysiologic control. The proposed model consists of three main components which are a skeletal structure modeling the body dynamics with joint actuators, a sensory detector and estimator for delay and disturbance, and an optimal nonlinear control scheme providing the required corrective response. Although these components are functioning concurrently, they were developed separately in this work to address the postural balance control problem.

A series of nonlinear optimal control problems are devised as mathematical models of human postural control during quiet standing. In our work, the human body is

modeled as a multiple segment inverted pendulum controlled by joint torques. Several performance criteria that are high even orders in the body state or functions of these states and quadratic in the joint control are utilized. By using the Model Predictive Control (MPC) technique, the discrete-time approximation to each of these problems can be converted into a nonlinear programming problem and then solved by optimization methods. The solution gives control schemes that agree with main features of the joint kinematics and their coordination as is shown by simulation of the model for different scenarios.

1.3 Thesis Outline

This dissertation is organized in eight chapters. Following this introduction is the background about human posture regulation. In that chapter, we briefly review the main physiological elements participating in human postural control, including the central nervous system, the peripheral nervous system, and the musculoskeletal system. Chapter 3 reviews the relevant balance control theories, experimental studies and the existing modeling work. In Chapter 4, a simple biomechanics model using a single inverted pendulum is derived. The resulting optimal control problem is then solved numerically by the same technique that is used in MPC and the major control features are extracted and discussed. Chapter 5 presents a scheme to model delay effects in the optimal control system. Also, a noise filtering and state estimator based on Kalman estimation is devised as an important part of the modeling frame work. In Chapter

6, we extended the model to the multiple joint coordination control problem. This is followed by a series of studies of different weightings within the performance criterion and their effect on posture regulation. Chapter 7 explores the role of center of mass and center of pressure in the optimal control scheme and provides an experimental validation mechanism. Finally, we conclude in Chapter 8 with a summary of the main findings of this work, and consider further prospects of this research field.

Chapter 2

Background

There has been an intensive biological and engineering effort to identify, understand, and model the underlying mechanisms of human postural control. Different approaches, tools, and frameworks have been proposed to tackle the postural control problem [84][82][51][36][40][63][64]. Research on human balance strategy not only enables neurologists to better understand some balance malfunction disorders such as Parkinson's disease, but also leads to more applicable bio-inspired control systems for important applications, such as humanoid robot control.

Traditionally, postural balance control has been considered to be reflex-like responses elicited automatically by a sensory stimulus; it is now commonly considered to be a fundamental motor skill learned by the CNS. Like any other motor skill, postural balance control strategies can become more efficient and effective with training and practice [7]. Balance control during quiet standing is a highly integrated task as shown in Figure 2.1. It consists of the central nervous system (CNS), musculoskeletal sys-

tem and sensorimotor processes using the vestibular system, joint angle proprioceptors, force sensors, and visual perception [40].

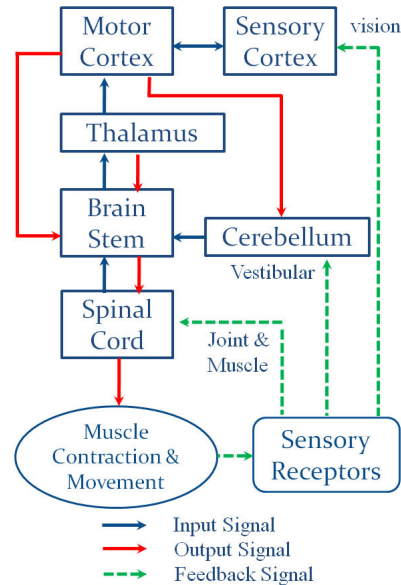


Figure 2.1: Balance control during quiet standing is a highly integrated task

The CNS, includes the brain and the spinal cord, integrates sensory information, makes decisions based on this information, and then directs the ensemble of muscles during the task. Specific balance control may vary due to individual goals and environmental context, but it always depends on the following basic function modules:[7]

- (1) The integration within the brain and spinal cord: to receive and process information, planning and programming movement.
- (2) Appropriate sensory input: visual, vestibular, joint-angle proprioceptive and force.
- (3) Skeletal system: complete movements developed by the central nervous system.
- (4) Normal muscle strength: to support the body and anti-gravity activity, but not impede the voluntary movement.

2.1 The Central Nervous System (CNS)

The central nervous system (CNS) plays a major role in human postural control. Modern approaches to understand postural control assume some sort of central processing of sensory information to produce body reactions to external (and internal) disturbances and thus they resemble sensorimotor feedback schemes. The CNS includes the brain and the spinal cord and is the site of information processing and control. The brain can be divided into three major parts as shown in Figure 2.2[55]: (i) forebrain, (ii) midbrain and (iii) hindbrain.

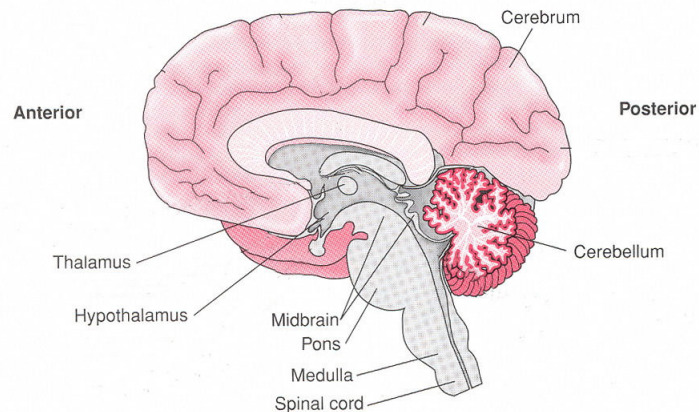


Figure 2.2: Central nervous system (CNS) [55]

The forebrain consists of cerebrum, thalamus and hypothalamus. The cerebral cortex contains motor areas, sensory areas and association areas that are responsible for complex functions such as intersensory associations, memory and communication. The cerebrum wraps around a structure called the thalamus, which is a major coordinating center for sensory and motor signaling. The thalamus relays sensory input to the primary sensory areas of the cerebral cortex. Another very important part of the

forebrain is called the hypothalamus, which lies at the base of the thalamus. The hypothalamus is the master control of the autonomic nervous system, parasympathetic and sympathetic. [65].

The midbrain (also called the mesencephalon) is located between the thalamus and hypothalamus of the forebrain and pons of the hindbrain. Through the body of the midbrain pass a substantial number of various fiber tracts especially related to vision, voluntary muscle activity and other important functions. The midbrain mainly contains the hippocampus and basal ganglia. The hippocampus is primarily responsible for short term memory. The basal ganglia are primarily but not exclusively responsible for crude motor movements. Injury to this area leads to rigidity, hypotonia, and Parkinson's disease.

The hindbrain comprises the pons, cerebellum and medulla. The pons relays information to the cerebellum and it contains fibers that descend from the cerebral cortex to control muscles of the head, limbs and trunk [65]. The cerebellum receives somatosensory input from the spinal cord, motor information from the cerebral cortex and input about balance from the vestibular system. It is primarily responsible for regulating muscle tone, for integrating the motor and sensory pathways, and for balance spatial awareness[65]. The medulla, along with the pons regulates blood pressure and the respiration.

The midbrain and hindbrain form the brainstem; the name given to the part of the brain which connects the spinal cord and the forebrain. Information regarding changes in the environment is received by the brain stem through the sensory organs.

This information is then processed and analyzed. The appropriate signals are then sent to the body's periphery to activate muscles and adjust sensors, so as to achieve motor goals.

The spinal cord receives and processes sensory information from the skin, joints, and muscles of the limbs and trunk. It contains motor neurons responsible for voluntary and reflex movements. Two types of neural roots form the spinal nerves. The dorsal roots receive the information transmitted into the spinal cord. The ventral roots innervate the muscles through outgoing motor axons.

2.2 The Peripheral Nervous System (PNS)

The PNS is divided into two parts: the somatic neural system and the autonomic neural system. The somatic neural system relays impulses from the CNS to skeletal muscles while the autonomic neural system transmits impulses from the CNS to the involuntary organs and smooth muscles of the body. The autonomic neural system is further classified into the sympathetic and the parasympathetic neural system.

Everyone is familiar with the clinical testing of the knee-jerk reflex, in which a tap to the patellar ligament activates the stretch receptors of the quadriceps, which in turn excites the motor neurons of the same muscles as part of a length-feedback servo controller. The entire process of response to a peripheral nervous stimulation, that occurs involuntarily, i.e., without conscious effort or thought and requires the involvement of a part of the central nervous system is called a reflex action. Its gain is

modulated as part of many voluntary motor behaviors and may become pathologically large or small as a result of different neurological disorders.

The reflex pathway comprises at least one afferent sensory (receptor) neuron and one motor (efferent or exciter) neuron appropriately arranged in series (Figure 2.3). The stimulus and response thus forms a reflex arc as shown below in the knee jerk reflex[65].

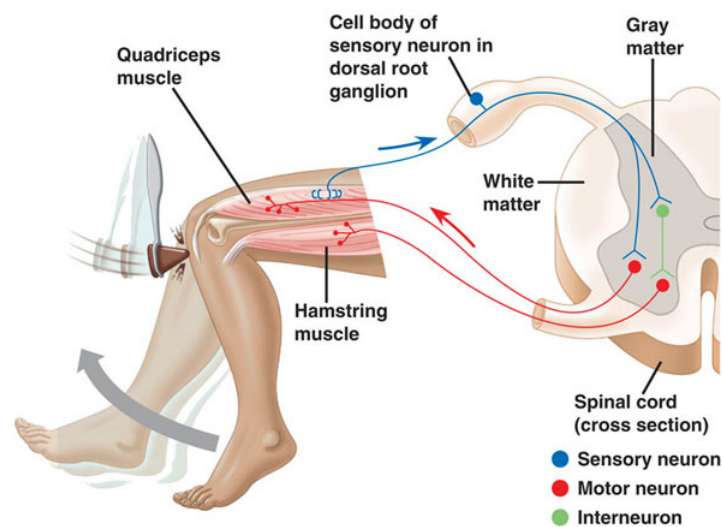


Figure 2.3: Diagrammatic presentation of knee jerk reflex action[65]

The peripheral nervous system is important in providing feedback from areas such as the skin, eyes, and muscles to the CNS. The somatosensory system, or somatic sensory system, processes different types of sensations: vision, sense of position and movement of the limbs, proprioception, discriminative touch, nociception or pain due to tissue damage, and temperature [65].

The visual, vestibular, and proprioceptive systems are the sensory modules that contribute heavily to motor control. Vision provides clues on head position and orien-

tation with respect to the surroundings whereas the vestibular receptors sense the head angular velocity and the resultant of the head translational and gravity accelerations.

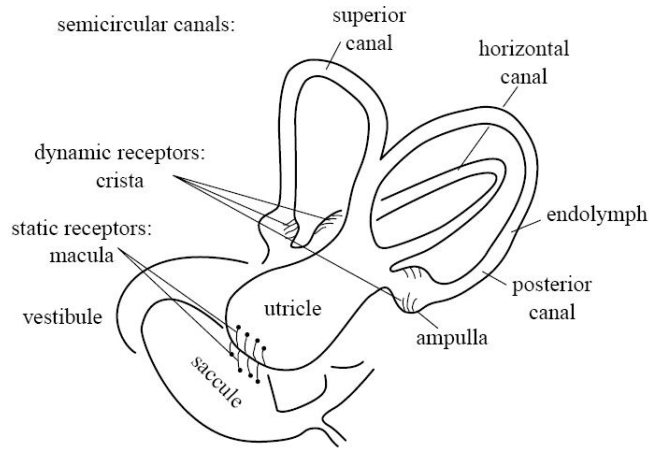


Figure 2.4: The static and dynamic receptors in the Labyrinth provide the necessary angle and angular velocity signals to balance the body in the presence of time delays in the auditory neural pathways [29].

The vestibular system is housed within the membranous labyrinth of the inner ear. The vestibular portion of the membranous labyrinth consists of a pair of otolith organs called the utricle and the saccule, as well as three semicircular ducts or canals as shown in Figure 2.4. The otolith organs sense angular position and translational acceleration of the head; the semicircular canals sense rotational acceleration of the head. Accelerations are registered through the bending of specialized vestibular hair cells. The semicircular canals, utricle, and saccule all have a dynamic function. They sense either rotational or translational acceleration. The utricle and saccule additionally have a static function and they sense the static angle of the head in space [29].

Proprioceptive information includes the angular displacement and velocity of body joints such as the ankle, knee, hip, and neck. Further, force sensors provide a measure

of reaction forces between the feet and the supporting surface. These sensory modalities are principal to postural control. First, they measure the current relative and absolute body (and body segments) position and orientation together with their time rate of change. Secondly, they measure the external disturbances acting on the body such as pushing forces or tilting of the supporting surface. On the other hand, the motor part comprises a complex set of skeletal muscles.

2.3 The Musculoskeletal System

The musculoskeletal system, innervated by the nervous system through motor neurons, causes the body to move voluntarily. This section provides a brief overview of the bones, joints and, muscles and other associated components of the motor system.

2.3.1 Bones, Joints and Ligament

Bones of the human body generally make contact through three types of joints: fibrous joints, cartilaginous joints, and synovial joints. Fibrous joints, such as sutures of the skull, are relatively immobile. Cartilaginous joints, such as the intervertebral discs, are slightly movable. Synovial joints, such as the hip and elbow, are much more mobile.

Ligaments attach the bones at a synovial joint, and friction is reduced by lubricated articular cartilage that covers the bone surfaces that form the joint. Synovial joints may have one to three degrees of rotational freedom with a limited range of rotational motion about each axis.

2.3.2 Muscles

Movement of bones about joints is caused by the contraction of skeletal muscles. When a muscle receives a signal from an innervating motor neuron, the neural action potential is converted to a sarcolemmal action potential through a process called neuromuscular propagation, and then results in muscle contraction. Note that a contraction does not always correspond to the shortening of a muscle. Muscles may perform isometric contractions, in which they provide a force but their length does not change, or a lengthening contraction, in which they provide a force while their length grows.

2.4 Neurophysiology of Balance Control

Postural balance control is defined as the act of maintaining, achieving or restoring a state of balance during any posture or activity. It has been identified to be associated with three broad classes of human activity:

- (1) The maintenance of a specified posture, such as sitting or standing.
- (2) Voluntary movement, such as the movement between postures.
- (3) The reaction to an external disturbance, such as a trip, a slip or a push

As balance is often classified into static balance and dynamic balance, the balance control strategies may be either 'reactive' (compensatory) or 'predictive' (anticipatory), or a combination of both.

- (a) Reactive postural control strategy which involves a movement or muscular response following environment interference or unpredicted disturbance (e.g., being pushed) [1][7]

(b) Predictive postural control strategy might involve a voluntary movement, or increase in muscle activity, in anticipation of a predicted disturbance.

Maintaining balance is an integrated action to daily life involving complicated movements. The ability to maintain balance is a fundamental prerequisite for the various postures and movements. Probably almost all muscles in the body are actuated in every simple posture adjustments. The overall control scheme includes contraction of different groups of muscles, shifting the center of gravity, tilt and rotation of pelvis, posterior/anterior movement of joints (hip, knee, ankle) as shown in Figure 2.5 [55].

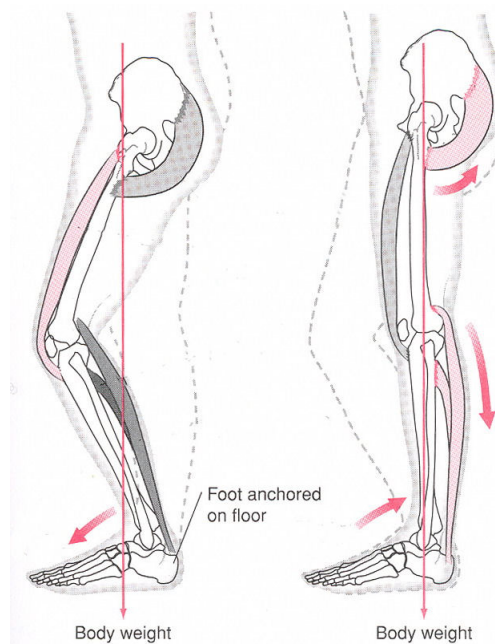


Figure 2.5: Contraction of different groups of muscles and posterior/anterior movement of joints (hip, knee, ankle) during balance control [55]

Balance malfunction often affects overall body function leading to a serious fall. Falling is a major health threat to the elderly because falling can result in many serious consequences[10][17][28]. Every year in China at least twenty million elderly experience

almost twenty-five million falls, costing more than one billion dollars/year in medication and rehabilitation[74]. A survey shows falling ranks as the sixth most prevalent cause of death of the elderly in the United States, and is the number one cause of death for people over the age of 75 in the United Kingdom[75]. Therefore, in clinical medicine, balance assessment is important for the following reasons:

- (1) Determine balance malfunction in the patient and determine the cause(if there is);
- (2) Determine the rehabilitation or treatment methodology and test their effectiveness;
- (3) Predict the risk of falls.

A systematic approach to clinical assessment of balance seeks to identify the underlying causes of the balance problem related to biomechanics, motor coordination and sensory organization. Some assessment indexes have proved to be useful to custom design a treatment problem, including *Falls Efficacy Scale* (FES) by Tinetti and Hill [36][38][81][35]; *Activities-Specific Balance Confidence Scale* (ABC) by Powell [73]. Sensitivity, bias, reliability, and efficiency are the criteria to evaluate an assessment technique [61] .

Chapter 3

Balance Control of Upright Posture

There has been an intensive biological and engineering effort to identify, understand, and model the underlying mechanisms of human postural control. Different approaches, tools, and frameworks have been proposed to tackle the postural control problem [84][82][51][36][40][63][64]. Understanding postural control as a biological process has its origins in physiology and is based on clinical and physiological tests. Modern electronic measurement technology makes it possible to conduct quantitative analysis of the various parts of the body, especially for lower limb movement and force during normal activities[77].

Balance of the human body is decided by the center of gravity, center of pressure, and the support surface area[11][32][33]. In static balance, if the body's center of gravity falls within the support area, the human body is stable, otherwise it may lose stability. For a long time, many biological features of quiet standing postural balance and its mechanisms have been studied, including the body's trajectory, joint angles, velocity,

cycle phase, muscle EMG, and muscle energy consumption. Results of such studies are collected and inferred in hypotheses and models explaining observed behaviors[80].

Control system theory is used as a tool in many fields (such as robotics, aerospace, computer science etc) to predict or estimate how a system will behave if controlled by a specific “control scheme.” Upright stance is inherently unstable without a scheme of automatic control; many feedback control models have been proposed to facilitate understanding of the neuromuscular mechanisms of human postural control. The theoretical study of quiet standing balance is useful for human nervous system disease diagnosis, disability assessment, joint orthotics prostheses design, and walking reconstruction for paraplegic patients. It has been a basic means in clinical research, in anthropology, kinesiology and aerospace science and other fields[10].

3.1 Experimental Studies

Early studies mainly focused on different sub-systems of the balance control through clinical test measurements, including the proprioceptive subsystem [24][32]; the visual subsystem:[22][71][78]; the vestibular subsystem [19] [27][46] and overall equilibrium control[20][36].

In experimental studies, a notable feature of postural control is a spontaneous body movement with small magnitude during quiet standing. Postural sway is anterior-posterior motion of the upright body as shown in Figure 3.1 [55]. It is the result of constant displacement and correction of the center of gravity within the base of support.

Good standing posture with good alignment will decrease the amount of stress placed on bones, ligaments, muscles, and tendons. It will also decrease the amount of muscle energy needed to keep the body upright.

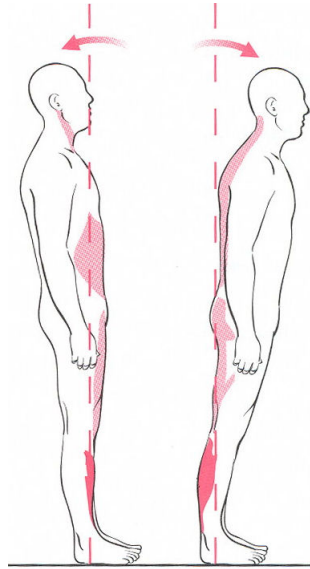


Figure 3.1: Spontaneous body sway movement with small magnitude [55].

The quantitative and qualitative properties of the constant sway phenomenon have been investigated by comparing the system's behavior under different physiological conditions. Early studies used the direct measurement of the trajectory of the ankle joint angle [24][25] and other body points [3][4]. Collins and Deluca studied the trajectory of the center of pressure (COP) [14][15][16][18] and Gatev et al. focused on the trajectory of the center of mass (COM)[30][68][85][86]. On the other side, the physiological impacts on the body sway have also been intensively studied, including: aging effects [3][68]; disruption/alteration of proprioception [24][26][59][45]; disruption or obstruction of visual feedback [3][16][22] and alteration of vestibular sense[18][27][52][85].

3.2 Biomechanic Models

Results of such experimental studies are collected and inferred in hypotheses and models explaining the observed behaviors. Inspired by these features, a series of biomechanical models resembling human balance control were devised to study the core principles of human postural control. These proposed frameworks commonly consisted of three main components, which are a mechanical structure describing the body dynamics with joint actuators, a sensory estimation system, and a control scheme providing corrective response. To validate and test the performance of the proposed postural control architecture, the control scheme is simulated given the derived model for different scenarios. The main difficulty is to derive a realistic model. Too strong assumptions may produce a simplified model not capable of capturing important dynamical aspects. On the other extreme, taking all aspects of interest into consideration will result in an intricate model that can be as hard to understand as the real system.

The human body exhibits redundant multi-degree-of-freedom motions due to the dynamics of multiple joints. However, when we study the balance control problem, only the most relevant body segments and joints are considered. Different models have been proposed in the literature to analyze balance posture, such as a single inverted pendulum model, two-segment model [70], and three-segment model [82][83][51].

The human postural balance control problem can be formulated as the following. Based on sensory information, choose in real time a suitable joint control torque to achieve a desired body balance position in the presence of external disturbances. Dif-

ferent motor strategies can be selected by the central nervous system (CNS) depending on the scenario. In general, the main body postural action takes place around the ankle in the so-called ankle strategy and this leads to an inverted-pendulum model. It is sometimes more feasible to move the hip back and forth (hip strategy) to stabilize the body when the support surface area is restricted. Swaying from the ankle or hip (ankle strategy or hip strategy) are commonly described fixed-support strategies, while grasping with a hand or stepping (stepping strategy) are common change-in-support posture stabilizing strategies [36]

The joint torques needed to stabilize the body during quiet stance can theoretically be generated actively and passively[62]. Passive torque components are the result of tension/stiffness produced by muscle tonus and by the stiffness of the surrounding tissue, such as ligaments and tendons. However, the stabilization of quiet stance by passive torque alone is a very challenging task[88]. An active component is required to maintain stability. The active torque component is controlled by the CNS, which modulates/controls muscle contractions based on the overall body kinematics and dynamics of spontaneous body sway that are influenced by external disturbances [84][87][94].

3.2.1 Linear Feedback Control Strategies

Numerous studies have demonstrated that quiet stance can be perturbed by stimulation of various sensory systems. These results suggest that active feedback-control mechanisms contribute to corrective torque generation based on body motion detected by sensory systems. [30][19][36][46][48][71]

Fitzpatrick et al. [25] investigates experimentally while feedback control can fully account for the entire torque required to maintain stance. In performing their study, they made the implicit assumption that various sensory systems make a fixed contribution to torque generation independent of environmental conditions or the reliability/accuracy of the various sensory measures of relative body motion. Based on this assumption, the corrective torque contribution from individual sensory systems was identified in separate experiments and summed to determine the total torque derived from sensory feedback mechanisms. The total torque was found to be insufficient to maintain stance, leading to the conclusion that feedback mechanisms alone are insufficient to explain our ability to maintain stance.

Bennett et al. [8] investigated the stretch-reflex contribution to limb stabilization and also demonstrated possible limitations in feedback control. Their results showed that stretch-reflex feedback control can only make a limited contribution to limb stabilization because this reflex (with essentially fixed dynamic properties of the limb, muscles, and stretch receptors) becomes unstable even with fairly low feedback gain. That is, a much higher reflex gain than knee jerk reflex would be needed for adequate compensation of a load disturbance, but this cannot be achieved by a stretch reflex because high gains produce instability. This occurs even though the time delay is relatively short (25-ms transmission delay plus an additional delay with similar magnitude due to muscle activation and force development). [42][77]. Longer time delays exacerbate the stability problem in feedback-control systems

Velocity feedback can play a significant role in anticipating body position change

because it carries information about the subsequent state of the body, i.e., a change in COM velocity indicates the direction and intensity with which the current COM displacement will be changed in the following time instant [14][15][16]. In general, the velocity feedback in addition to the position feedback, called proportional + derivative (PD) control, can potentially predict the future condition of the system and can stabilize it more effectively than only a position/proportional controller.

Application to a single joint inverted pendulum model to simulate human quiet stance revealed that the PD controller can facilitate stable control of the proposed model. However, there is no experimental study without perturbations that investigates the contribution of velocity information in controlling the body during quiet stance, and the tuning of the PD controller, i.e., the ratio of position and velocity information, remains unclear.

3.2.2 Nonlinear Control Strategies

Collins and De Luca postulated a nonlinear combination of open- and closed-loop control to explain their experimental findings for stance control [14]. They introduced a new analysis technique called stabilogram diffusion analysis, which measures the average similarity of the center-of-pressure signal at points in time separated by different time intervals. This analysis showed that quiet stance behavior is characterized by "persistence" over short time intervals and "anti-persistence" over longer time intervals. A possible explanation offered for this two-part behavior was that, over short time intervals, the postural system is not controlled (i.e., it operates open-loop), whereas at

longer time intervals, there is active feedback control (i.e., closed-loop control). This hypothesized dynamic switching between open- and closed-loop control would imply that the overall system cannot be completely characterized as a feedback-control system.

Peterka [70] showed that a feedback-control model could account for the persistence and anti-persistence behavior revealed by stabilogram diffusion analysis[15]. That is, it is not necessary that the system switch between open- and closed-loop control to explain the experimental findings from stabilogram diffusion analysis of quiet stance center-of-pressure measurements; a simple feedback-control system is sufficient[62]. However, the PD controller that demonstrates this behavior must include delay in the loop.

3.2.3 Optimal Control Strategies

In 1995, Kuo proposed a triple linked inverted pendulum model and a linear quadratic Gaussian (LQG) optimal controller to study the balance regulation [51]. The LQG controller consisted of a linear quadratic regulator (LQR) and a linear quadratic estimator (LQE) for state feedback information. Muscle dynamics are not included in Kuo's model and the neural efforts were directly proportional to joint torques. Neural transmission delays are mentioned but not quantified. While there is no evidence that the CNS functions as an LQG controller, there are presumably arguments that the CNS can be expected to behave like an optimizer because it utilizes redundant sets of both actuators and sensors.

If the optimization presumably performed by the CNS can be adequately described

by a quadratic function of states and controls, then LQG is a natural choice for modeling CNS behavior. LQR selects trajectories that minimize an objective function which weights the deviations of the controls and states from nominal. LQE on the other hand, relies on an internal model of the system to make the best possible use of information from sensors plus the Gaussian estimator. State estimators also incorporate coordinate transformations and time integration as necessary to integrate sensory information from more than one source.

Note that modeling of the postural motor control system as an LQG controller does not presume that the CNS performs such functions. Rather, the LQG system represents an ideal linear system, making best use of sensory information to minimize a quadratic function of states and controls, while satisfying the constraints. If the CNS has similar objectives and similar performance criteria, then the LQG system will produce a smooth, stable trajectory of states similar to the human response to perturbations. He, Levine and Loeb[34] developed a complex model of the cat neuromusculoskeletal system based on LQR control. They used this model to analyze various control schemes, including joint position servo, muscle length servo, muscle stiffness, and full state feedback control, which is augmented with sensor and muscle states.

3.3 Proposed Nonlinear Optimal Control Model

The models we have discussed represent a variety of schemes and ideas of postural control, each assuming some type of feedback mechanisms. The difficulty of implementing

control system theory to model a biological system is the limited understanding of the biological system itself.

The scope of models presented in this study is different from those models mentioned in the earlier parts of this chapter. Our model explains the observed kinematics by using a nonlinear optimal feedback control scheme. This model also investigates the trade-off effects in integration of sensory signal and control efforts in the CNS with delay factors. This feedback mechanism may be used to predict the Center of Pressure (COP) and Center of Mass (COM) kinematics including position, velocity and acceleration. Specifically,

- (1). A nonlinear optimal control mechanism with performance measure having higher order than quadratic costs for deviations of the states from the nominal.
- (2). A model of delay in both sensory feedback and control actuation of CNS.
- (3). Coordination of multiple joints by varying the weightings of the deviations of the states and controls from their nominal values, and by penalizing COP deviation from its nominal value.
- (4). Expandable structure for other complex system models.

The derived model is simulated for different scenarios to validate and test the performance of the proposed postural control architecture.

Chapter 4

Single Joint Balance Control

4.1 Single Inverted Pendulum Model

The human body exhibits redundant multi-degree-of-freedom motions due to the dynamics of multiple joints. However, when we study the balance control problem, only the most relevant body segments and joints are considered. The body segments of interest are the feet, legs, thighs, trunk, and head. Corresponding joints are ankle, knee, hip, and neck. Depending on the fineness of the desired model, different segmental combinations can be lumped.

For small deviations from the nominal postural position, upright standing in the sagittal plane is commonly modeled as a single-inverted pendulum comprising all body segments above the ankles lumped to form one rigid body whereas the feet are considered again as a part of the supporting surface (Figure 4. 1).

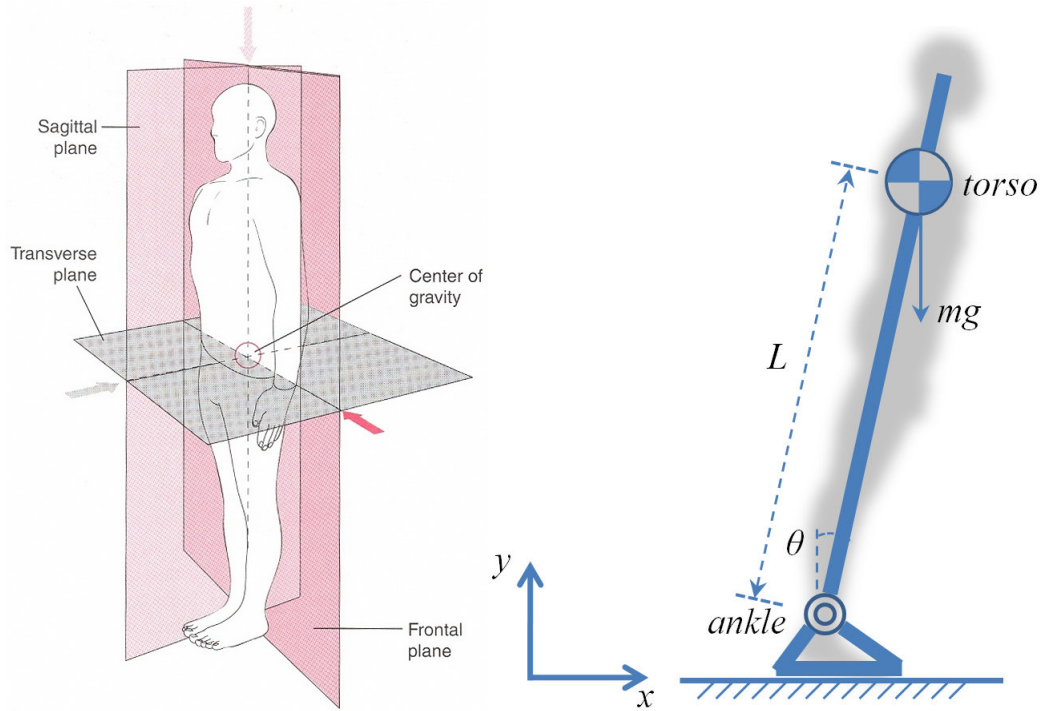


Figure 4.1: Single joint inverted pendulum model for postural balance control during quiet standing in the sagittal plane. (Left figure is from [55])

In this case, only motion about the ankle joint is assumed [85][62][71]. One reason is that experimental observations suggest that for small postural deviations, there is very little, if any, knee and hip angular motion. We will formulate the control scheme starting from a single inverted pendulum as the biomechanical model, and then develop a more realistic model of neuromusculoskeletal upright stance that is descriptive of observed postural responses, physiologically relevant, and straightforward to interpret.

Assuming that the body weight is mg and the distance of the Center of Mass (COM) from the ankle joint is L , then a gravitational torque $mgL\sin(\theta)$ acts on the body due to a shift of the COM a distance $L\sin(\theta)$ from the vertical. To stabilize posture, a counteractive muscle torque u is exerted by activating the related ankle-joint

muscles. The dynamics of a single inverted pendulum is expressed as,

$$I_o \frac{d^2\theta}{d\tau^2} = mgL\sin(\theta) + u + \epsilon \quad (4.1)$$

θ	Ankle angle	g	Gravitational acceleration
I_o	Moment of inertia of the body	L	Distance of COM from the ankle
m	The body mass	u	Ankle torque
τ	Time	ϵ	Disturbance torque

In this inverted pendulum model, the ankle torque that stabilizes the body during quiet stance can be generated actively and passively[54]. Passive torque [62] components are the result of tension/stiffness produced by muscle tonus and by the stiffness of the surrounding tissue, such as ligaments and tendons. The active torque [62][84][87] component is produced by muscle contractions.

Because the COM is normally located in front of the ankle joint, passive backward ankle torque is continuously applied to the body to prevent it from falling forward [79]. It is known that the stabilization of quiet stance by passive torque alone is not possible though, and therefore an active component is required to maintain stability[36]. Since ankle flexor activity is rare and ankle extensors are considerably activated, the ankle extensors contribute the most toward control of the ankle joint torque [30][47][57][58][68].

Dimensional analysis has been often used for qualitative reasoning about physical systems. For this human standing model $[\cdot]$ denotes dimension, M is mass, L is length, T is time and 1 indicates dimensionless.

$$\begin{aligned}
[\theta] &= 1 & [I_o] &= M(Ln)^2 \\
[g] &= L/T^2 & [h] &= L \\
[u] &= ML^2/T^2 & [\epsilon] &= ML^2/T^2
\end{aligned}$$

We introduce the quantities $t = \tau/\beta$ and the normalization factor $\beta = \sqrt{L/g}$, which has dimension $[\beta] = T$ (time). Given $\frac{d\tau}{dt} = \beta$ and $\tilde{\theta}(t) = \theta(\tau)$, we apply the chain rule to obtain a dimensionless first order derivative with respect to time and repeat the process for the second derivative

$$\frac{d\tilde{\theta}(t)}{dt} = \beta \frac{d\theta(\tau)}{d\tau} \text{ and } \frac{d^2\tilde{\theta}(t)}{dt^2} = \beta^2 \frac{d^2\theta(\tau)}{d\tau^2}$$

Let $\alpha = \frac{mgL}{I_o}$, we can simplify Eqn (4.1) into a completely dimensionless form:

$$\frac{d^2\tilde{\theta}(\tau)}{d\tau^2} = \alpha\beta^2 \sin\tilde{\theta}(\tau) + \frac{\tilde{u}(\tau)}{I_o}\beta^2 + \frac{\tilde{\epsilon}(\tau)}{I_o}\beta^2 \quad (4.2)$$

Note here $[\alpha] = \frac{1}{T^2}$, whereas $[\beta^2] = T^2$ and for the rest variables: $\left[\frac{d^2\tilde{\theta}(\tau)}{d\tau^2}\right] = 1$, $[\tilde{\theta}(\tau)] = 1$, $[\alpha\beta^2] = 1$, $\left[\frac{\tilde{u}(\tau)}{I_o}\beta^2\right] = 1$ and $\left[\frac{\tilde{\epsilon}(\tau)}{I_o}\beta^2\right] = 1$. Then, we omit the tilde and simplify as,

$$\ddot{\theta}(\tau) = \alpha\beta^2 \sin\theta(\tau) + \frac{u(\tau)}{I_o}\beta^2 + \frac{\epsilon(\tau)}{I_o}\beta^2 \quad (4.3)$$

Then let $x_1 = \theta$, $x_2 = \dot{\theta}$, further define $u = \frac{u(t)}{I_o}\beta^2$, $\epsilon = \frac{\epsilon(t)}{I_o}\beta^2$ and a nominal equilibrium posture of $x_1 = 10^\circ$, $x_2 = 0$. We can then apply $\sin(x_1-10) \rightsquigarrow (x_1-10) = x_1$ to simplify the system without losing generality, because the angular excursions possible during stable posture regulation are less than $\pm 5^\circ$. The dimensionless differential Equation (4.3) linearized about $x_1 = 10^\circ$, $x_2 = 0$ has the simplified form :

$$\begin{cases} \dot{x}_1(t) = x_2(t) \\ \dot{x}_2(t) = \alpha\beta^2 x_1(t) + u(t) + \epsilon(t) \end{cases} \quad (4.4)$$

where x_1 and x_2 are deviations from the nominal equilibrium point and u is defined as the difference between the actual control and the nominal passive control needed to maintain equilibrium at 10° . The two parameters α and β provide a body characteristic measurement for the description of the human [91][92].

Since the prior research [57, 59] suggests the postural controller is fairly insensitive to small errors, the plant model has two states and one control, and the noise is very small, we (temporarily) ignore the noise and use state space notation to represent the equations of motion Eqn (4.4).

The state variables for the single inverted pendulum are defined as the angle and angular velocity. For simplicity, we use the normal notation for the following section. Eqn(4.4) can be rewritten as:

$$\dot{\underline{x}}(t) = A\underline{x}(t) + Bu(t) \quad (4.5)$$

where $\underline{x} \in \mathbb{R}^2$ denotes the states and

$$A = \begin{bmatrix} 0 & 1 \\ \alpha\beta^2 & 0 \end{bmatrix}, B = \begin{bmatrix} 0 \\ 1 \end{bmatrix}$$

4.2 The Optimal Control Problem

The human body is modeled as a single inverted pendulum in the sagittal plane, and controlled by ankle joint torques. Then, a biomechanical model resembling human balance control is proposed and devised for the study of core principles of human postural control.

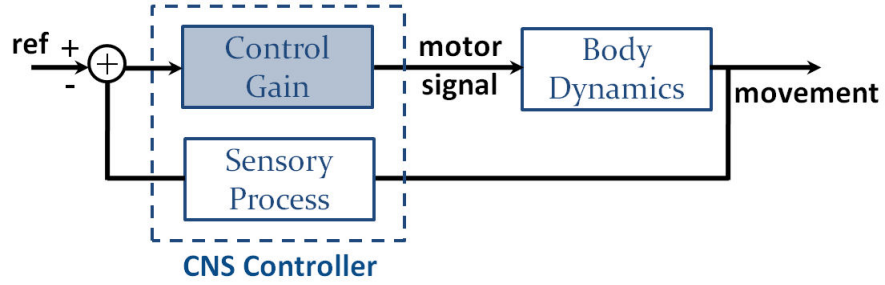


Figure 4.2: The single joint balance control system

The performance criteria that are of high even orders in the body state and quadratic in the joint control are utilized.

$$J_{SHOC} = \int_0^{\infty} [px_1^{2m}(t) + qx_2^{2n}(t) + ru^2(t)] dt$$

where p, q and r are cost coefficients, m, n are integers, and x_1, x_2 are deviations from the nominal equilibrium values of body angle and angular velocity in the sagittal plane.

The u are control torques of each joint. SHOC stands for a Single inverted pendulum model with Higher Order Control. The term $\int_0^{\infty} [px_1^{2m}(t) + qx_2^{2n}(t)] dt$ corresponds to the cost of the deviations of the balance position from its nominal value. The term $\int_0^{\infty} ru^2(t)dt$ approximate the energy of the control signal at the ankle joint.

The higher order objective function provides an extra degree of freedom in addition

to the cost coefficient. Note that this performance measure reduces the neuromuscular energy used by penalizing small postural errors very lightly.

When $m + n > 2$, this higher order performance measure will lead to a nonlinear optimal balance control scheme. It can be implemented to explain kinematics and investigate the trade-off effects in integration of sensory signal and control efforts in the CNS. It may be used to predict the Center of Mass (COM) kinematics including position, velocity and acceleration. To further simplify this problem, we introduce some assumptions for this model summarized as follows:

- A. No neural transmission delay is considered
- B. Full state feedback is available with perfect state estimation

These assumptions are probably incorrect; the dynamics of a real standing human body are much more complicated than this; but this model provides a very simple paradigm for us to start with. Then the optimal control problem is constructed as

$$\begin{aligned} \mathbf{min} \quad J_{SHOC} &= \int_0^{\infty} [px_1^{2m}(t) + qx_2^{2n}(t) + ru^2(t)] dt & (4.6) \\ \mathbf{s.t.} \quad \dot{\underline{x}}(t) &= A\underline{x}(t) + Bu(t) \end{aligned}$$

We use the relationship $t = k\delta$ to transform the continuous state-space system into a sampled discrete system:

$$\underline{x}[k] = \underline{x}(k\delta) = e^{Ak\delta}\underline{x}[0] + \int_0^{k\delta} e^{A(k\delta-\xi)}Bu(\xi)d\xi$$

Now, if we want to analyze the $k + 1$ term, we can use the same equation again:

$$x[k+1] = e^{A(k+1)\delta} \underline{x}[0] + \int_0^{(k+1)\delta} e^{A((k+1)\delta-\xi)} Bu(\xi) d\xi$$

Separating out the variables, and breaking the integral into two parts gives us:

$$\underline{x}[k+1] = e^{A\delta} e^{Ak\delta} \underline{x}[0] + \int_0^{k\delta} e^{A\delta} e^{A(k\delta-\xi)} Bu(\xi) d\xi + \int_{k\delta}^{(k+1)\delta} e^{A(k\delta+\delta-\xi)} d\xi$$

If we substitute in a new variable $\lambda = (k+1)\delta + \xi$, and use the following relationship $e^{Ak\delta} x[0] = x[k]$, we get our final result:

$$\underline{x}[k+1] = e^{A\delta} \underline{x}[k] + \left(\int_0^\delta e^{A\lambda} d\lambda \right) Bu[k]$$

Comparing this equation to our solution gives us a set of relationships for converting the continuous time system into a discrete time system. Here, we will use \bar{A} and \bar{B} denote the system matrices of a discrete system

$$\bar{A} = e^{A\delta} = \sum_{n=0}^{\infty} \frac{A^n (\delta)^n}{n!}, \quad \bar{B} = A^{-1}(\bar{A} - I)^{-1} B$$

Then the discretized dimensionless system is

$$\underline{x}[k+1] = \bar{A} \underline{x}[k] + \bar{B} u[k]$$

The above continuous time problem has been converted into discrete time as:

$$\mathbf{min} J_{SHOC} = \sum_{k=0}^{\infty} p x_1^{2m}(k) + q x_2^{2n}(k) + r u^2(k) \quad (4.7)$$

$$\mathbf{s.t.} \quad \underline{x}(k+1) = \bar{A} \underline{x}(k) + \bar{B} u(k)$$

Even though this simple model has linear time-invariant dynamics, due to the higher order terms in the performance measure, the solution to this problem is not straightforward.

4.3 LQR Case

If we choose m, n both equal to 1, the objective function is quadratic. Since the dynamics constraints are linear, this problem then becomes a linear-quadratic optimal control problem, which is one of the most fundamental optimal control problems:

$$\mathbf{min} J_{SLQR} = \sum_{k=0}^{\infty} px_1^2(k) + qx_2^2(k) + ru^2(k) \quad (4.8)$$

$$\mathbf{s.t.} \underline{x}(k+1) = \bar{A}\underline{x}(k) + \bar{B}u(k)$$

$$\underline{x}(0) = \underline{x}_0$$

where $\underline{x}(t_0)$ is the initial condition. It will be helpful to convert the performance measure into a canonical form as,

$$\mathbf{min} J_{SLQR} = \sum_{k=0}^{\infty} \underline{x}^T(k)Q\underline{x}(k) + u^T(k)Ru(k)$$

where

$$Q = \begin{bmatrix} p & 0 \\ 0 & q \end{bmatrix} \text{ and } R = r$$

The LQR optimal control sequence minimizing the performance index is given by $\underline{u}^*(k) = -L\underline{x}(k)$ where $L = (R + \bar{B}^T P \bar{B})^{-1} \bar{B}^T P \bar{A}$, and P is the solution of the algebraic *Riccati* Equation:

$$P = Q + \bar{A}^T (P - P \bar{B} (R + \bar{B}^T P \bar{B})^{-1} \bar{B}^T P) \bar{A}$$

If we choose m, n both equal to 2, and $r = 1$ then the objective function is no longer quadratic, it becomes quartic in the states and quadratic in the control:

$$\mathbf{min} J_{SHOC} = \sum_{k=0}^{\infty} px_1^4(k) + qx_2^4(k) + u^2(k) \quad (4.9)$$

$$\mathbf{s.t.} \underline{x}(k+1) = \bar{A}\underline{x}(k) + \bar{B}u(k)$$

$$\underline{x}(0) = \underline{x}_0$$

The constraints are still linear, but the solution to this optimal control problem cannot be found by analytical means. Most of the real world system models involve nonlinear optimization with complicated objective functions or constraints for which analytical solutions are not available [6].

4.4 Model Predictive Control

Model Predictive Control (MPC) refers to a class of control algorithms that compute a sequence of control inputs based on an explicit prediction of dynamic outputs within a finite future horizon.

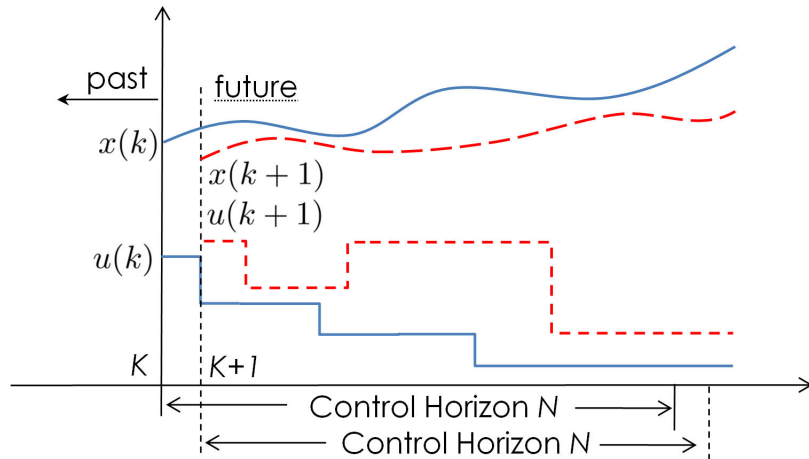


Figure 4.3: Moving horizon control

Consider the diagram in Figure. 4.3. At the time k , the current plant state $x(k)$ is sampled and a cost minimizing control is computed (via a numerical minimization algorithm) for a relatively short time horizon in the future $[k, k + N]$. The state path $[x(k)...x(k + N)]$ and the controls $[u(k)...u(k + N)]$ over a finite horizon N are computed and stored.

Then, only the first step of the control strategy $u(k)$ is implemented to the system, and at time $k + 1$ the plant state is sampled again. The calculations are repeated starting from the new current state $x(k + 1)$, yielding a new control $[u(k + 1)...u(k + 1 + N)]$ and new predicted state path $[x(k + 1)...x(k + 1 + N)]$. The prediction horizon $[k + 1, k + 1 + N]$ keeps being shifted forward, and for this reason MPC is also called receding horizon control. The iterative computation mainly exploits the similarity of subsequent problems and provides a feedback control scheme. We then try to solve the discrete-time optimal control problem using the same techniques of MPC, that is choose a finite horizon N and convert this into a finite time optimal control problem as

$$\mathbf{min} J_{SHOC} = \sum_0^N px_1^4(k) + qx_2^4(k) + u^2(k) \quad (4.10)$$

$$\mathbf{s.t.} \underline{x}(k+1) = \overline{A}\underline{x}(k) + \overline{B}u(k)$$

$$\underline{x}(0) = \underline{x}_0$$

Many numerical procedures have been developed to solve general optimal control problems. Today, it is commonly accepted [67] that the best approach is to discretize the problem in time and apply nonlinear programming algorithms.

4.5 The Optimization Problem

The discretized optimal control problem using MPC technique in a finite horizon N then becomes a nonlinear optimization problem, which has the canonical form as:

$$\begin{aligned} \mathbf{min} \quad & f_0(x) \\ \mathbf{s.t.} \quad & f_i(x) \leq 0, \quad i = 1, \dots, m \\ & h_i(x) = 0, \quad i = 1, \dots, p \end{aligned}$$

The problem is to find an optimal variable $x \in \mathbb{R}^n$ that minimizes the objective or cost function $f_0(x) : \mathbb{R}^n \rightarrow \mathbb{R}$ among all x that satisfy the inequality constraints $f_i(x) \leq 0$ and equality constraints $h_i(x) = 0$. If there are no constraints (*i.e.*, $m = p = 0$) the problem is unconstrained.

Certain problem classes can be solved efficiently and reliably, such as least squares problems, linear programming problems and convex optimization problems. If the

resulting discrete time optimization problem is convex (minimization problem) and the constraint set is convex, which means

$$f(\alpha x_1 + (1 - \alpha)x_2) \leq \alpha f(x_1) + (1 - \alpha)f(x_2)$$

$$\forall 0 < \alpha < 1$$

then the problem can be solved by convex optimization. Least squares problems are a special case of convex programming problems as we discussed in the LQR case. The convexity of the objective function and the constraints make the powerful tools of convex analysis applicable.

It's known to have a solution and to be comparatively easy to solve the convex programming problem using Newton-type optimization schemes. These methods depend on the first and possibly the second derivatives of the objective function include:

A Newton's Method: Newton's method is based on Taylor's series expansion.

The Taylor's series expansion of a function $f(x)$ at $x = x_k$ is given by:

$$f(x) = f(x_k) + \nabla f^T(x - x_k) + \frac{1}{2}(x - x_k)^T H(x_k)(x - x_k)$$

where $H(x_k)$ is the Hessian matrix evaluated at point x_k and we set

$$\nabla f(x_k) + H(x_k)(x - x_k) = 0$$

This can be solved to obtain an improved solution

$$x_{k+1} = x_k - H^{-1}(x_k)\nabla f(x_k)$$

The procedure is repeated till convergence for finding the optimal solution.

- B Quasi-Newton Method: Quasi-Newton methods are algorithms for finding maxima and minima of nonlinear functions. They are based on Newton's method, but they approximate the Hessian matrix, or its inverse, in order to reduce the amount of computation per iteration.

Under differentiability and constraint qualifications, the *Karush-Kuhn-Tucker (KKT)* conditions provide necessary conditions for a solution to be optimal [72]. Due to the convexity, these conditions are also sufficient. Our problem as defined in (4.9) satisfies this condition and therefore it is a convex programming problem. using a *Newton-KKT* interior point method. Interior point methods, also referred to as barrier methods, were inspired by Karmarkar's [49] concept to transform the convex optimization problem into minimizing (or maximizing) a linear function over a convex set [90]. They guarantee that the number of iterations of the algorithm is bounded by a polynomial in the dimension and accuracy of the solution. The virtues of convex optimization are

- A. Local optimum is a global optimum.
- B. The feasibility of a convex problem can be determined unambiguously.
- C. Precise stopping criteria can be defined by duality.

4.6 The MPC Solution

We have converted the optimal control problem into a optimization problem using the MPC technique, and due to the higher even order (quartic in this case), this leads to a convex programming problem as following:

$$\begin{aligned}
 \mathbf{min} \quad & J_{SHOC} = \sum_0^N px_1^4(k) + qx_2^4(k) + u^2(k) \\
 \mathbf{s.t.} \quad & \underline{x}(k+1) = \bar{A}\underline{x}(k) + \bar{B}u(k) \\
 & \underline{x}(0) = \underline{x}_0
 \end{aligned} \tag{4.11}$$

where

$$\bar{A} = e^{A\delta} = \sum_{n=0}^{\infty} \frac{A^n(\delta)^n}{n!}, \quad \bar{B} = A^{-1}(\bar{A} - I)^{-1}B$$

$$A = \begin{bmatrix} 0 & 1 \\ \alpha\beta^2 & 0 \end{bmatrix} \quad B = \begin{bmatrix} 0 \\ 1 \end{bmatrix}$$

We introduce a overall variable that contains the state and control variables

$$\underline{s} = \left[\underline{x}(0)^T, u(0), \underline{x}(1)^T, u(1), \dots, \underline{x}(k), u(k) \dots, \underline{x}(N)^T, u(N) \right]^T$$

The objective function $J(\underline{x}, u)$ then becomes $J(\underline{s})$ and the variable $\underline{s} \in \mathbb{R}^{3N+1}$. We introduce the following notation for the *Newton-KKT* iteration algorithm.

$\underline{s}^{(i)}$ is the overall variable at i^{th} iteration

$\underline{r}^{(i)}$ is the gradient for the overall variable at i^{th} iteration, $\underline{r}^{(i)} = \nabla J(\underline{s}^{(i)})$

$H^{(i)}$ is the Hessian matrix for overall variable at i^{th} iteration, $H^{(i)} = \nabla^2 J(\underline{s}^{(i)})$

Note that the Hessian $H^{(i)}$ is block diagonal

$$H^{(i)} = \text{diag}[R_0^{(i)}, Q_1^{(i)}, R_1^{(i)}, \dots, Q_k^{(i)}, R_k^{(i)}, \dots, Q_N^{(i)}, R_N^{(i)}]$$

$$R_k^{(i)} = \nabla^2 f(u_k^{(i)}) = 2 \quad \forall i$$

$$Q_k^{(i)} = \nabla^2 f(\underline{x}_k^{(i)}) = \begin{bmatrix} \frac{\partial^2 f(\underline{x}_k^{(i)})}{\partial x_1(k) \partial x_1(k)} & 0 \\ 0 & \frac{\partial^2 f(\underline{x}_k^{(i)})}{\partial x_2(k) \partial x_2(k)} \end{bmatrix} \quad \forall i$$

Each term on the diagonal of the Hessian $H^{(i)} = \nabla^2 J(\underline{s}^{(i)})$ is positive definite, except at $x_1(k) = 0$ or $x_2(k) = 0$ for some $k = 0, 1, 2, \dots, N$.

4.6.1 Newton-KKT Methods

In this section, we describe an iterative interior-point algorithm to solve the *Newton KKT* system [12]. The Newton step $\Delta \underline{s}_{nt}^{(i)}$ for our equality constrained problem is characterized by the following *Newton KKT* system:

$$\begin{bmatrix} H^{(i)} & A_s^T \\ A_s & 0 \end{bmatrix} \begin{bmatrix} \Delta \underline{s}_{nt}^{(i)} \\ \underline{w} \end{bmatrix} = \begin{bmatrix} -\underline{r}^{(i)} \\ 0 \end{bmatrix} \quad (4.12)$$

$$A_s = \begin{bmatrix} I & 0 & \dots & \dots & \dots & O \\ -\bar{A} & -\bar{B} & I & 0 & \dots & \vdots \\ \vdots & \vdots & \vdots & \vdots & \vdots & \vdots \\ O & \dots & -\bar{A} & -\bar{B} & I & 0 \end{bmatrix}$$

Using the Schur Complement to solve the *Newton KKT* system

$$H^{(i)} \Delta \underline{s}_{nt}^{(i)} + A_s^T \underline{w} = -\underline{r}^{(i)} \quad (4.13)$$

We use the following algorithm to solve the optimization problem.

Algorithm 4.1 Regular Convex Optimization

Input: $\underline{s}^{(0)} = [\underline{x}(0), \underline{u}(0), \overline{A}\underline{x}(0), \underline{u}(1), \dots, \overline{A}^k \underline{x}(0), \underline{u}(1), \dots, \overline{A}^N \underline{x}(0), \underline{u}(N)]^T$ **Output:** \underline{s}^* such that the given cost function is minimized

```
1  Start
2    For  $i = 1$  to  $N^i$ 
3      Compute  $R = -A_s[H^{(i)}]^{-1}A_s^T$ 
4      Solve for  $\underline{w}$  from  $R\underline{w} = A_s[H^{(i)}]^{-1}\underline{r}^{(i)}$ 
5      Compute  $\Delta_{\underline{s}_{nt}}^{(i)} = [H^{(i)}]^{-1}(-A_s\underline{w} - \underline{r}^{(i)})$ 
6        IF  $\lambda(\Delta_{\underline{s}_{nt}}^{(i)}) = \sqrt{[\Delta_{\underline{s}_{nt}}^{(i)}]^T H^{(i)} \Delta_{\underline{s}_{nt}}^{(i)}} > \epsilon$ 
7          DO  $\underline{s}^{(i+1)} \leftarrow \text{LinearSearchAlgorithm}(\underline{s}^{(i)}, \Delta_{\underline{s}_{nt}}^{(i)})$ 
8          ELSE DO  $\underline{s}^{(i+1)} = \underline{s}^{(i)}$ 
9        End For
10     Output  $\underline{s}^* = \underline{s}^{(i+1)}$ 
11  End
```

Algorithm 4.2 Backtracking Linear Search

Input: $\underline{s}, \Delta_{\underline{s}_{nt}}$ **Output:** \underline{s}^* linear search in the $\Delta_{\underline{s}_{nt}}$ direction

```
1  Start
2    Choose  $\mu \in (0, 0.5)$   $\eta \in (0, 1)$   $\rho = 1$ 
3    While  $J(\underline{s} + \rho\Delta_{\underline{s}_{nt}}) > J(\underline{s}) + \mu\rho[\nabla J(\underline{s})]^T \Delta_{\underline{s}_{nt}}$ 
4      DO  $\rho := \rho\eta$ 
5      Update  $\underline{s} = \underline{s} + \rho\Delta_{\underline{s}_{nt}}$ 
6    End While
7    Output  $\underline{s}^*$ 
8  End
```

This would give us a nonlinear, approximately optimal, full-state feedback regulator for posture. In fact, all of the elements of the state of this system are measured by sensors in the human body. Biologically, this nonlinear controller can be learned over time and would not impose any computational burden on the human nervous system.

4.7 Results

4.7.1 The Nonlinear Full-State Feedback Solution

The simulations of the designed control system are based on the simplified sway model defined in Eqn (4.9) using Peterka’s body parameters[70] as shown in Table 4.1.

Table 4.1: Body Characteristics and Dimensionless Model Parameters

Symbol	Quantity	Value
M	Body mass	76 kg
I_0	Moment of body inertia	66 kg.m ²
L	CM height over ankle joint axis	0.87 m
g	Acceleration of gravity	9.8 m/s ²
α	mgh/I_0	9.26
β	$\sqrt{h/g}$	0.092

We apply the model predictive control (MPC) to find the closed-loop solution. The control gain was obtained by solving the convex programming problem starting at each sampling instant as a finite horizon open-loop optimal control problem, using the current state of the plant as the initial state. Optimization yielded an optimal control sequence and the first control in this sequence was applied to the plant. The performance criteria used were of the form

$$J_{SHOC}(\underline{x}, u) = \sum_0^N [px_1^{2m}(k) + qx_2^{2n}(k) + u^2(k)]$$

Four different optimal control problems were solved and simulated for different scenarios. We chose $[m, n]=[1, 1], [1, 2], [2, 1]$ and $[2, 2]$. The open loop optimal control problem was solved for every initial condition in a grid as indicated in Table 4.2.

Table 4.2: Open-loop Simulation Parameters

Symbol/Quantity	Values
Feasible angular range	$[-5^\circ, 5^\circ]$
Angular step interval size	0.05°
Feasible velocity range	$[-1.5^\circ/s, 1.5^\circ/s]$
Velocity step interval size	$0.005^\circ/s$
N^h - Length of horizon	20
N^i - Iteration numbers	20
p - Angular cost coefficient	0.1
q - Velocity cost coefficient	0.5

This array consisted of the following feasible sway range:

- Angular displacements $x_1 \in [-5^\circ, 5^\circ]$ with step interval size is 0.05°
- Angular velocity $x_2 \in [-1.5^\circ/s, 1.5^\circ/s]$ with step interval size is $0.005^\circ/s$.

The $[1, 1]$ result is for an LQR optimal control — a linear system. The $[2, n]$ results, as expected, have considerably more movement for small x_1 . The choice of $p = 0.1$ means that the main effects will appear for $|x_1| < 0.5^\circ$. In order to obtain an approximation to the optimal feedback control, we then interpreted the first value of the control signal as the optimal feedback gain for any state identical to the initial state, resulting in the control torque as a function of state (feedback control) as shown in Figure. 4.4. The feedback control for an arbitrary initial condition was then computed by interpolating from this grid.

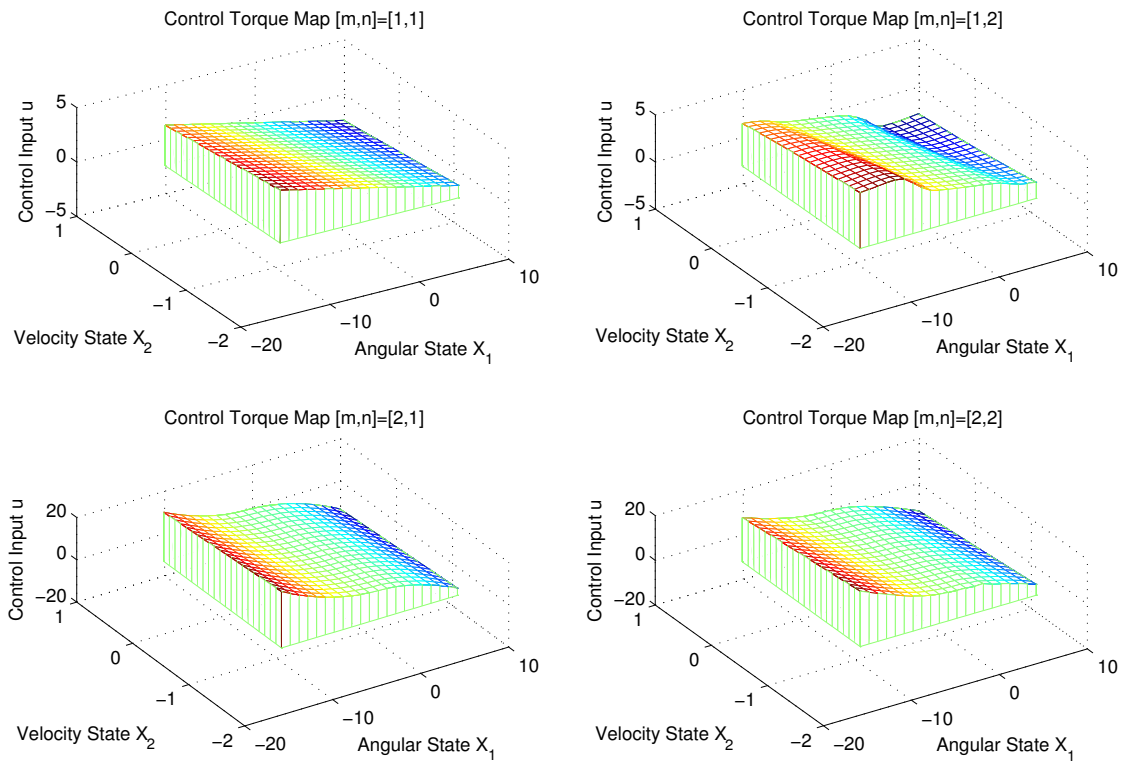


Figure 4.4: Control Torque Map in the Feasible Sway Range

As can be seen in Figure 4.4. the $[1, 1]$ feedback control is linear — it is the LQR optimal feedback control. The other three feedback controls $[m, n]=[1, 2]$, $[2, 1]$ and $[2, 2]$ have nearly zero slope at $|x_1| = 0$ and steep slope for large $|x_1|$. The $[1, 2]$ feedback controller seems to have an interesting skewness. We can use the obtained control torque map over the feasible sway range to fully describe the SHOC system with fixed noise level as is discussed in the following sections.

4.7.2 The Performance of the Full-State Feedback Solution

We simulated the closed-loop SHOC system with a fixed noise level using the optimal feedback control obtain from the torque map in Figure 4.4. The noise is white Gaussian noise with zero-mean and standard deviation equal to 0.1.

Transient Response (Balance Restoration)

The parameters for simulation of transient response are listed in Table 4.3. The simulation results are depicted in Figure. 4.5.

Table 4.3: Fixed Initial State and Noise Level Parameters

Symbol	Quantity	Value
x_1	Angular displacement	$+3^\circ$
x_2	Angular velocity	$+0.1^\circ/s$
ϵ	Noise level	0.1
T	Simulation duration	20 <i>secs</i>
δ	Sampling interval	1/50 <i>secs</i>

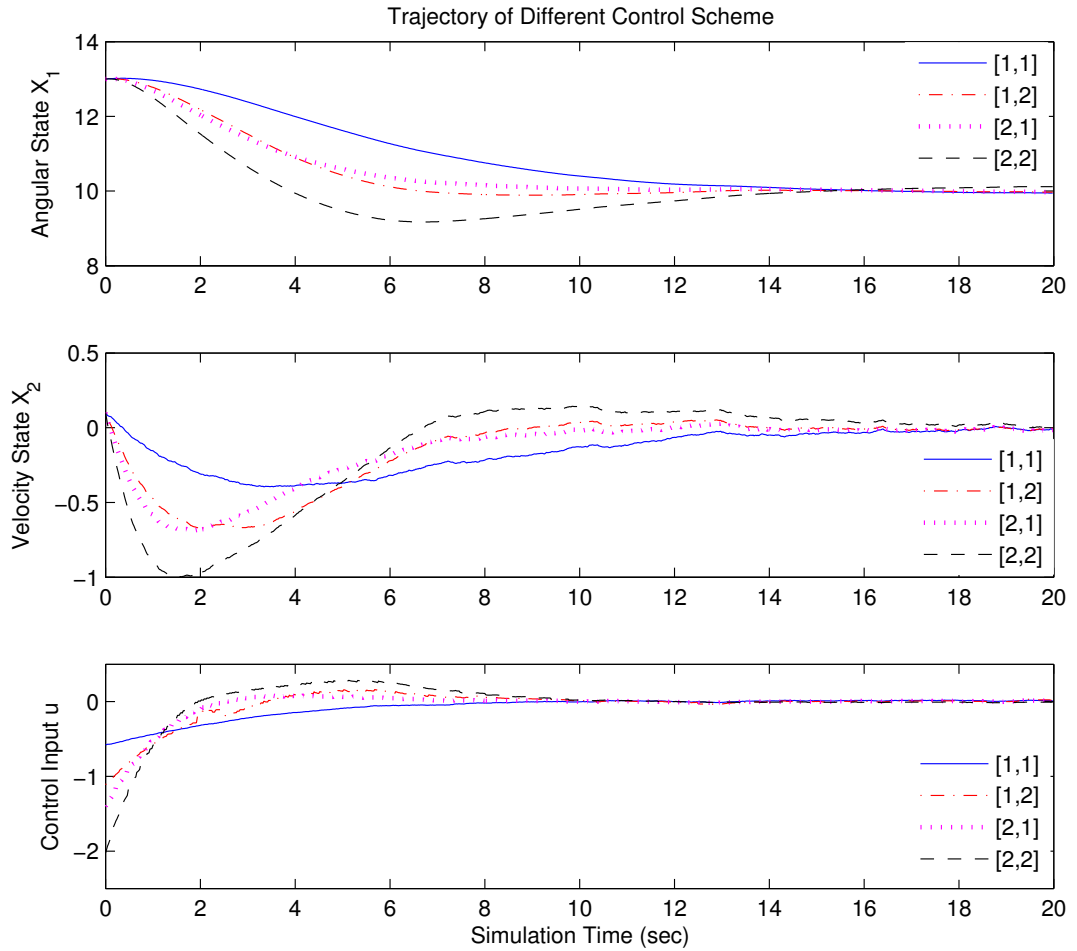


Figure 4.5: Trajectories of angular state x_1 , angular velocity x_2 and the control input u for different performance criteria with fixed noise level

Notice that the optimal controls for all three SHOC performance criteria are much more aggressive in reducing the large initial deviations than the LQR optimal control. However, all three respond less to the small deviations that remain after roughly 10 seconds. Similar as the kinetic energy $k = \frac{1}{2}mv^2$, the rotational kinetic energy is $k_{rot} = \frac{1}{2}I\dot{\theta}^2$. The ankle torque is defined as $\tau = I\ddot{\theta}$, so when the torque act through a rotational distance, the rotation work is defined as

$$W = \int_{\theta_1}^{\theta_2} \tau d\theta = \int_{t_1}^{t_2} \tau \frac{d\theta}{dt} dt$$

Work is the reason that makes the energy change:

$$W = \Delta E$$

Therefore, the torque energy for the ankle will be

$$E = \int_{t_1}^{t_2} \tau \frac{d\theta}{dt} dt \simeq \sum_{k=n_1}^{n_2} u(k) * x_2(k)$$

We then calculated the control torque energy $E_{ab} = \sum_a^b u(k) * x_2(k)$ for different time intervals $[a, b]$: $[0s, 5s]$ $[5s, 10s]$ $[10s, 15s]$ $[15s, 20s]$. The results are listed in Table 4.4.

Table 4.4: Torque Energy E_{ab} at Different Time Interval for Four Control Strategies under Same Noise Level

Noise Level	$E_{[0,5]}$	$E_{[5,10]}$	$E_{[10,15]}$	$E_{[15,20]}$
[1, 1]	1.8480	0.03	0.0014	0.0034
[1, 2]	3.1806	0.1337	0.0032	0.0021
[2, 1]	3.6549	0.0180	0.0017	0.0014
[2, 2]	6.6331	0.5014	0.0008	0.0008

As we can see from the table, the control torque energy for all four control strategies decreases rapidly when the system is far from the equilibrium position. But near the equilibrium state, the LQR control strategy consumes the most energy, while the SHOC control schemes require less torque energy. In the long run, as long as there are only small disturbances introduced to the system, a SHOC control will be the most energy-efficient control scheme to maintain the inverted pendulum in a stable equilibrium state.

Steady State Response (Balance Maintenance)

It is interesting to simulate the system starting from an equilibrium state but driven by different levels of noise. This is the case for balance maintenance. The results are shown in Figure 4.6. Note that the noise sequences are identical for all four trajectories in each of the figures.

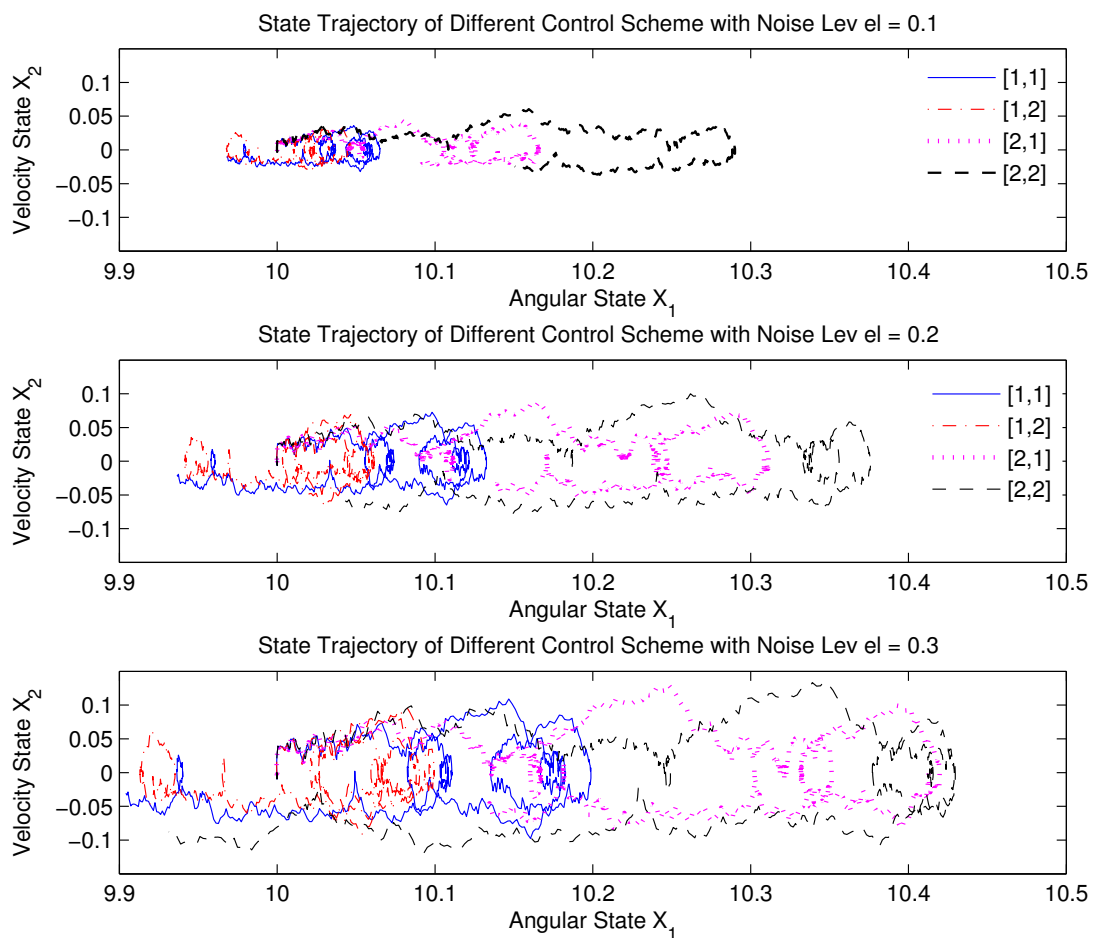


Figure 4.6: State trajectories of four different control schemes to maintain the equilibrium state driven by different levels of noise

The noise in each figure is, except for a scale factor, also identical. As expected,

all of the SHOC controllers result in greater sway than the LQR optimal controller. Surprisingly, all four controllers produce trajectories that seem to cluster near some nominal state, drift from that state, and then cluster elsewhere. The $[2, n]$ controllers have the most sway, The $[1, 2]$ controller seems to have the least.

Stabilogram Diffusion Function (SDF)

As we mentioned in section 2, to better demonstrate the difference between two state trajectories, Collins and DeLuca proposed a new analysis technique called the *Stabilogram Diffusion Function* (SDF) [14]. This analysis is very sensitive to sway amplitude and velocity. It showed that quiet stance behavior is characterized by "persistence" over short time intervals and "anti-persistence" over long time intervals.

The SDF describes the relationship between the time interval of motion and the average of corresponding changes in position [14]. It is sufficient and sensitive to detect differences in postural sway. The SDF is defined to be:

$$\langle \Delta l_{cop}^2(t) \rangle = \langle [l_{cop}(t + \Delta t) - l_{cop}(t)]^2 \rangle$$

where $\langle \cdot \rangle$ denotes the ensemble mean of the time series, as Δt ranges from 0 to 10 seconds in the simulation. The computation of l_{cop} , the displacement of the COP is based on the Horizontal projection of the COM x_{com} , and its acceleration \ddot{x}_{com}

$$I_0 \ddot{x}_{com} = mgL(x_{com} - l_{cop})$$

At $\Delta t = 0$, the SDF $\langle \Delta l_{cop}^2 \rangle$ value is zero. As Δt increases, $\langle \Delta l_{cop}^2 \rangle$ will also increase, because $l_{cop}(t)$ and the time-shifted version, $l_{cop}(t + \Delta t)$, becomes less similar to each

other. The SDF measures the similarity of the average center of pressure (COP) between different time intervals. The SDFs for different control schemes are plotted in Figs 4.7.

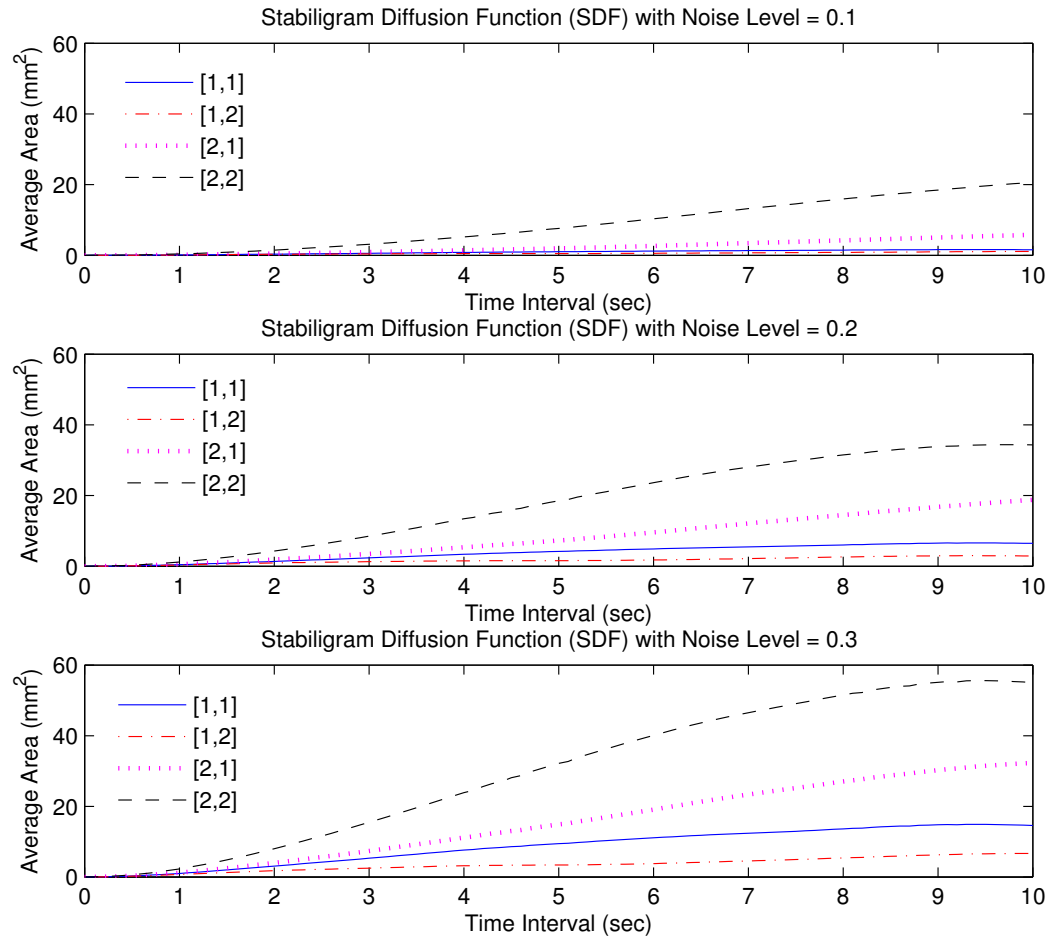


Figure 4.7: SDF function of four different control schemes to maintain the equilibrium state driven by different levels of noise

The conditions for the SDFs plotted in Figure 4.7 are the standard ones. Lastly, we computed the energy expended by each of the controllers in maintaining the posture when starting from equilibrium and perturbed by white Gaussian noise. The results are shown in Table 4.5.

Table 4.5: Torque Energy E_{ab} at $[0s, 20s]$ of Four Control Strategies under Different Noise Level

Noise level	[1, 1]	[1, 2]	[2, 1]	[2, 2]
$\epsilon = 0.1$	0.0261	0.0098	0.014	0.0076
$\epsilon = 0.2$	0.064	0.0387	0.0391	0.0305
$\epsilon = 0.3$	0.1128	0.84	0.077	0.0687

They demonstrate that the [1, 1] controller expends the most energy and the [2, 2] the least. Note that stability is not an issue. None of the controllers allows enough sway to jeopardize stability in any way.

4.8 Summary

The optimal control problem consisting of a simple dimensionless inverted pendulum model of the human and a performance criterion that is quartic in at least some states and quadratic in the control has been formulated, solved by the *Newton-KKT* method, and shown to exhibit, in many respects, similar behavior to humans standing quietly. Although the simple inverted pendulum model is standard in the literature on human postural regulation, one value of the work reported here may well be the ease with which it can be extended.

Chapter 5

Model with Delay and Noise

5.1 Neurophysiology of Neural Delay

There is a substantial time delay caused by the finite speed of signal propagation and transmission in the nervous system[66]. Neural delay is defined as the time interval between the change in the stimulation and the change in neural activity at the target site [66]. Major sources of delay are the sensory process and the transmission of internal motor commands to muscles and musculoskeletal systems.

Neural delays vary substantially across sensory modalities. In simple reaction time tasks, for example pressing a button in response to a stimulus such as a flash of light, a sound burst, or a tactile stimulus[89]. The stimulus response interval for the light stimulus is 200 - 250 ms, whereas for sound or touch it is about 150 msec. The minimum latency for a voluntary motor response appears to be around 100–120 ms[89]. The fact that reaction time to a light flash is longer than that to a sound burst is

because humans have a quicker auditory sensory process than visual [89].

From the transmission point of view, a response requiring a longer neural pathway will be slower. The reflex behaviors such as the knee jerk can be produced in about 40 ms via a shorter pathway involving only the spinal cord. For the voluntary motor response behaviors such as those in button pressing experiments, which involve additional cortical processing, the decisions are slower and the delay is therefore longer.

The sensorimotor delay – the time loss from muscle activation to active torque generation due to the neuromusculoskeletal dynamics – has been recently shown to play a significant role in the balance control system of quiet stance. The larger the delay, the more difficult it is to find appropriate control gains to stabilize the system. It is still unclear how the CNS evokes a timely active torque despite a long sensory-motor time delay in the feedback control loop.

In engineering, if delays are long and external conditions change rapidly, specific feedback corrections may not be appropriate by the time they are implemented[31]. In this chapter, we introduced a model which includes the sensory process and neural transmission delay in the MPC-based nonlinear optimal control system.

5.2 Model with Delay

In the previous chapter, we have derived a dimensionless differential equation linearized around the equilibrium that has the simplified form Eqn (4.5). In this dynamic model, the delay effects in the nervous system are not taken into account. There is significant

delay in the feedback due to neural transmission, muscle activation, and possibly neural processing. There are actually two delays in our postural control system: to model this delay in the CNS receiving the sensory data. we introduce a vector of delayed observations with a delay of $\bar{\tau}_d$,

$$\underline{y}(t) = \underline{x}(t - \bar{\tau}_d)$$

At this step, the observer is noise free and therefore has the full state available. For the delay in the application of the control, we introduce the new delayed controller:

$$u(t - \bar{\tau}_d)$$

Note that we assume the neural transmission delay is the same for both input and output [71]. The dynamics including sensory and transmission delay is modeled as,

$$\begin{aligned} \dot{\underline{x}}(t) &= A\underline{x}(t) + B\underline{u}(t - \bar{\tau}_d) \\ \underline{y}(t) &= \underline{x}(t - \bar{\tau}_d) \end{aligned}$$

The model includes the sensory process and neural transmission delay in the MPC-based nonlinear optimal control system is shown in Figure 5.1.

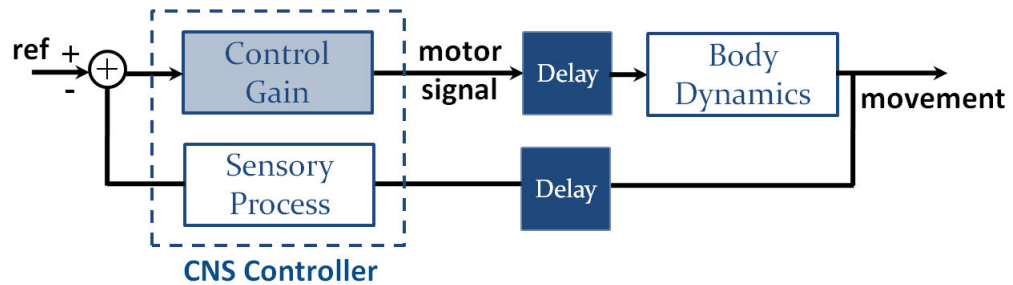


Figure 5.1: The balance control system with delay

If we choose the discrete time step $t = k\delta$, where δ is the sampling interval and then we define n_d is the number of sample in the delay, and $\bar{\tau}_d = \delta n_d$. Now we want to incorporate delay in the discretized model, we introduce the new vector variable \underline{z} as

$$\begin{aligned}
z_1(k) &= x_1(k - n_d) & z_{2n_d+1}(k) &= x_1(k) \\
z_2(k) &= x_2(k - n_d) & z_{2n_d+2}(k) &= x_2(k) \\
&\vdots & z_{2n_d+3}(k) &= u(k - n_d) \\
z_{2n_d-1}(k) &= x_1(k - 1) & &\vdots \\
z_{2n_d}(k) &= x_2(k - 1) & z_{3n_d+2}(k) &= u(k - 1)
\end{aligned}$$

The delay effects due to neural transmission and possibly neural processing is modeled by adding the delayed states to the linear model as,

$$\begin{bmatrix} z_1(k+1) \\ z_2(k+1) \\ \vdots \\ z_{3n_d+2}(k+1) \end{bmatrix} = A_z \begin{bmatrix} z_1(k) \\ z_2(k) \\ \vdots \\ z_{3n_d+2}(k) \end{bmatrix} + \begin{bmatrix} 0 \\ 0 \\ \vdots \\ 0 \\ u(k) \end{bmatrix}, \underline{y}(k) = \begin{bmatrix} z_1(k) \\ z_2(k) \\ z_{2n_d+3}(k) \\ \vdots \\ z_{3n_d+2}(k) \end{bmatrix}$$

The expression for $\underline{y}(k)$ reflects the facts that the state is only available to the controller after a delay $\bar{\tau}_d = \delta n_d$. The controller effect is also delayed due to muscle activation.

Then we convert this into the state space format as follows:

$$\underline{z}(k+1) = A_z \underline{z}(k) + B_z u(k)$$

$$\underline{y}(k) = C_z \underline{z}(k)$$

where

$$A_z = \begin{bmatrix} 0 & I_{2 \times 2} & 0 & \cdots & \cdots & 0 \\ & \ddots & \ddots & \ddots & & \vdots \\ \vdots & & 0 & I_{2 \times 2} & 0 & \vdots \\ & & & \bar{A}_{2 \times 2} & \bar{B}_{2 \times 2} & \vdots \\ 0 & \cdots & \cdots & \cdots & \cdots & 0 \end{bmatrix}, B_z = \begin{bmatrix} 0 \\ 0 \\ \vdots \\ 1 \end{bmatrix},$$

$$C_z = \begin{bmatrix} I_{2 \times 2} & 0_{2 \times 2n_d} & 0_{2 \times n_d} \\ 0_{n_d \times 2} & 0_{n_d \times 2n_d} & I_{n_d \times n_d} \end{bmatrix}$$

We can convert the continuous time system into a discrete time system with,

$$\bar{A} = e^{A\bar{\tau}} = \sum_{n=0}^{\infty} \frac{A^n (\bar{\tau})^n}{n!}, \bar{B} = A^{-1}(\bar{A} - I)^{-1}B$$

The dimensions of the coefficient matrices are

$$A_z \in \mathbb{R}^{(3n_d+2) \times (3n_d+2)}$$

$$B_z \in \mathbb{R}^{(3n_d+2) \times 1}$$

$$C_z \in \mathbb{R}^{(3n_d+2) \times (n_d+2)}$$

Then, the optimal control problem for single inverted pendulum with delay is

$$\begin{aligned} \mathbf{min} \quad J_{SDHOC} &= \sum_0^N d_1 z_1^{2m}(k) + d_2 z_2^{2n}(k) + \cdots + d_{2n_d+2} z_{2n_d+2}^{2n}(k) \\ &+ \sum_0^N d_{2n_d+3} z_{2n_d+3}^2(k) + \cdots + d_{3n_d+2} z_{3n_d+2}^2(k) + \sum_0^N u^2(k) \\ \mathbf{s.t} \quad \underline{z}(k+1) &= A_z \underline{z}(k) + B_z u(k) \end{aligned} \quad (5.1)$$

Here, *SDHOC* stands for Single inverted pendulum with Delay effects and Higher order Optimal Control.

5.2.1 Example - Single Unit Delay Model

We start by considering one step delay effects ($n_d = 1$) both on the observations and control variable, the variable z is defined as:

$$z_1(k) = x_1(k - 1)$$

$$z_2(k) = x_2(k - 1)$$

$$z_3(k) = x_1(k)$$

$$z_4(k) = x_2(k)$$

$$z_5(k) = u(k - 1)$$

and the dynamics will be:

$$\begin{bmatrix} z_1(k+1) \\ z_2(k+1) \\ z_3(k+1) \\ z_4(k+1) \\ z_5(k+1) \end{bmatrix} = \begin{bmatrix} 0 & I & 0 \\ 0 & \bar{A} & \bar{B} \\ 0 & \dots & 0 \end{bmatrix} \begin{bmatrix} z_1(k) \\ z_2(k) \\ z_3(k) \\ z_4(k) \\ z_5(k) \end{bmatrix} + \begin{bmatrix} 0 \\ 0 \\ 0 \\ 0 \\ 1 \end{bmatrix} u(k)$$

which converts into the state space format as follows:

$$\underline{z}(k+1) = A_z \underline{z}(k) + B_z u(k)$$

$$\underline{y}(k) = C_z \underline{z}(k)$$

$$A_z = \begin{bmatrix} 0 & I & 0 \\ 0 & \bar{A} & \bar{B} \\ 0 & \dots & 0 \end{bmatrix}, B_z = \begin{bmatrix} 0 \\ 0 \\ 0 \\ 0 \\ 1 \end{bmatrix}, C_z^T = \begin{bmatrix} 1 & 0 \\ 0 & 1 \\ 0 & 0 \\ 0 & 0 \\ 0 & 0 \end{bmatrix}.$$

The nonlinear optimal control problem is defined as

$$J_{SDHOC}(z, u) = \sum_0^N [d_1 z_1^{2m}(k) + d_2 z_2^{2n}(k) + d_3 z_3^{2m}(k) + d_4 z_4^{2n}(k) + d_5 z_5^2(k) + u^2(k)]$$

$$\mathbf{s.t.} \quad \underline{z}(k+1) = A_z \underline{z}(k) + B_z u(k)$$

This system includes one unit of delay for each of the state and control vectors. We use the the overall optimization variable which contains all the state and control:

$$\underline{s} = [\underline{z}(0), u(0), \underline{z}(1)^T, u(1), \underline{z}(2)^T, u(2) \dots, \underline{z}(N)^T, u(N)]^T$$

and $\underline{s} \in \mathbb{R}^{6(N+1)}$. We then implement the *Newton-KKT* iteration algorithm as before.

$\underline{s}^{(i)}$ is the overall variable at i^{th} iteration

$\underline{r}^{(i)}$ is the gradient for the overall variable at i^{th} iteration and $\underline{r}^{(i)} = \nabla J(\underline{s}^{(i)})$

$H^{(i)}$ is the Hessian matrix for overall variable at i^{th} iteration and $H^{(k)} = \nabla^2 J(\underline{s}^{(i)})$

Note that the Hessian $H^{(i)}$ size is increased substantially, but it is block diagonal

$$H^{(i)} = \text{diag} [Q_1^{(i)}, R_1^{(i)}, Q_2^{(i)}, R_2^{(i)}, \dots, Q_N^{(i)}, R_N^{(i)}]$$

where,

$$R_n^{(i)} = \nabla^2 f(u_n^{(i)}) = 2 \quad \forall i$$

$$Q_n^{(i)} = \nabla^2 f(\underline{z}_n^{(i)}) = \begin{bmatrix} \frac{\partial^2 f(\underline{z}_n^{(i)})}{\partial z_1 \partial z_1} & 0 & \dots & \dots & 0 \\ 0 & \frac{\partial^2 f(\underline{z}_n^{(i)})}{\partial z_2 \partial z_2} & \ddots & & \vdots \\ \vdots & \ddots & \frac{\partial^2 f(\underline{z}_n^{(i)})}{\partial z_3 \partial z_3} & \ddots & \vdots \\ \vdots & & \ddots & \frac{\partial^2 f(\underline{z}_n^{(i)})}{\partial z_4 \partial z_4} & 0 \\ 0 & \dots & \dots & 0 & \frac{\partial^2 f(\underline{z}_n^{(i)})}{\partial z_5 \partial z_5} \end{bmatrix} \quad \forall i$$

Each term on the diagonal of the Hessian $H^{(i)} = \nabla^2 J(\underline{s}^{(i)})$ is positive, except at

$$z_1(k) = 0, z_2(k) = 0, z_3(k) = 0, z_4(k) = 0, z_5(k) = 0 \text{ for some } k = 0, 1, 2, \dots, N.$$

The Newton step $\Delta \underline{s}_{nt}^{(i)}$ for is then characterized by the following *Newton-KKT* system, we use the same iterative interior point algorithm to solve it [12]:

$$\begin{bmatrix} H^{(i)} & A_s^T \\ A_s & 0 \end{bmatrix} \begin{bmatrix} \Delta \underline{s}_{nt}^{(i)} \\ \underline{w} \end{bmatrix} = \begin{bmatrix} -\underline{r}^{(i)} \\ 0 \end{bmatrix} \quad (5.2)$$

with new constraint matrix as

$$A_s = \begin{bmatrix} I & 0 & \dots & \dots & \dots & O \\ -A_z & -B_z & I & 0 & \dots & \vdots \\ \vdots & \vdots & \vdots & \vdots & \vdots & \vdots \\ O & \dots & -A_z & -B_z & I & 0 \end{bmatrix},$$

then we use the Schur Complement to solve the KKT system

$$H^{(i)} \Delta \underline{s}_{nt}^{(i)} + A_s^T w = -\underline{r}^{(i)}$$

Use the same algorithm 4.1 in chapter 4. For the LQR problem, the Hessian H is independent of z_0 . As m increases to any even order higher than quadratic, the performance measure for small errors will be very close to zero. This will result in some

difficult problems for the Newton-KKT method: the *Hessian* $H^{(i)}$ at the i^{th} iteration in the Newton-KKT Eqn (5.2) is singular or close to singular. For the LQR problem, the Hessian H is independent of z_0 . But for any even order higher than quadratic, the Hessian for fairly small errors will be very close to singular.

To solve the singular Hessian problem, quasi-Newton method is one approach. The concept is: replace H with a carefully chosen matrix $W = H + E$ where E is a positive semi-definite correction [12]. This method will heavily depend on the choice of E and consequently affect the convergence rate of the Newton iteration.

We introduced a computational algorithm to deal the singular or close to singular Hessian problem. Due the special system structure and the biological feature of sensory dead zone effect, the optimization iteration could be modified with respect to different Hessian. The rational for the new algorithm is: when the dynamics are equal to zero (or close to zero), the controller would treat them all as “zero” or stable states, therefore no corrective torques will be applied for the small deviation. Inspired by this feature, the new optimization scheme is updated as:

Algorithm 5.1 Modified Convex Optimization

Input: $\underline{s}^{(0)} = [\underline{z}(0), \underline{u}(0), \overline{A}\underline{z}(0), \underline{u}(1), \dots, \overline{A}^k \underline{z}(0), \underline{u}(1), \dots, \overline{A}^N \underline{z}(0), \underline{u}(N)]^T$ **Output:** \underline{s}^* such that the given cost function is minimized

```
1  Start
2    For  $i = 1$  to  $N^i$ 
3      IF  $H^{(i)} > 0 \forall k$ 
4        Compute  $R = -A_s[H^{(i)}]^{-1}A_s^T$ 
5        Solve for  $\underline{w}$  from  $R\underline{w} = A_s[H^{(i)}]^{-1}\underline{r}^{(i)}$ 
6        Compute  $\Delta\underline{s}_{nt}^{(i)} = [H^{(i)}]^{-1}(-A_s\underline{w} - \underline{r}^{(i)})$ 
7        IF  $\sqrt{[\Delta\underline{s}_{nt}^{(i)}]^T H^{(i)} \Delta\underline{s}_{nt}^{(i)}} > \epsilon$ 
8          DO  $\underline{s}^{(i+1)} \leftarrow \text{LinearSearchAlgorithm}(\underline{s}^{(i)}, \Delta\underline{s}_{nt}^{(i)})$ 
9          ELSE DO  $\underline{s}^{(i+1)} = \underline{s}^{(i)}$  ENDIF
10       IF  $H^{(i)} > 0$  for  $k = 1, 2, \dots, n$  AND  $H^{(i)} = 0$  for  $k = n + 1, \dots, N$ 
11         Find  $\underline{k}$  where  $H^{(i)} = 0$ 
12         Let  $\underline{s}^{(i)}(\underline{k}) = 0$  and  $\Delta\underline{s}_{nt}^{(i)}(\underline{k}) = 0$ 
13         IF  $\sqrt{[\Delta\underline{s}_{nt}^{(i)}]^T H^{(i)} \Delta\underline{s}_{nt}^{(i)}} > \epsilon$ 
14           Update  $A_s$  and  $H^{(i+1)} \leftarrow H^{(i)}$  for  $k = 1, 2, \dots, n$ 
15           DO  $\underline{s}^{(i+1)} \leftarrow \text{LinearSearchAlgorithm}(\underline{s}^{(i)}, \Delta\underline{s}_{nt}^{(i)})$ 
16           ELSE DO  $\underline{s}^{(i+1)} = \underline{s}^{(i)}$  ENDIF
17       IF  $H^{(i)} = 0 \forall k$ 
18         Update  $\underline{s}^{(i+1)} = \underline{s}^{(i)}$  ENDIF
19     End For
20   Output  $\underline{s}^* = \underline{s}^{(i+1)}$ 
21 End
```

Simulation Results

The simulations are based on the simplified sway model defined before using Peterka's body parameters [70] as shown again in Table 5.1. Four different optimal control problems were solved and their operation simulated for different scenarios.

Table 5.1: Body Characteristics and Dimensionless Model Parameters

Symbol	Quantity	Value
M	Body mass	76 kg
I_0	Body moment of inertia	66 kg.m ²
L	CM height over ankle joint axis	0.87 m
g	Acceleration of gravity	9.8 m/s ²
δ	Sampling interval	1/50 secs
α	Mgh/I_0	9.26
β	$\sqrt{h/g}$	0.092

We first solved the postural problems with performance measure as

$$J_{SDHOC}(z, u) = \sum_0^N [pz_1^{2m}(k) + qz_2^{2n}(k) + pz_3^{2m}(k) + qz_4^{2n}(k) + z_5^2(k) + u^2(k)]$$

We simulated the SDHOC by MPC using the iterative optimal feedback control algorithm with $[m, n]=[1, 1]$ and $[2, 2]$. The parameters for these simulations are listed in Table 5.2. The simulation results are also compared with LQR controller as depicted in Figure. 5.2.

Table 5.2: Simulation Parameters

Symbol	Quantity	Values
$z_1(0)$	Initial angular offset	$[0.1^\circ, 0.5^\circ, 2^\circ, 10^\circ]$
$z_2(0)$	Initial angular velocity	$[0.1^\circ/s, 0.5^\circ/s, 2^\circ/s, 10^\circ/s]$
N	Ending point	40
i	Number of iterations	20
p	Angular cost coefficient	0.1
q	Velocity cost coefficient	0.1

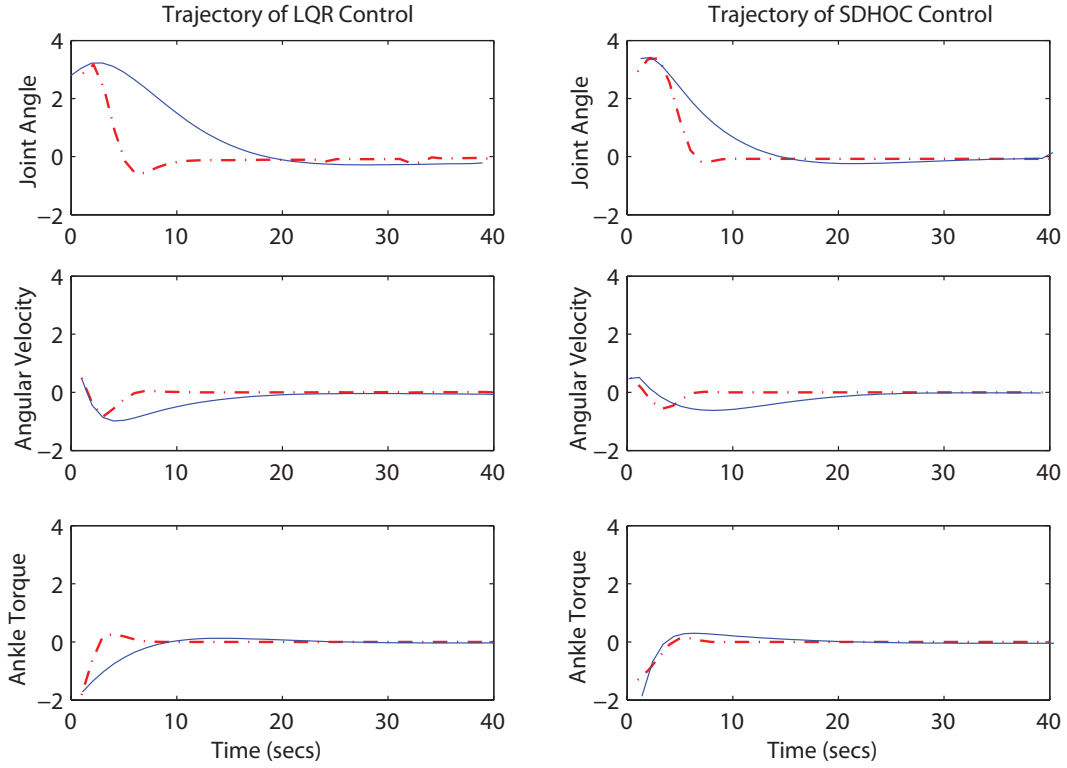


Figure 5.2: Trajectories of angular state x_1 , angular velocity x_2 and the control input u for SDHOC and LQR

As we can see from Figure 5.2, for both LQR and SDHOC control, the delay effect created more body sway than the model without delay. We then computed the energy expended by each of the controllers in maintaining the posture. The results are shown in Table 5.3. They demonstrate that for the overall energy used during the balance restoration, the LQR control strategy consumes the more energy, while the SDHOC control schemes require less torque energy. .

Table 5.3: Torque Energy of Two Control Strategies starting from different initial points

$[z_1(0), z_2(0)]$	$[0.1, 0.1]$	$[0.5, 0.5]$	$[2, 2]$	$[10, 10]$
<i>LQR</i>	0.3161	0.7243	1.4204	3.0829
<i>SDHOC</i>	0.2145	0.4795	0.9591	1.9658

In the long run, as long as there are only small disturbances introduced to the system,

the SDHOC control will be the more energy-efficient control scheme to maintain the inverted pendulum in a stable equilibrium state.

This approach provides an effective way to study the delays in the optimal control system, although with the somewhat unrealistic restriction that the full state is available to the controller. Because the dynamics are linear, the excursions from equilibrium are small and the performance criteria are symmetric about zero, certainty equivalence is likely to hold, at least approximately. Please note that here we assume perfect observation for the optimal state estimator.

5.3 Optimal State Estimator

Inclusion of the delay in the observations changes the optimal control problem substantially. Now we have to include another important effect into the system — noise as shown in Figure 5.3.

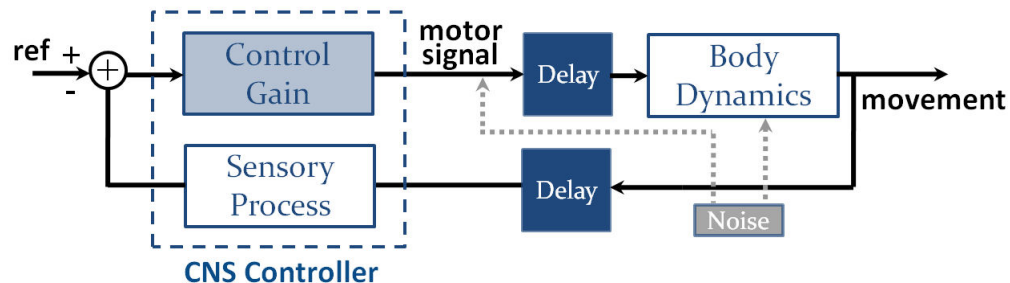


Figure 5.3: The system diagram of Single inverted pendulum model with state Estimator and Higher order Optimal Control (SEHOC)

The correct formulation would include noise on the input and output and would replace the present deterministic performance criterion with an expected value of the

performance. We now extend the single unit delay model by adding White Gaussian Noise (*WGN*) as following:

$$\underline{z}(k+1) = A_z \underline{z}(k) + B_z u(k) + \underline{\nu}(k)$$

$$\underline{y}(k) = C_z \underline{z}(k) + \underline{w}(k)$$

The process noise $\underline{\nu}(k)$ and measurement noise $\underline{w}(k)$ are independent White Gaussian Noise (*WGN*) with mean zero and covariance Ξ and Θ respectively, i.e., $\underline{\nu} \sim N(0, \Xi)$ and $\underline{w} \sim N(0, \Theta)$. The new optimal control problem with state estimator is then defined as

$$\begin{aligned} \mathbf{min} \quad & J_{SEHOC}(\underline{z}, u) = E \left\{ \sum_0^N d_1 z_1^{2m}(k) + d_2 z_2^{2n}(k) + \dots + d_{2n_d+2} z_{2n_d+2}^{2n}(k) \right\} \\ & + E \left\{ \sum_0^N d z_{2n_d+3}^2(k) + \dots + d_{3n_d+2} z_{3n_d+2}^2(k) \right\} + E \left\{ \sum_0^N u^2(k) \right\} \\ \mathbf{s.t} \quad & \underline{z}(k+1) = A_z \underline{z}(k) + B_z u(k) + \underline{\nu}(k) \\ & \underline{y}(k) = C_z \underline{z}(k) + \underline{w}(k) \end{aligned}$$

5.3.1 *LQG Case*

The discrete-time control problem is precisely a linear quadratic Gaussian (LQG) optimal control problem when $m = n = 1$. This solution is well known in the case of a quadratic performance criterion. It is the deterministic full state feedback controller computed by solving the linear quadratic regulator (LQR) problem concatenated with a Kalman filter to estimate the state from the observations.

The Linear quadratic estimator (LQE), i.e, a Kalman filter is used to estimate the state of a linear system, with complete/incomplete state information, disturbed by additive Gaussian noises $\underline{v}(k)$ and $\underline{w}(k)$:

$$\underline{z}(k+1) = A_z \underline{z}(k) + B_z u(k) + \underline{v}(k)$$

$$\underline{y}(k) = C_z \underline{z}(k) + \underline{w}(k)$$

The LQE is the optimal least square and minimum variance unbiased estimator under the given assumptions of the zero mean and covariance:

$$E[\underline{v}(k)] = 0, E[\underline{w}(k)] = 0 \forall k$$

$$Cov[\underline{v}(k)] = \underline{V}(k), Cov[\underline{w}(k)] = \underline{W}(k)$$

The LQR controller under these assumptions and with the performance measure,

$$J_{LQG} = E \left\{ \sum_0^N [\underline{z}^T Q \underline{z} + u^T R u] \right\}$$

is the certainly equivalence controller. That is, the LQE is used to produce a state estimate $\hat{\underline{z}}(k)$ which replaces $\underline{z}(k)$ in the controller. The LQR and LQE can be designed, computed and implemented independently. The optimal estimator is specified by the following equations:

$$\hat{\underline{z}}(t+1) = A_z \hat{\underline{z}}(k) + B_z u(k) + K(\underline{y}(k) - C \hat{\underline{z}}(k))$$

$$u(k) = -L \hat{\underline{z}}(k)$$

$$\hat{\underline{z}}(0) = E[\underline{z}_0]$$

At each time instance, this filter generates $\hat{z}(k)$ to estimate the true state $z(k)$ using the past measurements $y(k)$ and inputs $u(k)$. The matrix K , the Kalman gain, is computed from A_z , C_z and the covariance matrices $\underline{V}(k)$ and $\underline{W}(k)$.

$$K = A_z P(k) C_z^T \left[C_z P(k) C_z^T + \underline{W}(k) \right]^{-1}$$

The Kalman gain is determined by the following matrix Riccati difference equation:

$$P(k+1) = A_z \left[P(k) - P(k) C_z^T \left[C_z P(k) C_z^T + \underline{W}(k) \right]^{-1} C_z P(k) \right] A_z^T$$

The feedback gain matrix equals:

$$L = \left[B_z^T S(k+1) B_z + R \right]^{-1} B_z^T S(k+1) A_z$$

where $S(k+1)$ is determined by the following matrix Riccati difference equation:

$$S(k+1) = A_z^T \left[S(k) - S(k) B_z \left[B_z^T S(k) B_z + R \right]^{-1} B_z^T S(k) \right] A_z + Q$$

When $m = 2$ or $n = 2$, the problem is much harder because certainty equivalence does not apply. However, for small noise and small excursions from equilibrium, it is reasonable to believe that the optimal controller based on an assumption of certainty equivalence is a good approximation to the truly optimal controller.

5.3.2 SEHOC Case

There are also neurophysiological reasons to believe in certainty equivalence. It is easy for motor units to exert the nonlinear control. There is evidence for state prediction in the spinal cord (Central Pattern Generation). Thus when $m = 2$, we divide the

optimal control problem into a certainty equivalent controller (i.e., the optimal feedback controller assuming no noise and complete state observations) and an optimal state estimator. We use the Kalman filter to estimate the state because, under small noise and small excursions, it should be very close to the optimal filter.

In the case of a higher order performance measure, we assume that we can approximate the optimal feedback controller by the solution to the deterministic optimal control problem specified here concatenated with a Kalman filter to estimate the state from the observations. The Kalman filter/predictor for this system is then

$$\hat{z}(k|k) = \hat{z}(k|k-1) + K[y(k) - C_z \hat{z}(k|k-1)]$$

$$\hat{z}(k+1|k) = A_z \hat{z}(k|k) + Bu(k)$$

where K is the gain matrix of the Kalman filter calculated using MATLAB's *dlqe* command. With the estimate of the current state as the initial state, we then apply model predictive control (MPC), or receding horizon control (RHC), to find the closed-loop optimal solution. The algorithm is as follows

♣START Choose True Initial State $\underline{z}(0)$
 Choose Estimated Initial State $\hat{\underline{z}}(0) \sim N(0, \Xi)$
 FOR $k = 0$ TO N DO
 • Compute Optimal Controller
 $u(k)$ = certainty equivalent MPC control with $\hat{\underline{z}}(k)$ as the initial state
 • Update State Estimate, True State, and Observation
 $\underline{z}(k+1) = A_z \underline{z}(k) + B_z u(k) + \underline{\nu}(k)$
 $\underline{y}(k) = C_z \underline{z}(k) + \underline{w}(k)$
 • State Estimation by Kalman Filter
 $\hat{\underline{z}}(k+1) = A_z \hat{\underline{z}}(k) + B_z u(k) + K(\underline{y}(k) - C_z \hat{\underline{z}}(k))$
 $u(k) = -L \hat{\underline{z}}(k)$
 END

The control input is then obtained by solving the convex programming problem in a finite horizon open-loop optimal control problem, using the estimated state of the plant as the initial state as shown in Figure 5.4.

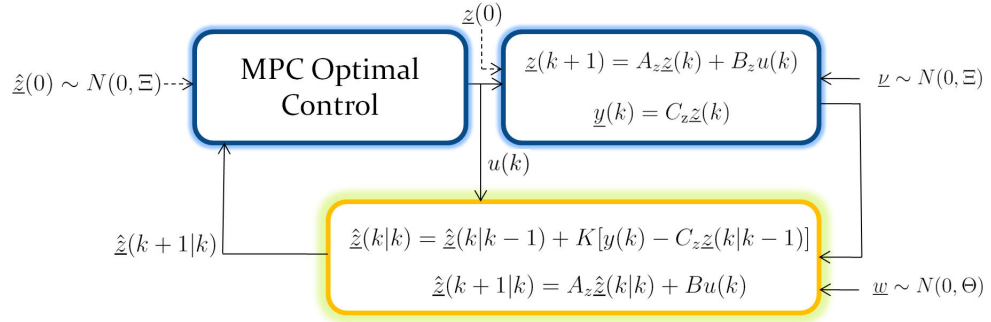


Figure 5.4: The SEHOC control scheme

The Optimization yields an optimal control sequence and the first control in this sequence is applied to the plant. For the closed-loop, start at some initial condition and compute the complete open-loop optimal solution but save only the first control value. Apply this control as the input to the system with the added noise to update the next state. This new state is estimated by the Kalman filter.

Simulation Results

The simulations use Peterka’s body parameters [70] as shown in Table 5.1. We solved the postural optimal control problems for both transient and steady state response. The parameters for the LQG and SEHOC case are shown in Table 5.4. To better compare the results with Peterka’s, we normalized the PID coefficients to work with our dimensionless model as $[k_p, k_i, k_d] = [1.95, 0.25, 4.5] * \delta$.

Table 5.4: Parameters for Controller Candidates

Symbol	LQG	SEHOC
m	1	2
$[p, q]$	[10, 10]	[10, 10]
i	1	20

Transient Response

The transient response of a balance restoration scenario was solved for the initial conditions listed in Table 5.5.

Table 5.5: Balance Restoration Simulation Parameters

Symbol	Quantity	Values
$z_1(0)$	Angular displacement	$+3^\circ$
$z_2(0)$	Angular velocity	$+0.5^\circ/s$
Ξ, Θ	Noise standard deviation	0.1
T	Simulation Duration	20 <i>sec</i>

The state trajectory results under small disturbance are shown in Figure 5.5. Note that the noise sequences are identical for all trajectories in each of the figures. In all figures the dotted line is the PID result, the dashed line is the LQG result and the solid line is the SEHOC result.

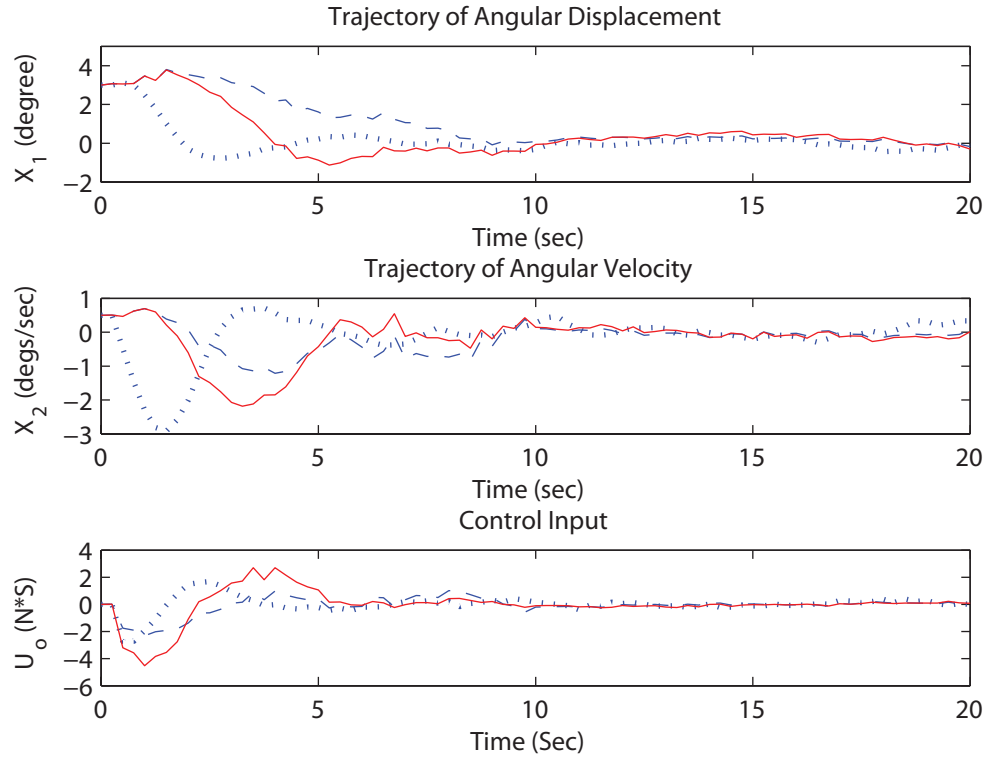


Figure 5.5: Trajectories of angular state x_1 , angular velocity x_2 and the control input u during balance restoration for PID (\cdots), LQG ($--$) and SEHOC($—$)

As we can see from Figure 5.5, both the error and the control torque for all the control strategies decrease rapidly when the system is far from the equilibrium position. The fastest transient response is that of the PID with SEHOC second. However, the control amplitude by SEHOC control is the largest.

Steady-State Response

The parameters for the steady state (balance maintenance) simulation are listed in Table 5.6. The simulation results are depicted in Figure. 5.6. and Figure 5.7.

Table 5.6: Balance Maintenance Simulation Parameters

Symbol	Quantity	Values
$z_1(0)$	Angular displacement	$+0.01^\circ$
$z_2(0)$	Angular velocity	$+0.01^\circ/s$
Ξ, Θ	Noise standard deviation	0.1
T	Simulation Duration	20 sec

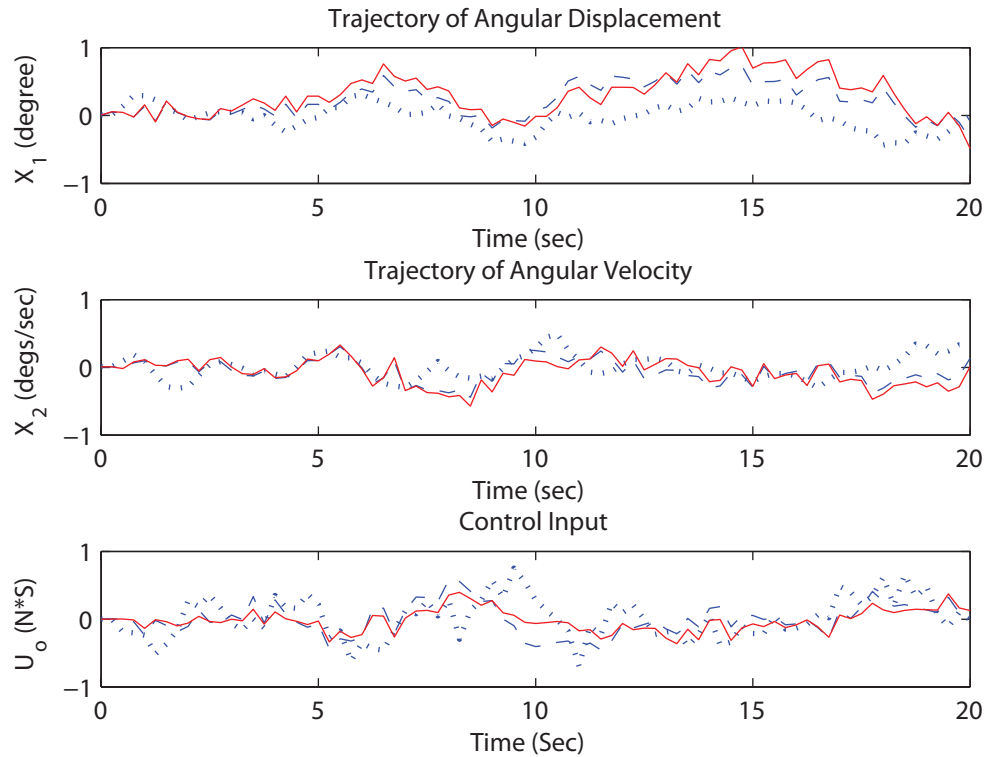


Figure 5.6: Trajectories of angular state x_1 , angular velocity x_2 and the control input u during balance maintenance for PID (\cdots), LQG ($--$) and SEHOC($—$)

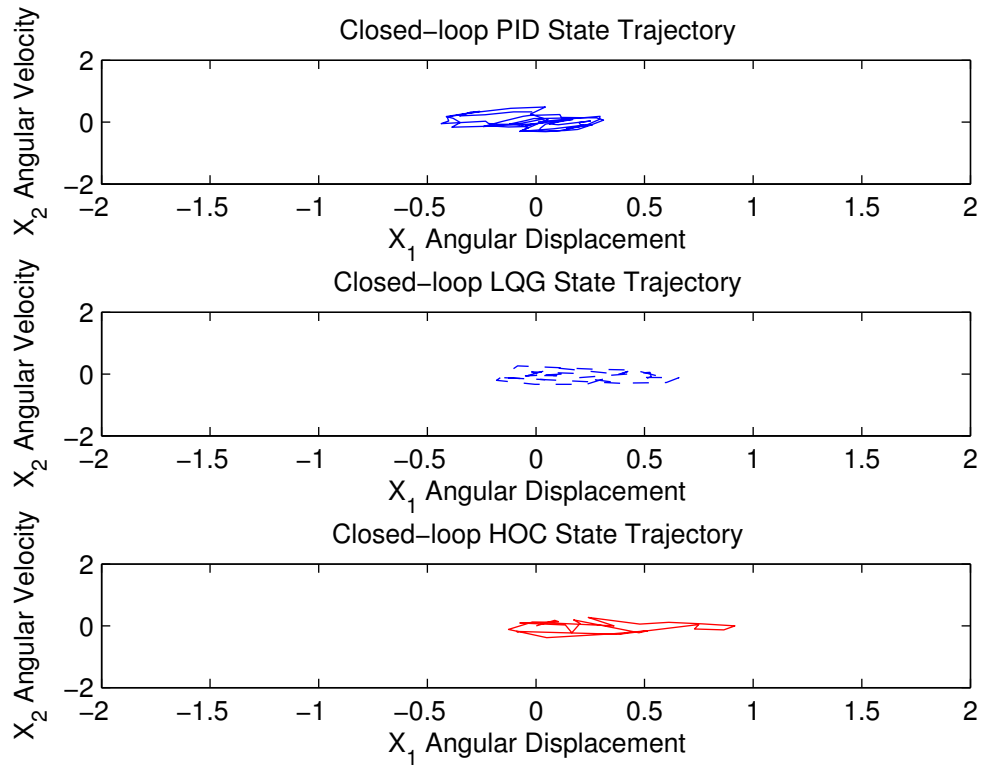


Figure 5.7: State trajectories of angular state x_1 , angular velocity x_2 during balance maintenance for PID (\cdots), LQG ($--$) and SEHOC($—$)

As we can see from Figure 5.6 and Figure 5.7, the SEHOC controllers have the larger sway, The PID controller seems to have the least. It is interesting that the PID controller seems to produce sway centered at -0.25° , which the LQG centers its sway at $+0.25^\circ$ and the SEHOC at a lightly larger position angle.

We then computed the energy expended by each of the controllers in maintaining the posture when starting from equilibrium and perturbed by white Gaussian noise. The results of the control torque energy are shown in Table 5.7.

Table 5.7: Torque Energy of Three Control Strategies During Balance Maintenance

<i>Controller</i>	<i>PID</i>	<i>LQG</i>	<i>SEHOC</i>
<i>E</i>	1.4157	0.5787	0.2159

For the overall energy used during balance maintenance, the PID control strategy consumes the most energy, while the SEHOC control scheme requires the least control energy. In the long run, as long as there are only small disturbances introduced to the system, a SEHOC control will be the more energy-efficient control scheme to maintain a stable equilibrium state. Note that stability is not an issue. None of the controllers allows enough sway to jeopardize stability in any way.

We then applied the SDF to measure the similarity of the average center of pressure (COP) between different time intervals. The SDFs for the designed SEHOC control scheme compared with LQG and PID control results from Peterka’s paper are plotted in Figure 5.8.

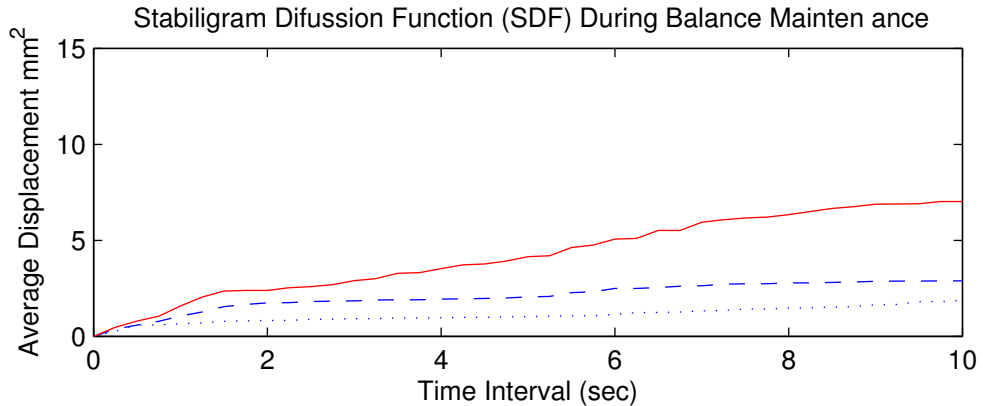


Figure 5.8: Stabiligram diffusion function (SDF) of angular state x_1 during steady state response for PID (\cdots), LQG ($---$) and SEHOC ($—$)

The conditions for the SDFs are the standard ones. That is, the subjects start at

equilibrium. The SDF's measured by Collins [14] and studied by Peterka [70] are similar to those we obtained for the LQG and SEHOC controllers. They exhibit two slopes with the steeper slope at small time intervals. As we can see from Figure. 5.8, at the same noise levels the SEHOC controller generates more sway than the LQR controller. This difference in amplitude can probably be corrected by adjusting the weights in the performance criteria.

5.4 Summary

These results demonstrate two especially significant features. First, postural sway appears to result from the delay inherent in the human postural regulation system. It seems evident that appropriately weighting state errors can make both the LQG and SEHOC controllers match the PID postural sway. Thus, determining what controller actually is used will require other data besides the observed sway. Second, with the same weights, the SEHOC controller uses much less control energy than the LQG controller which were much less than the PID controller. It would be interesting to further adjust the weights so as to make the amount of sway identical and then compare the amount of control energy used by the two optimal controllers and Peterka's PID control. This might provide an experimental test of the three hypotheses by measuring the energy used in maintaining posture under small random disturbance. It is likely that humans do try to minimize the muscular energy or fatigue in regulating posture.

Chapter 6

Coordinated Control

6.1 Double Inverted Pendulum Model

Although the human body is often approximated and simplified as an inverted pendulum that rotates about the ankle joint, the posture control problem is clearly much more complicated. Moreover, experimental data indicates that the response to perturbations during quiet standing varies with the size of the disturbance [62][71][85]. As explained earlier, there is a range of perturbations for which the response involves primarily motion at the ankle and hip.

In this chapter, we present a computational model of a quietly standing human which uses three rigid and connected segments to represent the foot, leg (locked knee), and torso. This is the simplest situation in which the coordination of the controls at multiple joints can be studied. This two joint, three segment model is controlled by torques on the ankle and hip joints as depicted in Figure 6.1.

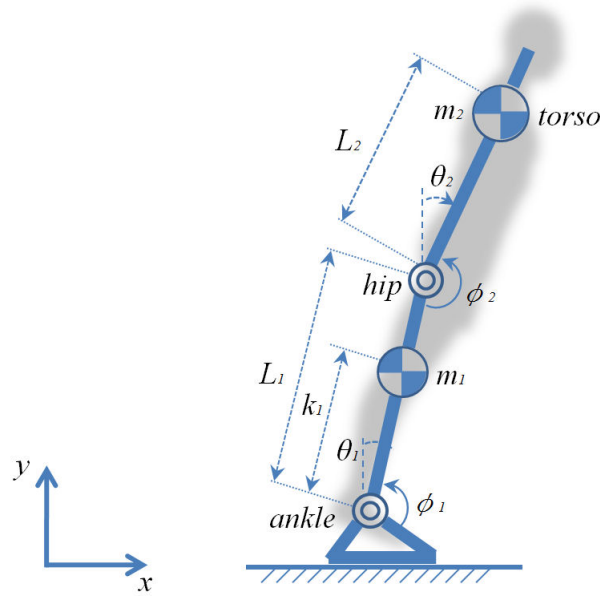


Figure 6.1: The three link sagittal biped is composed of three rigid links. The term k for $i = 1, 2, 3$ is the distance from the bottom of link i to the center of mass of link i . The term L_i is the length of link i .

We first derive the equations of motion using the Euler-Lagrange method defined as:

$$\begin{aligned} \frac{d}{dt} \left(\frac{\partial \mathcal{L}}{\partial \dot{\phi}_1} \right) - \frac{\partial \mathcal{L}}{\partial \phi_1} &= u_{ankle} \\ \frac{d}{dt} \left(\frac{\partial \mathcal{L}}{\partial \dot{\phi}_2} \right) - \frac{\partial \mathcal{L}}{\partial \phi_2} &= u_{hip} \end{aligned}$$

where

$$\mathcal{L} = \mathcal{K} - \mathcal{P} \tag{6.1}$$

and \mathcal{K} is the total kinetic energy of the system; \mathcal{P} is the total potential energy. The generalized coordinates for this system are $[\phi_1, \phi_2]$. The torques at ankle and hip joint are u_{ankle} and u_{hip} .

The total kinetic energy is the sum of the rotational and translational kinetic energies of the components of the system, and all the potential energy is due to gravity. These quantities can be written in terms of the angles ϕ_i and the position of the center

of mass(x_i, y_i) of each link i as

$$\mathcal{K} = \frac{1}{2} \sum_{i=1}^2 [I_i \dot{\phi}_i^2 + m_i(x_i^2 + y_i^2)]$$

$$\mathcal{P} = \sum_{i=1}^2 g m_i y_i$$

We write each x_i and y_i in terms of the generalized coordinates to express the kinetic energy and potential energy,

$$\begin{aligned} x_1 &= L_0 \cos(\phi_0) + k_1 \cos(\phi_0 - \phi_1) \\ y_1 &= L_0 \sin(\phi_0) - k_1 \sin(\phi_0 - \phi_1) \\ x_2 &= L_0 \cos(\phi_0) + L_1 \cos(\phi_0 - \phi_1) - L_2 \cos(\phi_0 - \phi_1 - \phi_2) \\ y_2 &= L_0 \sin(\phi_0) - L_1 \sin(\phi_0 - \phi_1) + L_2 \sin(\phi_0 - \phi_1 - \phi_2) \end{aligned}$$

Then, we derive the equations of motion with the vector of general coordinates $q = [\phi_1, \phi_2]$ which only includes the ankle and hip joints. The dynamic equation is,

$$J(q)\ddot{q} + G(q, \dot{q}) = U_q \quad (6.2)$$

Since the body dynamics during standing have been demonstrated to be well-approximated by a linear model for small perturbations [91][92][93], we linearize the double inverted pendulum model around the unstable equilibrium point:

$$\begin{pmatrix} \phi_1^* \\ \phi_2^* \\ u_{ankle}^* \\ u_{hip}^* \end{pmatrix} = \begin{pmatrix} \frac{\pi}{2} \\ \pi \\ 0 \\ 0 \end{pmatrix}$$

and also define the small angular deviations from the vertical equilibrium.

$$\begin{pmatrix} \phi_1 \\ \phi_2 \\ u_{ankle} \\ u_{hip} \end{pmatrix} = \begin{pmatrix} \phi_1^* \\ \phi_2^* \\ u_{ankle}^* \\ u_{hip}^* \end{pmatrix} + \begin{pmatrix} \Delta\phi_1 \\ \Delta\phi_2 \\ \Delta u_{ankle} \\ \Delta u_{hip} \end{pmatrix}$$

Then the linearized dynamical model in the neighborhood of vertical will be

$$\begin{bmatrix} \Delta\ddot{\phi}_1 \\ \Delta\ddot{\phi}_2 \end{bmatrix} = -Q^{-1}F \begin{bmatrix} \Delta\phi_1 \\ \Delta\phi_2 \end{bmatrix} + Q^{-1} \begin{bmatrix} \Delta u_{ankle} \\ \Delta u_{hip} \end{bmatrix} \quad (6.3)$$

where $Q = \begin{bmatrix} Q_{11} & Q_{12} \\ Q_{21} & Q_{22} \end{bmatrix}$ and the elements in this matrix are,

$$Q_{11} = I_1 + I_2 + m_1\ell_1^2 + m_2(L_1^2 + L_2^2 + 2L_1L_2)$$

$$Q_{12} = I_2 + m_2L_2^2 + m_2L_1L_2$$

$$Q_{21} = I_2 + m_2L_2^2 + m_2L_1L_2$$

$$Q_{22} = I_2 + m_2L_2^2$$

$$F = \begin{bmatrix} m_1g\ell_1 + m_2gL_1 + m_2gL_2 & m_2gL_2 \\ m_2gL_2 & m_2gL_2 \end{bmatrix}$$

The most basic body dimension is the length of the segments between each joint. These vary with age, gender, and race. An average set of segment lengths expressed as a percentage of body height was prepared by Drillis and Continit (1966) [84].as shown in Figure 6.2. These segment proportions serve as a good approximation to convert into a dimensionless model. This makes it easier to apply the model to a variety of humans having different height, weight, moments of inertia, etc[84].

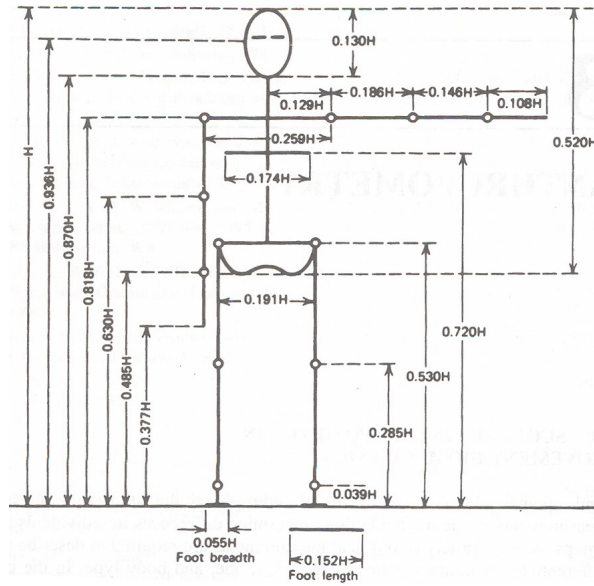


Figure 6.2: Body segment length expressed as a fraction of body height [84]

Define M to be the total body mass and L to be the height of the upright body. Then, each segment is proportional to these two quantities. We have used typical numerical values for simplicity. In reality, the fractions would have to be measured or estimated for a specific individual.

<i>Ankle-Hip</i>	<i>Hip-Torso</i>
$m_1 = \frac{1}{3}M$	$m_2 = \frac{2}{3}M$
$k_1 = 0.424L$	$L_2 = 0.47L$
$L_1 = 0.53L$	

We introduce the quantities $t = \tau/\beta$ and the normalization factor $\beta = \sqrt{L/g}$, which has dimension $[\beta] = T$ (time). Given $\frac{d\tau}{dt} = \beta$ and $\phi_i(\tau) = \phi_i(\beta t)$, for $i = 1, 2$, (for simplicity, we use ϕ_i as the normalized variable in the rest of the paper) Eqn (6.3) can be simplified into a completely dimensionless form:

$$\begin{bmatrix} \Delta\ddot{\phi}_1(\tau) \\ \Delta\ddot{\phi}_2(\tau) \end{bmatrix} = \beta^2 \left(\frac{Q}{ML^2}\right)^{-1} \frac{F}{ML^2} \begin{bmatrix} \Delta\phi_1 \\ \Delta\phi_2 \end{bmatrix} + \frac{\beta^2}{ML^2} \left(\frac{Q}{ML^2}\right)^{-1} \begin{bmatrix} \Delta u_{ankle} \\ \Delta u_{hip} \end{bmatrix}$$

Now we introduce the new state space variables:

$$\underline{z} = \begin{bmatrix} z_1 \\ z_2 \\ z_3 \\ z_4 \end{bmatrix} = \begin{bmatrix} \Delta\phi_1 \\ \Delta\phi_2 \\ \frac{d}{dt}(\Delta\phi_1) \\ \frac{d}{dt}(\Delta\phi_2) \end{bmatrix}, \quad \underline{u} = \begin{bmatrix} u_1 \\ u_2 \end{bmatrix} = \begin{bmatrix} \Delta u_{ankle} \\ \Delta u_{hip} \end{bmatrix}$$

Substitute the new variables and we have the new dynamics in the form

$$\dot{\underline{z}} = A\underline{z} + B\underline{u} \quad (6.4)$$

where

$$A = \begin{bmatrix} 0_{2 \times 2} & I_{2 \times 2} \\ \beta^2 \left(\frac{Q}{ML^2}\right)^{-1} \frac{F}{ML^2} & 0_{2 \times 2} \end{bmatrix}$$

$$B = \begin{bmatrix} 0_{2 \times 2} \\ \frac{\beta^2}{ML^2} \left(\frac{Q}{ML^2}\right)^{-1} \end{bmatrix}$$

Next, we use the relationship $t = k\delta$ to sample the continuous system and create a discrete time approximation to the original system

$$\underline{z}[k+1] = e^{A\delta} \underline{z}[k] + \left(\int_0^\delta e^{A\lambda} d\lambda \right) B\underline{u}[k]$$

Comparing this equation to the continuous time one gives us a set of relationships for converting the continuous-time system into a discrete-time system. Then the discretized dimensionless system is

$$\underline{z}[k+1] = \overline{A}\underline{z}[k] + \overline{B}\underline{u}[k] + \underline{\nu}(k)$$

$$\underline{y}[k] = \overline{C}\underline{z}[k] + \underline{w}(k)$$

Here, we use \overline{A} and \overline{B} to denote the system matrices of the discrete time system

$$\overline{A} = \sum_{n=0}^{\infty} \frac{A^n (\delta)^n}{n!}$$

$$\overline{B} = A^{-1}(\overline{A} - I)^{-1}B$$

Note that we have added some process $\underline{\nu}(k)$ and measurement noises $\underline{w}(k)$ which are assumed to be independent White Gaussian Noise (*WGN*) with mean zero and covariance Ξ and Θ respectively, i.e., $\underline{\nu} \sim N(0, \Xi)$ and $\underline{w} \sim N(0, \Theta)$ as a way to incorporate the perturbations.

6.2 Optimal Coordinated Control

The new problem is defined as Double Inverted Pendulum with Coordinated Higher order Optimal Control (DCHOC):

$$\mathbf{min} J_{DCHOC} = \sum_{i=1}^4 \sum_{k=0}^N d_i z_i^{2p}[k] + \sum_{n=0}^N d_5 u_1^{2q}[k] + d_6 u_2^{2q}[k]$$

$$\mathbf{s.t.} \underline{z}[k+1] = \overline{A}\underline{z}[k] + \overline{B}\underline{u}[k]$$

where, $p, q \in \mathbb{R}_+$ are integers greater than or equal to 1. d_i with $i = 1, 2, \dots, 6$ are the weights for the state and the control input. We solve the optimal control problem with partial state feedback, WGN disturbance, and a finite final time, N . Furthermore, for

large N the first few values of the control are a reasonable approximation to those that would be valid in the infinite time case.

This finite time problem involves a convex performance measure and a linear system. It is thus a convex programming problem for which there are very good solution methods. We first display the problem in its convex programming form. Define

$$\underline{s} = [\underline{z}(0), \underline{u}(0), \underline{z}(1), \underline{u}(1), \dots, \underline{z}(N), \underline{u}(N)]^T$$

We rewrite the performance measure and dynamics in terms of the overall variable as

$$\mathbf{min} J(\underline{s}) = \sum_{n=0}^N \bar{D}_s \underline{s}^\Lambda [k]$$

$$\mathbf{s.t.} A_s \underline{s} = b$$

where $\Lambda \in \{p, q\}$, $\bar{D}_s = \text{diag}(d_1, d_2, \dots, d_6)$ and

$$A_s = \begin{bmatrix} I & 0 & \dots & \dots & \dots & O \\ -\bar{A} & -\bar{B} & I & 0 & \dots & \vdots \\ \vdots & \vdots & \vdots & \vdots & \vdots & \vdots \\ O & \dots & -\bar{A} & -\bar{B} & I & 0 \end{bmatrix}, b = \begin{bmatrix} \underline{z}(0) \\ O \\ \vdots \\ O \end{bmatrix}$$

The *Newton-KKT* method is a good choice for solving this problem. The key step in the Newton-KKT algorithm is the repeated solution of the following system of linear equations involving the gradient and the Hessian of $J(\underline{s})$.

$$\begin{bmatrix} \nabla^2 J(\underline{s}^{(i)}) & A_s^T \\ A_s & O \end{bmatrix} \begin{bmatrix} \Delta_{\underline{s}_{nt}}^{(i)} \\ \underline{w} \end{bmatrix} = \begin{bmatrix} -\nabla J(\underline{s}^{(i)}) \\ O \end{bmatrix} \quad (6.5)$$

where $\Delta_{\underline{s}_{nt}}^{(i)}$ is the Newton's step at i^{th} iteration and using the *Schur Complement* this can be reduced to

$$\nabla^2 J(\underline{s}^{(i)}) \Delta \underline{s}_{nt}^{(i)} + A_s^T w = -\nabla J(\underline{s}^{(i)}) \quad (6.6)$$

We could use the same modified convex programming algorithm in chapter 5 to solve the optimal control problem. This would give us a nonlinear, approximately optimal, full-state feedback regulator for posture. In fact, all of the elements of the state of this system are measured by sensors in the human body. Biologically, this nonlinear controller can be learned over time and would not impose any computational burden on the human nervous system. Technologically, it is easier to implement this controller as an MPC.

Because we want to study the effect of perturbations, and because the sensors in the human are believed to be noisy, we need to modify our deterministic optimal control problem because the real optimal control problem is stochastic. We simplify the stochastic problem by enforcing the separation of filtering and control and use a Kalman filter to deal with the noise. Note that this separation almost certainly does exist in the human nervous system (as we explain in the conclusions section) even though this may not be optimal. The Kalman filter/predictor for this system is then

$$\begin{aligned} \hat{\underline{z}}[k|k] &= \hat{\underline{z}}[k|k-1] + K[\underline{z}(k) - \overline{C}\underline{z}(k|k-1)] \\ \hat{\underline{z}}[k+1|k] &= \overline{A}\hat{\underline{z}}[k|k] + \overline{B}\underline{u}[k] \end{aligned}$$

where K is the gain matrix of the Kalman filter calculated using MATLAB's *dlqe* command. With the estimate of the current state as the initial state, we then apply model predictive control (MPC), to find the closed-loop optimal solution.

6.3 The Results

We have successfully solved the constrained nonlinear optimal control problem using the method described before. In this section, we demonstrate that the proposed control could automatically adjust and coordinate different balance strategies according to the state information and the disturbance level.

The parameters and coefficients in the simulations are based on the simplified sway model defined in Eqn (6.4) using body parameters from Peterka [70] as shown in Table 6.1. and Winter [84]. The approximately optimal control, with a look-ahead time of 4 seconds and a sampling interval of 0.1 seconds, makes $N^d = 40$.

Table 6.1: Body Characteristics, Model Parameters and Simulation Variables

M	76 <i>kg</i>	δ	0.1 <i>s</i>
L	1.7 <i>m</i>	N	200
I_1	60 <i>kg · m²</i>	N^d	40
I_2	45 <i>kg · m²</i>	N^{it}	30

6.3.1 Ankle strategy

The parameters for the “ankle strategy” are given in Table 6.2. Note that d_1 , the weight on deviations in ankle angle, is roughly 1/4 times d_2 , the weight on the hip angle deviations. Also, the weight on ankle angular velocity is 1/2 the weight on the hip angular velocity.

Table 6.2: Ankle Strategy simulation parameters

p	2	$z_1[0]$	$\frac{\pi}{8} \text{ rad}$
q	2	$z_2[0]$	$\frac{\pi}{800} \text{ rad}$
d_1	80	$z_3[0]$	$\frac{\pi}{16} \text{ rad/sec}$
d_2	350	$z_4[0]$	$\frac{\pi}{1600} \text{ rad/sec}$
d_3	100	$u_1[0]$	0 Nm
d_4	200	$u_2[0]$	0 Nm
d_5	1	$\ \epsilon\ $	0.01
d_6	1	$\ \psi\ $	0.01

In Figure 6.3 and 6.4, the ankle joint angle starts away from its equilibrium point and the hip joint angle is initially at its equilibrium point. We explore how the resulting optimal joint control torques affect the ankle and hip movement. As the ankle angle is returned to its equilibrium value, the ankle torque is, of course, larger than the hip torque. Interestingly it generally remains larger throughout the movement. Both the hip torque and the ankle torque remain relatively low.

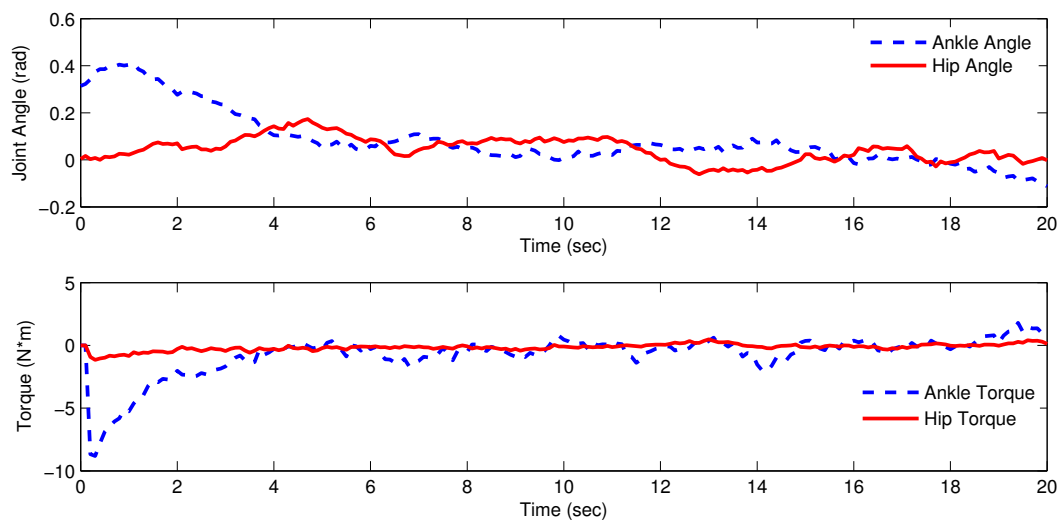


Figure 6.3: Trajectories of ankle and hip angle under control of ankle strategy

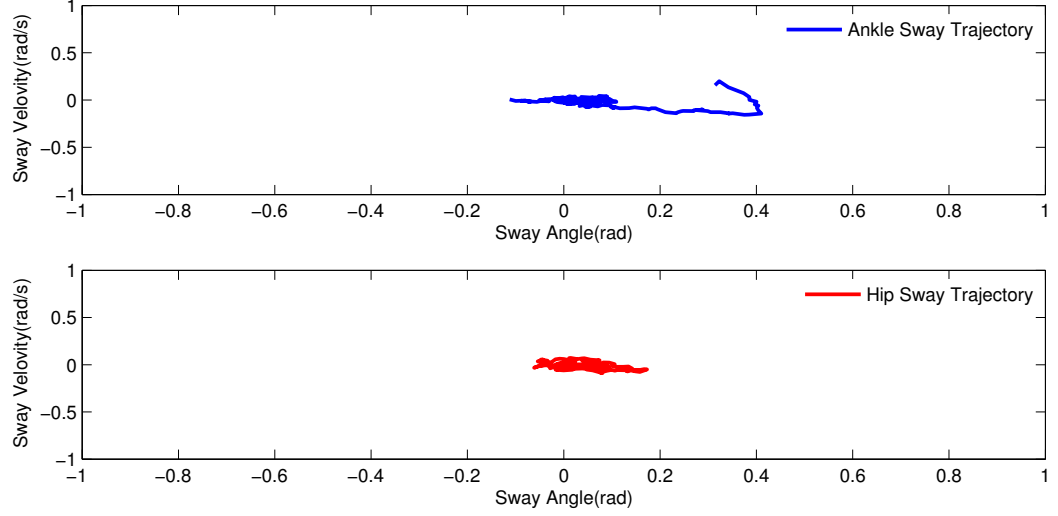


Figure 6.4: State trajectories of angular state and angular velocity for ankle and hip joint under control of ankle strategy

6.3.2 Hip Strategy

The parameters for the “hip strategy” are given in Table 6.3. Note that d_1 , the weight on deviations in ankle angle, is roughly 4 times d_2 , the weight on the hip angle deviations while the weight on ankle angular velocity is double that on the hip angular velocity.

Table 6.3: Hip Strategy simulation parameters

p	2	$z_1[0]$	$\frac{\pi}{800} \text{ rad}$
q	2	$z_2[0]$	$\frac{\pi}{8} \text{ rad}$
d_1	350	$z_3[0]$	$\frac{\pi}{1600} \text{ rad/sec}$
d_2	80	$z_4[0]$	$\frac{\pi}{16} \text{ rad/sec}$
d_3	200	$u_1[0]$	0 Nm
d_4	100	$u_2[0]$	0 Nm
d_5	1	$\ \epsilon\ $	0.01
d_6	1	$\ v\ $	0.01

In Figures 6.5 and 6.6, the ankle joint angle starts at its equilibrium point and the hip joint angle is initially away from its equilibrium point. We explore how the resulting joint control torques affect the ankle and hip movement. In this case, the hip joint angle is brought close to its equilibrium point by means of a rather large hip torque of short duration. There is some movement of the ankle joint.

Note that the hip joint angle is not returned exactly to its equilibrium. Because of the relatively low weight on hip angle deviations, it is optimal to allow the hip to remain away from its equilibrium. This is actually observed experimentally in humans, who do not necessarily stand at the exact vertical nor do they adopt exactly the same posture every time.

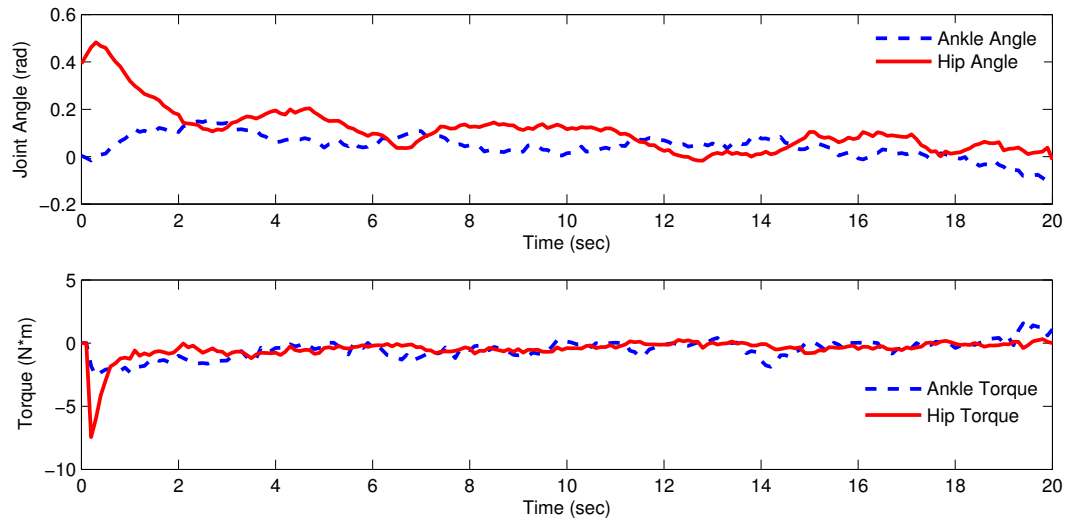


Figure 6.5: Trajectories of ankle and hip angle under control of hip strategy

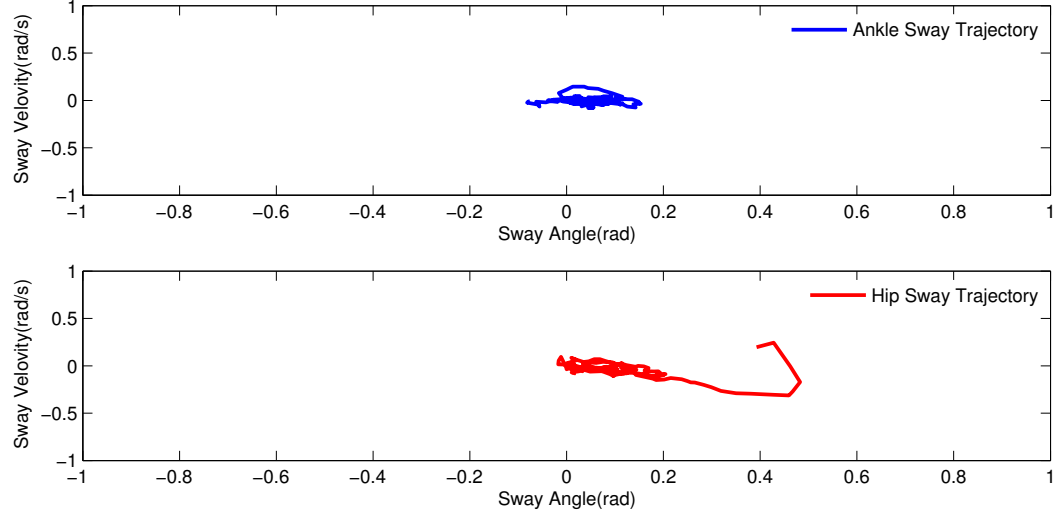


Figure 6.6: State trajectories of angular state and angular velocity for ankle and hip joint under control of hip strategy

6.3.3 Ankle and Hip Coordination

In this simulation, both the ankle and hip are start from their equilibrium position but are driven away by white Gaussian noise. The white noise has a standard deviation of 0.01 for the first 10 seconds, and 0.1 for the remaining 10 seconds. The other parameters of the simulations are given in Table 6.4.

Table 6.4: Parameters for Ankle Hip Coordination during Balance Maintenance

p	2	$z_1[0]$	$\frac{\pi}{800} \text{ rad}$
q	2	$z_2[0]$	$\frac{\pi}{800} \text{ rad}$
d_1	350	$z_3[0]$	$\frac{\pi}{1600} \text{ rad/sec}$
d_2	350	$z_4[0]$	$\frac{\pi}{1600} \text{ rad/sec}$
d_3	200	$u_1[0]$	0 Nm
d_4	200	$u_2[0]$	0 Nm
d_5	1	$\ \epsilon\ $	0.01 and 0.1
d_6	1	$\ v\ $	0.01 and 0.1

As we can see from Figure 6.7 and 6.8, for the small disturbances during the first 10 seconds, the controller is applying correction torque at the ankle only. The hip joint has very little control input and this leads to a slightly bigger sway for the upper body. This is, in fact, opposite to what is observed experimentally in the following sense. The experimentally observed hip motion is very small. It is not possible to observe the hip torque experimentally. Our results suggest two things. First, that there is substantial hip torque applied in order to reduce the hip angular motion. Second, that we should use a different combination of weights to replicate the experimental results.

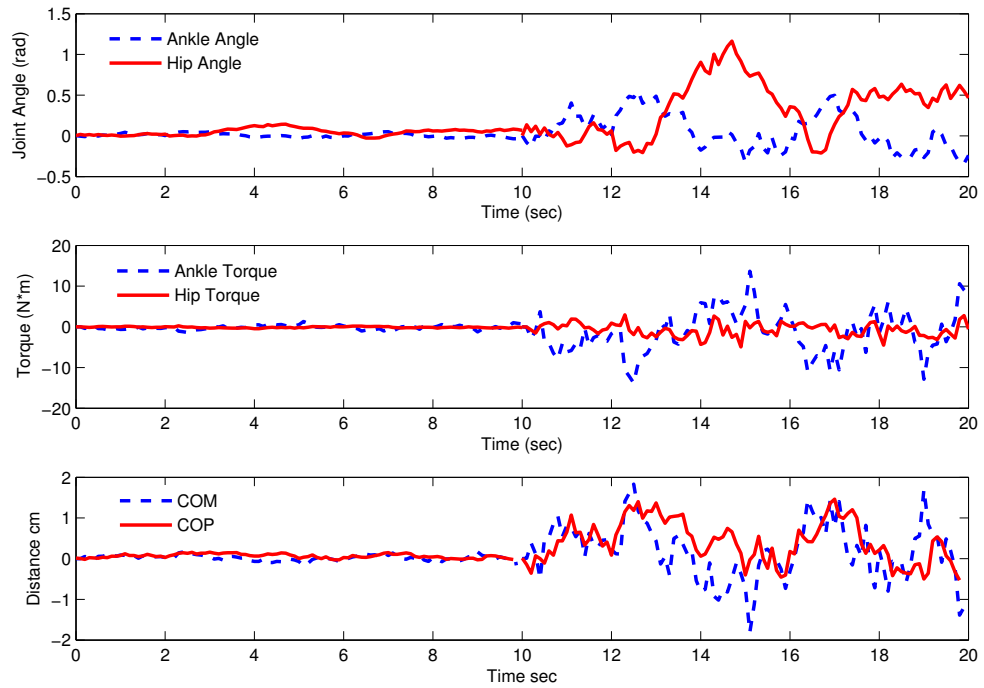


Figure 6.7: Trajectories of angular state, control torque and COM/COP for ankle and hip joints starting from equilibrium point driven by different noise levels

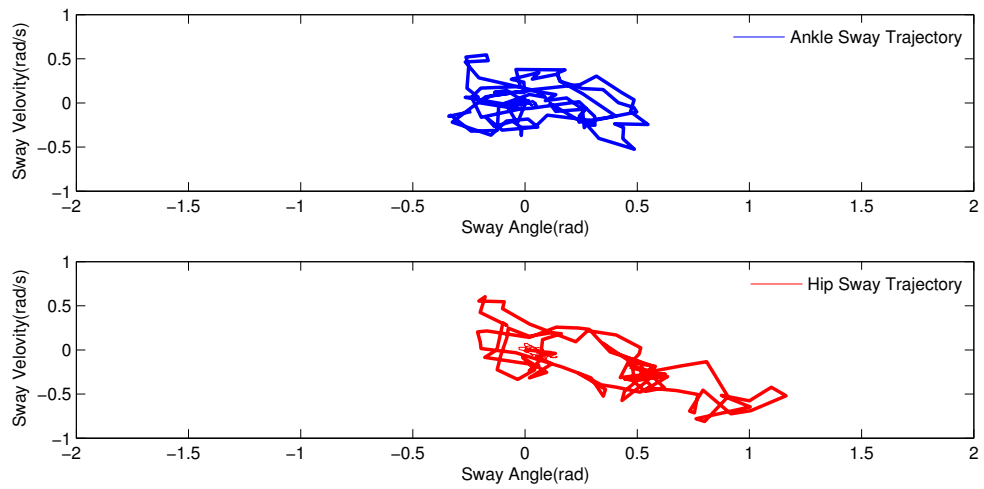


Figure 6.8: State trajectories of angular state and angular velocity for ankle and hip joint under control of ankle and hip coordination

When the disturbance increases, bending the hip creates an additional restoring torque to help maintain a stable posture. Still, the hip torque is relatively low and the hip angular sway relatively large. This is also reflected in the state trajectories in Figure 6.8; there are two clusters for the hip state trajectories corresponding to different noise levels, while the ankle is less sensitive to the noise change. Note that the hip motions needs to be complementary to the angle motion in order to keep the COP close to the middle of the foot.

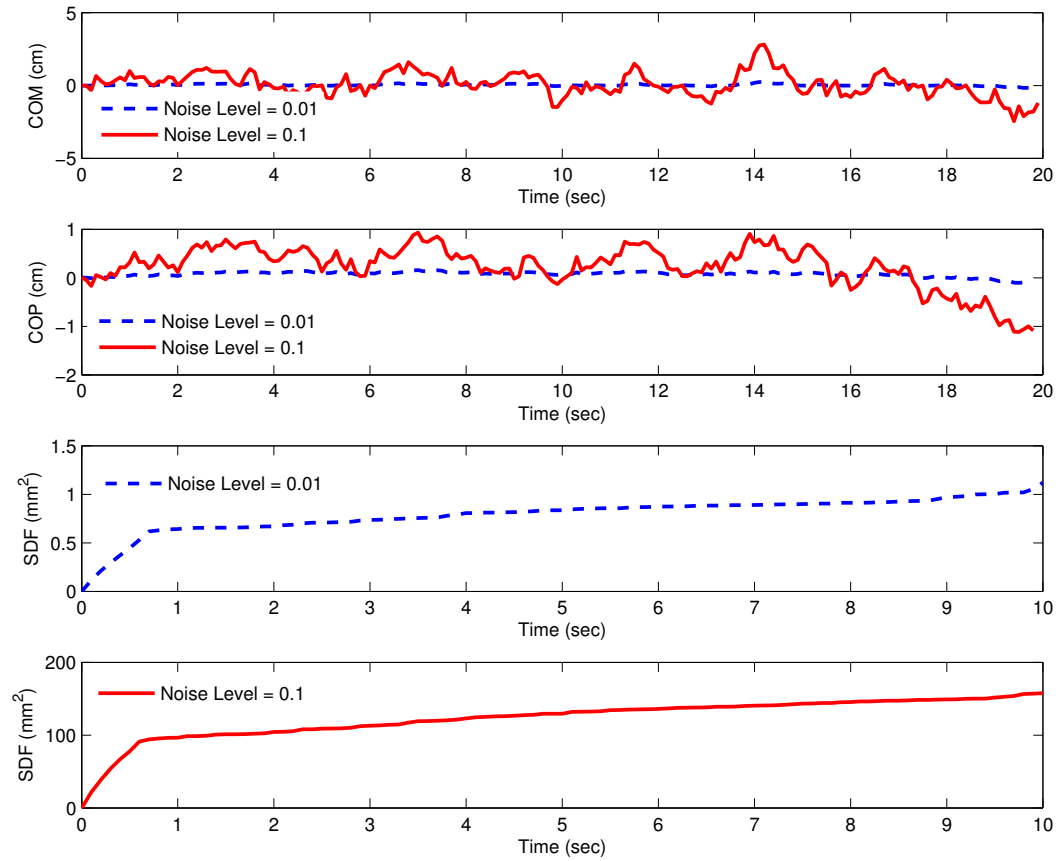


Figure 6.9: Trajectories of COM, COP and SDF starting from equilibrium point driven by different noise level

The SDF plots in Figure 6.9 indicates that the increasing noise level will generate more sway for the entire body. Note that the SDF plots are qualitatively similar to those seen experimentally.

Chapter 7

Control of Center of Pressure

To address stability, many of the proposed approaches consider a way to deal with the center of pressure (COP). The COP is defined as the point on the ground where the resultant of the ground-reaction force acts. Classically, reaction forces are considered to be the result of gravity (weight) and applied torque at the ankle joint. Thus, the COP has been mainly used to address static postural stability.

In this work, we present a computational model of a quietly standing human body which uses three rigid and connected segments to represent the foot, leg (locked knee), and torso as depicted in Figure 7.1. This is consistent with considerable experimental data which indicates that humans keep their knee angle nearly constant when there are small perturbations to their posture.

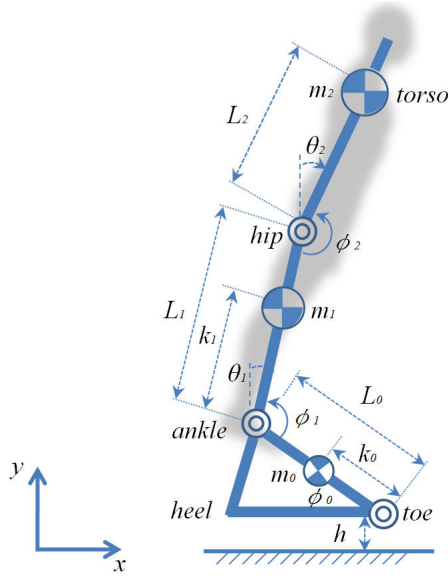


Figure 7.1: The three link sagittal biped is composed of three rigid links. The term k_i for $i = 1, 2, 3$ is the distance from the bottom of link i to the center of mass of link i . The term L_i is the length of link i . The torque at toe, ankle and hip joint are u_{toe} , u_{ankle} and u_{hip} .

We first derive the equations of motion using the Euler-Lagrange method for this two joint, three segment model controlled by torques on the ankle and hip joints:

$$\begin{aligned}
 \frac{d}{dt} \left(\frac{\partial \mathcal{L}}{\partial \dot{\phi}_0} \right) - \frac{\partial \mathcal{L}}{\partial \phi_0} &= u_{toe} \\
 \frac{d}{dt} \left(\frac{\partial \mathcal{L}}{\partial \dot{\phi}_1} \right) - \frac{\partial \mathcal{L}}{\partial \phi_1} &= u_{ankle} \\
 \frac{d}{dt} \left(\frac{\partial \mathcal{L}}{\partial \dot{\phi}_2} \right) - \frac{\partial \mathcal{L}}{\partial \phi_2} &= u_{hip} \\
 \frac{d}{dt} \left(\frac{\partial \mathcal{L}}{\partial \dot{h}} \right) - \frac{\partial \mathcal{L}}{\partial h} &= f_v
 \end{aligned}$$

where

$$\mathcal{L} = \mathcal{K} - \mathcal{P} \tag{7.1}$$

and \mathcal{K} is the total kinetic energy of the system; \mathcal{P} is the total potential energy. The generalized coordinates for this system are $[\phi_0, \phi_1, \phi_2, h]$. The torque at toe, ankle and

hip joint are u_{toe} , u_{ankle} and u_{hip} . f_v is the vertical component of the ground reaction force.

The two extra degrees of freedom, h and ϕ_0 , are introduced so we can calculate the center of pressure, l_{cop} . The center of pressure is located at the distance from the toe at which the vertical force, f_v has to be placed in order to create a torque about the toe equal to u_{toe} . It is a very good indication of how stable a posture is.

The total kinetic energy is the sum of the rotational and translational kinetic energies of the components of the system, and all the potential energy is due to gravity. These quantities can be written in terms of the angles ϕ_i and the position of the center of mass (x_i, y_i) of each link i as

$$\mathcal{K} = \frac{1}{2} \sum_{i=1}^3 [I_i \dot{\phi}_i^2 + m_i (x_i^2 + y_i^2)]$$

$$\mathcal{P} = \sum_{i=1}^3 g m_i y_i$$

We write each x_i and y_i in terms of the generalized coordinates to express the kinetic energy and potential energy,

$$\begin{aligned} x_0 &= k_0 \cos(\phi_0) \\ y_0 &= k_0 \sin(\phi_0) + h \\ x_1 &= L_0 \cos(\phi_0) + k_1 \cos(\phi_0 - \phi_1) \\ y_1 &= L_0 \sin(\phi_0) - k_1 \sin(\phi_0 - \phi_1) + h \\ x_2 &= L_0 \cos(\phi_0) + L_1 \cos(\phi_0 - \phi_1) - L_2 \cos(\phi_0 - \phi_1 - \phi_2) \\ y_2 &= L_0 \sin(\phi_0) - L_1 \sin(\phi_0 - \phi_1) + L_2 \sin(\phi_0 - \phi_1 - \phi_2) + h \end{aligned}$$

Then, we derive the equations of motion for the system with the vector of general coordinates $q = [\phi_0, \phi_1, \phi_2, 0]$ because $h = 0$ and $\phi_0 = \text{constant}$ are constraints.

$$J(q)\ddot{q} + G(q, \dot{q}) = U_q \tag{7.2}$$

The complete expression for ankle and hip torque will be:

$$\begin{aligned}
u_{ankle} = & [I_1 + I_2 + m_1k_1^2 + m_2L_1^2 + m_2L_2^2]\ddot{\phi}_1 \\
& +(I_2 + m_2L_2^2)\ddot{\phi}_2 \\
& +m_2L_1L_2(2\dot{\phi}_1\dot{\phi}_2 + (\dot{\phi}_2)^2)\sin(\phi_2) \\
& -m_2L_1L_2(2\ddot{\phi}_1 + \ddot{\phi}_2)\cos(\phi_2) \\
& +(m_1\ell_1 + m_2L_1)g\cos(\phi_1) \\
& -m_2gL_2\cos(\phi_1 + \phi_2)
\end{aligned}$$

$$\begin{aligned}
u_{hip} = & (I_2 + m_2L_2^2)(\ddot{\phi}_1 + \ddot{\phi}_2) \\
& -m_2L_1L_2\ddot{\phi}_1\cos(\phi_2) \\
& -m_2L_1L_2(\dot{\phi}_1)^2\sin(\phi_2) \\
& -m_2gL_2\cos(\phi_1 + \phi_2)
\end{aligned}$$

There is also a equation for u_{toe} and for f_v similar to these two equations. Now we have the nonlinear dynamics as

$$\begin{bmatrix} \ddot{\phi}_1 \\ \ddot{\phi}_2 \end{bmatrix} = Q^{-1} \begin{bmatrix} -G_1(\underline{\phi}) \\ -G_2(\underline{\phi}) \end{bmatrix} + Q^{-1} \begin{bmatrix} u_{ankle} \\ u_{hip} \end{bmatrix}$$

where

$$Q(1, 1) = I_1 + I_2 + m_1k_1^2 + m_2L_1^2 + m_2L_2^2 - 2m_2L_1L_2\cos(\phi_2)$$

$$Q(1, 2) = I_2 + m_2L_2^2 - m_2L_1L_2\cos(\phi_2)$$

$$Q(2, 1) = I_2 + m_2L_2^2 - m_2L_1L_2\cos(\phi_2)$$

$$Q(22) = I_2 + m_2L_2^2$$

$$G_1(\underline{\phi}) = m_2 L_1 L_2 (2\dot{\phi}_1 \dot{\phi}_2 + (\dot{\phi}_2)^2) \sin(\phi_2) + (m_1 k_1 + m_2 L_1) g \cos(\phi_1) - m_2 g L_2 \cos(\phi_1 + \phi_2)$$

$$G_2(\underline{\phi}) = -m_2 L_1 L_2 (\dot{\phi}_1)^2 \sin(\phi_2) - m_2 g L_2 \cos(\phi_1 + \phi_2)$$

To understand the *COP* one first needs to understand that the ground acts on the foot by means of a force vector f_v and a torque about the toe u_{toe} .

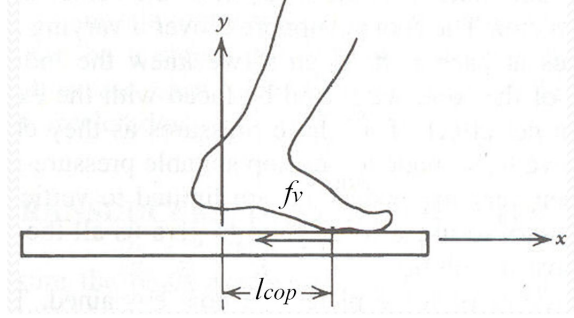


Figure 7.2: f_v is the horizontal component of the ground reaction force.

One can replace the toe torque by applying the force at the distance from the toe that creates u_{toe} . That distance is the *COP*. Mathematically, denoting the position of the *COP* by l_{cop} ,

$$l_{cop} = \frac{u_{toe}}{f_v} \quad (7.3)$$

where f_v is the vertical component of the ground reaction force (the component orthogonal to l_{cop}). We compute l_{cop} during standing by means of the Euler-Lagrange method. The key is that the foot does not move. Hence, ϕ_0 is a fixed constant and $\dot{\phi}_0 = \ddot{\phi}_0 = 0$ and $h = \dot{h} = \ddot{h} = 0$.

The toe torque required to satisfy these constraints is calculated by substituting them into the expression derived earlier for the toe torque, resulting in

$$u_{toe} = a_1 \ddot{\phi}_1 + a_2 \ddot{\phi}_2 + a_0$$

where

$$\begin{aligned}
a_1 = & -m_1k_1^2 - m_2L_1^2 - m_2L_2^2 \\
& m_1L_0k_1\cos(2\phi_0 - \phi_1) \\
& m_2L_0L_1\cos(2\phi_0 - \phi_1) \\
& -m_2L_0L_2\cos(2\phi_0 - \phi_1 - \phi_2) \\
& 2m_2L_1L_2\cos(\phi_2) \\
a_2 = & -m_2L_2^2 \\
& -m_2L_0L_2\cos(2\phi_0 - \phi_1 - \phi_2) \\
& m_2L_1L_2\cos(\phi_2) \\
a_0 = & -(m_0k_0 + m_1L_0 + m_2L_2)g\cos(\phi_0) \\
& (m_1k_1 + m_2L_1)g\cos(\phi_0 - \phi_1) \\
& -m_2L_2g\cos(\phi_0 - \phi_1 - \phi_2)
\end{aligned}$$

The vertical component of the ground force is similarly computed to be

$$f_v = b_1\ddot{\phi}_1 + b_2\ddot{\phi}_2 + b_0$$

where

$$\begin{aligned}
b_1 = & m_1k_1\cos(\phi_0 - \phi_1) + m_2L_1\cos(\phi_0 - \phi_1) - m_2L_2\cos(\phi_0 - \phi_1 - \phi_2) \\
b_2 = & -m_2L_2\cos(\phi_0 - \phi_1 - \phi_2) \\
b_0 = & -(m_0 + m_1 + m_2)g
\end{aligned}$$

Now we have

$$l_{cop} = f(\phi_1, \phi_2, \dot{\phi}_1, \dot{\phi}_2, u_{ankle}, u_{hip})$$

The next step is to linearize the problem about the nominal vertical posture. This is reasonable because the perturbations of the upright posture that are being considered are small. Thus, we linearize the double inverted pendulum model around the unstable equilibrium point:

$$\begin{pmatrix} \phi_1^* \\ \phi_2^* \\ u_{ankle}^* \\ u_{hip}^* \end{pmatrix} = \begin{pmatrix} \frac{\pi}{2} \\ \pi \\ 0 \\ 0 \end{pmatrix}$$

and also define the small angular deviations from the vertical equilibrium.

$$\begin{pmatrix} \phi_1 \\ \phi_2 \\ u_{ankle} \\ u_{hip} \end{pmatrix} = \begin{pmatrix} \phi_1^* \\ \phi_2^* \\ u_{ankle}^* \\ u_{hip}^* \end{pmatrix} + \begin{pmatrix} \Delta\phi_1 \\ \Delta\phi_2 \\ \Delta u_{ankle} \\ \Delta u_{hip} \end{pmatrix}$$

We introduce the new state space variables:

$$\underline{z} = \begin{bmatrix} z_1 \\ z_2 \\ z_3 \\ z_4 \end{bmatrix} = \begin{bmatrix} \Delta\phi_1 \\ \Delta\phi_2 \\ \frac{d}{dt}(\Delta\phi_1) \\ \frac{d}{dt}(\Delta\phi_2) \end{bmatrix} \quad \underline{u} = \begin{bmatrix} u_1 \\ u_2 \end{bmatrix} = \begin{bmatrix} \Delta u_{ankle} \\ \Delta u_{hip} \end{bmatrix}$$

Define M to be the total body mass and L to be the height of the upright body. Then, each segment is proportional to these two quantities. We have used typical numerical values for simplicity. In reality, the fractions would have to be measured or estimated for a specific individual.

<i>Toe-Ankle</i>	<i>Ankle-Hip</i>	<i>Hip-Torso</i>
$m_0 = \frac{1}{60}M$	$m_1 = \frac{1}{3}M$	$m_2 = \frac{13}{20}M$
$k_0 = 0.122L$	$k_1 = 0.424L$	$L_2 = 0.47L$
$L_0 = 0.152L$	$L_1 = 0.53L$	

We introduce the quantities $t = \tau/\beta$ and the normalization factor $\beta = \sqrt{L/g}$, which has dimension $[\beta] = T$ (time). Given $\frac{d\tau}{dt} = \beta$ and $\phi_i(\tau) = \phi_i(\beta t)$, for $i = 1, 2$, (for simplicity, we use ϕ_i as the normalized variable in the rest of the paper) Eqn (2) can be simplified into a completely dimensionless form:

$$\begin{bmatrix} \Delta \ddot{\phi}_1(\tau) \\ \Delta \ddot{\phi}_2(\tau) \end{bmatrix} = \beta^2 \left(\frac{Q}{ML^2} \right)^{-1} \frac{F}{ML^2} \begin{bmatrix} \Delta \phi_1 \\ \Delta \phi_2 \end{bmatrix} + \frac{\beta^2}{ML^2} \left(\frac{Q}{ML^2} \right)^{-1} \begin{bmatrix} \Delta u_{ankle} \\ \Delta u_{hip} \end{bmatrix}$$

$$Q(1, 1) = I_1 + I_2 + m_1 k_1^2 + m_2 L_1^2 + m_2 L_2^2 + 2m_2 L_1 L_2$$

$$Q(1, 2) = I_2 + m_2 L_2^2 + m_2 L_1 L_2$$

$$Q(2, 1) = I_2 + m_2 L_2^2 + m_2 L_1 L_2$$

$$Q(2, 2) = I_2 + m_2 L_2^2$$

$$G_1(\Delta \phi) = m_2 L_1 L_2 (2x_3 x_4 + x_4^2)(-x_2) + (m_1 \ell_1 + m_2 L_1)g(-x_1) - m_2 g L_2 (x_1 + x_2)$$

$$G_2(\Delta \phi) = m_2 L_1 L_2 x_3^2 x_2 - m_2 g L_2 (x_1 + x_2)$$

This becomes, in state space format

$$\dot{\underline{z}} = \underline{A}\underline{z} + \underline{B}u \tag{7.4}$$

where

$$A = \begin{bmatrix} 0_{2 \times 2} & I_{2 \times 2} \\ \beta^2 \left(\frac{Q}{ML^2} \right)^{-1} \frac{F}{ML^2} & 0_{2 \times 2} \end{bmatrix}$$

$$B = \begin{bmatrix} 0_{2 \times 2} \\ \frac{\beta^2}{ML^2} \left(\frac{Q}{ML^2} \right)^{-1} \end{bmatrix}$$

Then linearize the center of pressure l_{cop}

$$\begin{bmatrix} u_{toe} \\ f_v \end{bmatrix} = \begin{bmatrix} a_1 & a_2 \\ b_1 & b_2 \end{bmatrix} \begin{bmatrix} \ddot{\phi}_1 \\ \ddot{\phi}_2 \end{bmatrix} + \begin{bmatrix} a_0 \\ b_0 \end{bmatrix}$$

Substituting in the second derivation gives

$$\begin{bmatrix} u_{toe} \\ f_v \end{bmatrix} = \Gamma_{ab} \frac{\beta^2}{ML^2} \left(\frac{Q}{ML^2} \right)^{-1} F \begin{bmatrix} z_1 \\ z_2 \end{bmatrix} + \Gamma_{ab} \frac{\beta^2}{ML^2} \left(\frac{Q}{ML^2} \right)^{-1} \begin{bmatrix} u_1 \\ u_2 \end{bmatrix} + \Lambda_{ab}$$

with

$$\Gamma_{ab} = \begin{bmatrix} \frac{a_1}{ML^2} & \frac{a_2}{ML^2} \\ \frac{b_1}{ML} & \frac{b_2}{ML} \end{bmatrix}$$

$$\Lambda_{ab} = \begin{bmatrix} \frac{a_0}{ML^2} \\ \frac{b_0}{ML} \end{bmatrix}$$

where

$$\begin{aligned}
a_1 = & -m_1 k_1^2 - m_2 L_1^2 - m_2 L_2^2 \\
& m_1 L_0 k_1 (c_1 - c_0 x_1) \\
& m_2 L_0 L_1 (c_1 - c_0 x_1) \\
& -m_2 L_0 L_2 [c_0 (x_1 - x_2) + c_1 (1 - x_1 x_2)] \\
& 2m_2 L_1 L_2
\end{aligned}$$

$$\begin{aligned}
a_2 = & -m_2 L_2^2 \\
& -m_2 L_0 L_2 [c_0 (x_1 - x_2) + c_1 (1 - x_1 x_2)] \\
& m_2 L_1 L_2
\end{aligned}$$

$$\begin{aligned}
a_0 = & -\bar{c}_0 (m_0 k_0 + m_1 L_0 + m_2 L_2) g \\
& (m_1 k_1 + m_2 L_1) (\bar{c}_1 - \bar{c}_0 x_1) g \\
& -m_2 L_2 g [\bar{c}_0 (x_1 - x_2) + \bar{c}_1 (1 - x_1 x_2)]
\end{aligned}$$

$$\begin{aligned}
b_1 = & m_1 k_1 (\bar{c}_1 - \bar{c}_0 x_1) \\
& + m_2 L_1 (\bar{c}_1 - \bar{c}_0 x_1) \\
& -m_2 L_2 [\bar{c}_0 (x_1 - x_2) + \bar{c}_1 (1 - x_1 x_2)]
\end{aligned}$$

$$b_2 = -m_2 L_2 [\bar{c}_0 (x_1 - x_2) + \bar{c}_1 (1 - x_1 x_2)]$$

$$b_0 = -(m_0 + m_1 + m_2) g$$

$$c_0 = \cos(2\phi_0) \quad \bar{c}_0 = \cos(\phi_0)$$

$$c_1 = \sin(2\phi_0) \quad \bar{c}_1 = \sin(\phi_0)$$

7.1 Optimal Control of COP

The designed cost function is selected in a way to penalize large deviations of the COP from its nominal value while also penalizing the control efforts. The performance measure is a novel mixture of ankle strategy, hip strategy, and COP.

$$\begin{aligned}
 J_{DPHOC} = & \int_0^{\infty} \left[d_1 l_{cop}^{2m}(t) + d_2 \dot{\phi}_1^{2m}(t) + d_3 \dot{\phi}_2^{2m}(t) \right] dt \\
 & + \int_0^{\infty} \left[d_4 u_{ankle}^2(t) + d_5 u_{hip}^2(t) \right] dt
 \end{aligned} \tag{7.5}$$

where d_1, d_2, \dots, d_5 are cost coefficients, m is an integer (m is 1 in this paper), and l_{cop} , u_{ankle} and u_{hip} are deviations from the nominal equilibrium values of the COP and controls respectively. Here, *DPHOC* stands for Double inverted pendulum model with COP and Higher order Optimal Control scheme. Note that the linearization causes the components of the COP that are quadratic in the angular velocities to disappear, so we include the velocity terms in the performance criterion to avoid a singular Hessian.

Inspired by the way in which Model Predictive Control problems are solved, we discretized the entire optimal control problem and replace the infinite time horizon of the original problem by the limited time duration N , and the resulting discrete time optimal control problem is:

$$\begin{aligned}
 \mathbf{min} \ J_{DPHOC} = & \sum_{n=0}^N d_1 (l_{cop})^{2m}[k] + d_2 z_3^2[k] + d_3 z_4^2[k] \\
 & + \sum_{n=0}^N d_4 u_1^2[k] + d_5 u_2^2[k] \\
 \mathbf{s.t.} \ \underline{x}[k+1] = & \bar{A}\underline{x}[k] + \bar{B}\underline{u}[k]
 \end{aligned}$$

define

$$\underline{s} = [\underline{z}(0), \underline{u}(0), \underline{z}(1), \underline{u}(1), \dots, \underline{z}(N), \underline{u}(N)]^T$$

The constraint then becomes

$$A_s \underline{s} = b$$

$$A_s = \begin{bmatrix} I & 0 & \dots & \dots & \dots & O \\ -\bar{A} & -\bar{B} & I & 0 & \dots & \vdots \\ \vdots & \vdots & \vdots & \vdots & \vdots & \vdots \\ O & \dots & -\bar{A} & -\bar{B} & I & 0 \end{bmatrix}, b = \begin{bmatrix} \underline{z}(0) \\ O \\ \vdots \\ O \end{bmatrix}$$

where \bar{A} and \bar{B} denote the system matrices of the discrete time system:

$$\bar{A} = \sum_{n=0}^{\infty} \frac{A^n (\delta)^n}{n!}$$

$$\bar{B} = A^{-1}(\bar{A} - I)^{-1}B$$

This nonlinear programming problem can be solved by the Newton-KKT algorithm [12], the key step of which is the repeated solution of the following system of linear equations involving the gradient and the Hessian of $J(\underline{s})$.

$$\begin{bmatrix} \nabla^2 J(\underline{s}^{(i)}) & A_s^T \\ A_s & O \end{bmatrix} \begin{bmatrix} \Delta \underline{s}_{nt}^{(i)} \\ \underline{w} \end{bmatrix} = \begin{bmatrix} -\nabla J(\underline{s}^{(i)}) \\ O \end{bmatrix} \quad (7.6)$$

Here $\Delta \underline{s}_{nt}^{(i)}$ is the Newton step at the i^{th} iteration. To solve more efficiently, use the *Schur Complement* to reduce the Newton KKT system to

$$\nabla^2 J(\underline{s}^{(i)}) \Delta \underline{s}_{nt}^{(i)} + A_s^T \underline{w} = -\nabla J(\underline{s}^{(i)}) \quad (7.7)$$

The Hessian will be in diagonal block form as

$$\nabla^2 J(\underline{s}^{(i)}) = \begin{bmatrix} H^1 & O & \dots & & O \\ O & \ddots & & & \\ \vdots & & H^n & & \vdots \\ & & & \ddots & O \\ O & \dots & O & H^N & \end{bmatrix}$$

where H^n is the Hessian matrix at time step n , which is a symmetric matrix with elements in the upper triangle as follows

$$\begin{bmatrix} \frac{\partial^2 J}{\partial z_1 \partial z_1} & \frac{\partial^2 J}{\partial z_1 \partial z_2} & \frac{\partial^2 J}{\partial z_1 \partial z_3} & \frac{\partial^2 J}{\partial z_1 \partial z_4} & \frac{\partial^2 J}{\partial z_1 \partial u_1} & \frac{\partial^2 J}{\partial z_1 \partial u_2} \\ \vdots & \frac{\partial^2 J}{\partial z_2 \partial z_2} & \frac{\partial^2 J}{\partial z_2 \partial z_3} & \frac{\partial^2 J}{\partial z_2 \partial z_4} & \frac{\partial^2 J}{\partial z_2 \partial u_1} & \frac{\partial^2 J}{\partial z_2 \partial u_2} \\ & \vdots & \frac{\partial^2 J}{\partial z_3 \partial z_3} & \frac{\partial^2 J}{\partial z_3 \partial z_4} & \frac{\partial^2 J}{\partial z_3 \partial u_1} & \frac{\partial^2 J}{\partial z_3 \partial u_2} \\ & & \vdots & \frac{\partial^2 J}{\partial z_4 \partial z_4} & \frac{\partial^2 J}{\partial z_4 \partial u_1} & \frac{\partial^2 J}{\partial z_4 \partial u_2} \\ \vdots & & & \vdots & \frac{\partial^2 J}{\partial u_1 \partial u_1} & \frac{\partial^2 J}{\partial u_1 \partial u_2} \\ \frac{\partial^2 J}{\partial u_2 \partial z_1} & \dots & & & \dots & \frac{\partial^2 J}{\partial u_2 \partial u_2} \end{bmatrix}$$

We could use the same modified convex programming algorithm in chapter 5 to solve the optimal control problem. This would give us a nonlinear, approximately optimal, full-state feedback regulator for posture. In fact, all of the elements of the state of this system are measured by sensors in the human body. Biologically, this nonlinear controller can be learned over time and would not impose any computational burden on the human nervous system. Technologically, it is easier to implement this controller as an MPC.

In reality, the human postural control system includes significant delays[44][43]. These would require inclusion of a predictor in the feedback controller. However, we

ignore the delays here because the overall control problem can be separated into two parts by imposing certainty equivalence and the full state feedback problem needs to be solved first. Inclusion of the delays and the predictor will complicate the controller and the exposition but add little to our understanding of the coordination.

7.2 The Results

We have successfully solved the constrained nonlinear optimal control problem using the method described in the preceding sections. In this section, we demonstrate that the proposed control could automatically adjust and coordinate different balance strategies according to the disturbance level.

The parameters and coefficients in the simulations are based on the simplified sway model defined in Eqn (7.4) using body parameters from Peterka [70] and Winter from last chapter[84]. The approximately optimal control, with a look-ahead time of 4 seconds and a sampling interval of 0.1 seconds, makes $N^d = 40$. The dimensionless results are then converted back to the real units in order to have a fair comparison with the experimental measurements.

7.2.1 Transient Response

The first simulation is to test the system's ability to recover from an initial disturbance. The parameters for the transient response simulation are listed in Table 7.1, d_1 is the weight on the *COP* deviation, and the initial *COP* deviation is chosen as 0.5 cm. The

parameters d_2 and d_3 are the weights on the angular velocity of the ankle and hip, and d_4 and d_5 are the weights on the control torques at the ankle and hip joints.

Table 7.1: Simulation parameters for transient response

d_1	100	$l_{cop}[0]$	0.5 <i>cm</i>
d_2	100	$z_3[0]$	0.001 <i>rad/sec</i>
d_3	100	$z_4[0]$	0.001 <i>rad/sec</i>
d_4	10	$u_1[0]$	0 <i>Nm</i>
d_5	10	$u_2[0]$	0 <i>Nm</i>
$\ \epsilon\ $	0.01,0.1	$\ v\ $	0.01,0.1

In order to investigate the coordination control of ankle and hip under different perturbations, the model is perturbed by white Gaussian noise with a standard deviation of 0.01 and 0.1 respectively. In Figure 7.3, the COM_x and COP are plotted for the two different noise levels. The trajectories of the ankle and hip angles are depicted in Figure 7. 4; The corresponding control torques are shown in Figure 7.5.

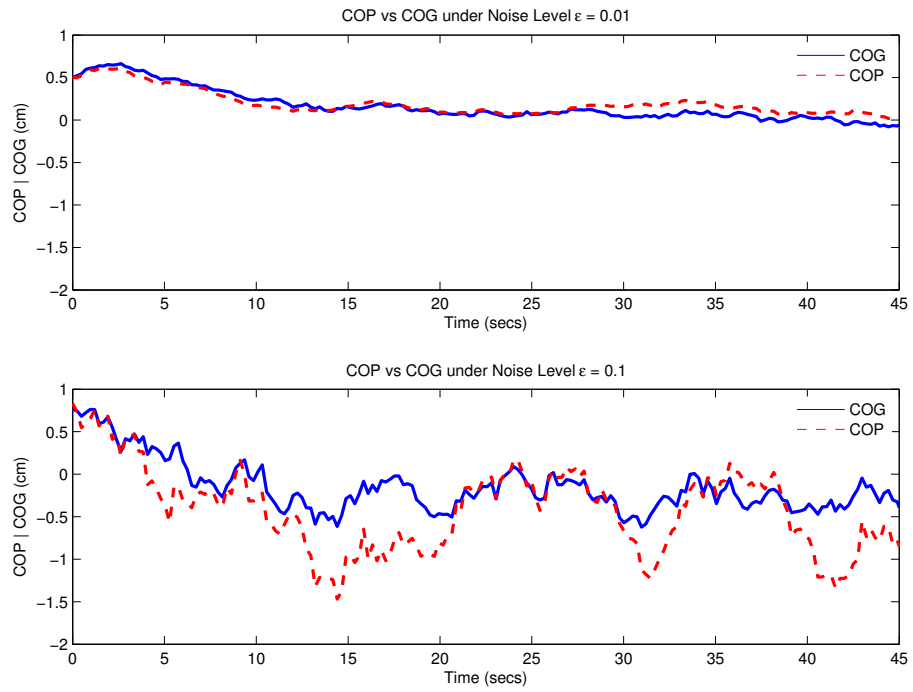


Figure 7.3: Trajectories of COM and COP during transient response

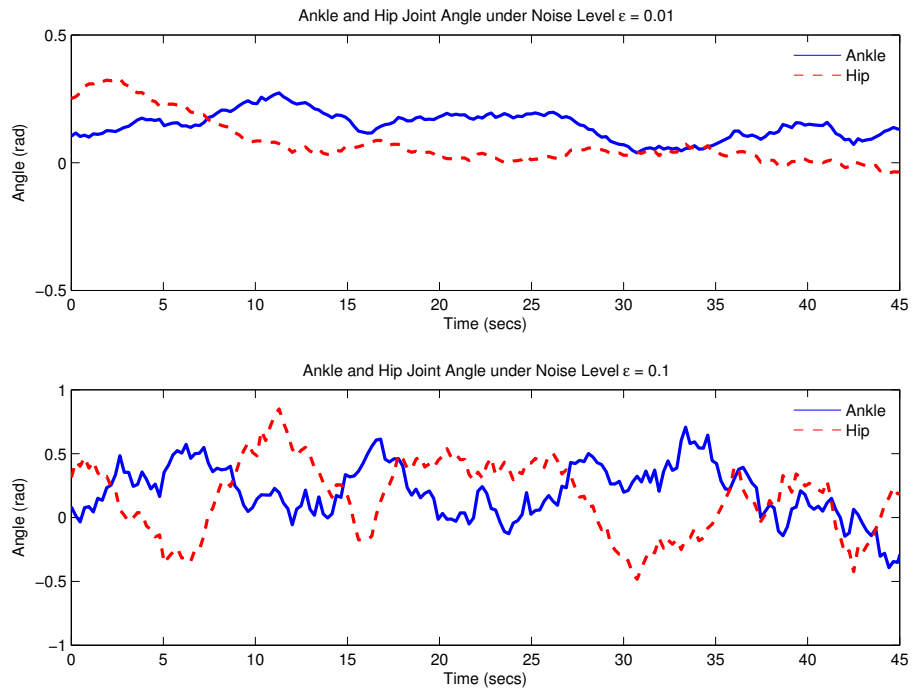


Figure 7.4: Trajectories of ankle and hip angle during transient response

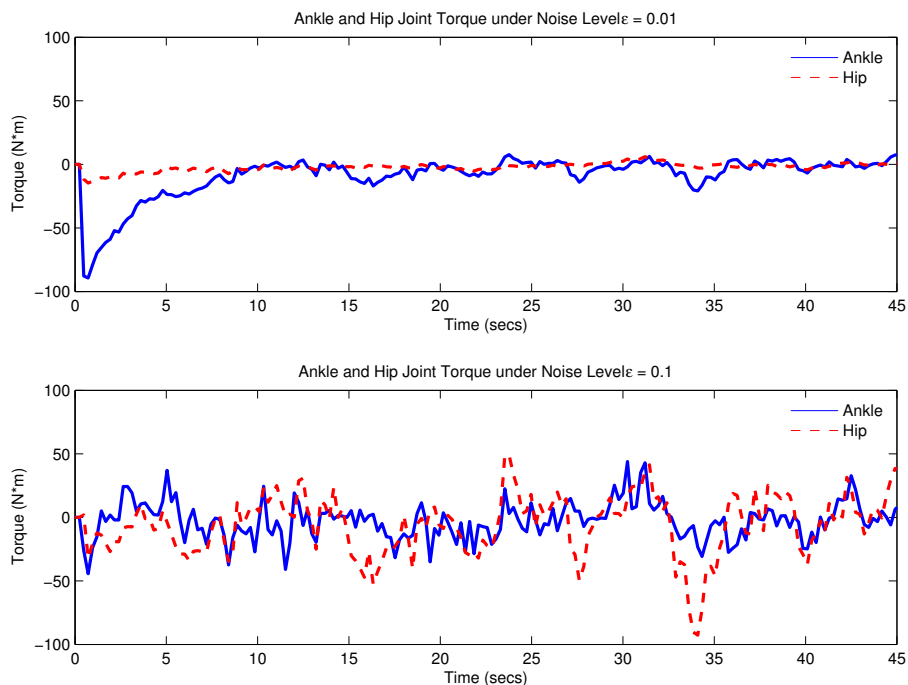


Figure 7.5: Control torque of ankle and hip joint during transient response

Since the postural motion is normally a small amplitude sway around the equilibrium position, it is interesting to simulate the optimally controlled system during steady state. In the following simulation of the steady state response, all the parameters are kept the same as for the transient response, but the initial position is set to its equilibrium value as shown in Table 7.2. Note that two different noise levels are considered.

Table 7.2: Simulation parameters for steady response

d_1	100	$l_{cop}[0]$	0 <i>cm</i>
d_2	100	$z_3[0]$	0.001 <i>rad/sec</i>
d_3	100	$z_4[0]$	0.001 <i>rad/sec</i>
d_4	10	$u_1[0]$	0 <i>Nm</i>
d_5	10	$u_2[0]$	0 <i>Nm</i>
$\ \epsilon\ $	0.01,0.1	$\ v\ $	0.01,0.1

7.2.2 *Steady State Response*

This section shows that our controller is trading off control effort versus motion of the *COP*, which is plotted in Figure 7.6 along with the trajectory of COM_x for both noise levels. Not unexpectedly, the *COP* exhibits greater displacements. This is because it includes the effects of control while the COM_x ignores the applied torques completely.

Figure 7.7 shows the applied torques at the two joints, again for both noise levels. It is interesting that the torque applied at the hip is substantially larger than that applied at the ankle. This does not contradict any experimental data because the joint torques are generally not observed during normal posture regulation.

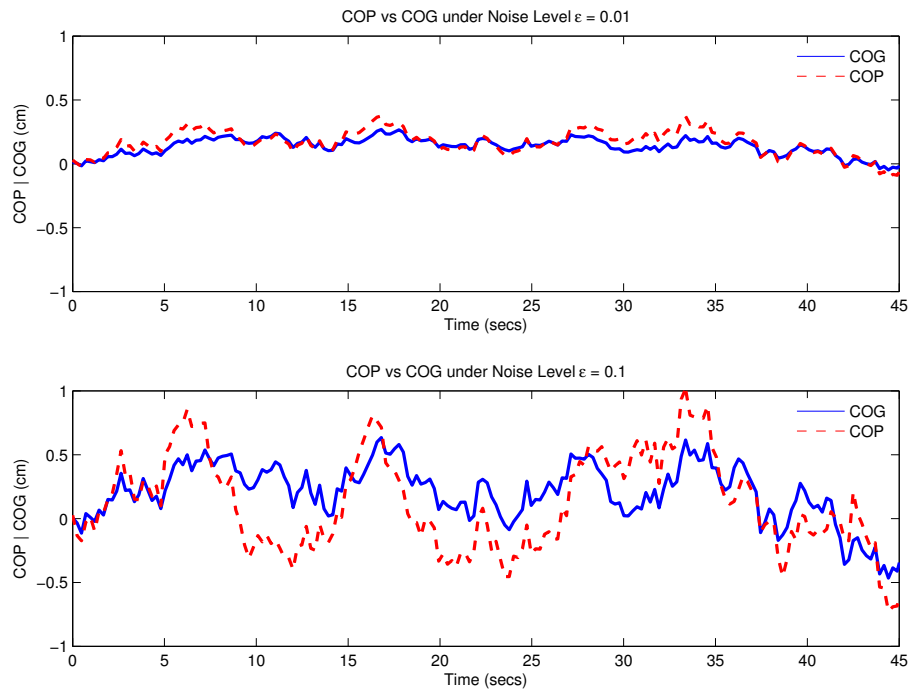


Figure 7.6: Trajectories of COM and COP during steady state response

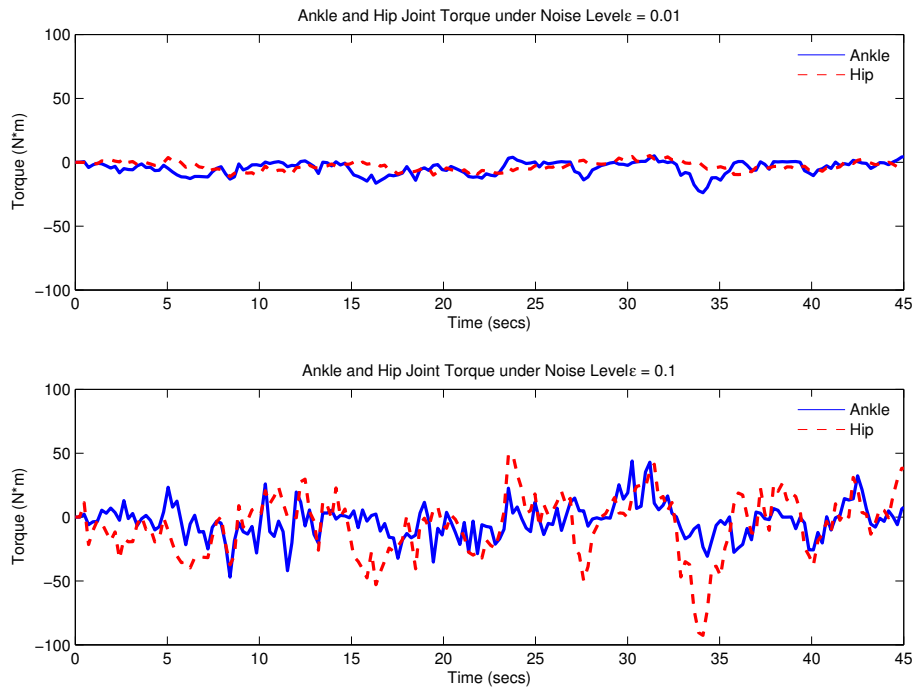


Figure 7.7: Control torque of ankle and hip joint during steady state response

In Figure 7.8, we plot the trajectories of the ankle and hip angles for the two different noise levels. Observe that, although both responses are small, the ankle response is slightly larger than that of the hip when the small noise level is used. In contrast, when the larger noise level is simulated, the hip angular displacement is larger than that of the ankle angle. This same difference is observed experimentally, albeit more noticeably. This suggests that regulating the location of the COP automatically produces the experimentally observed hip and ankle coordination.

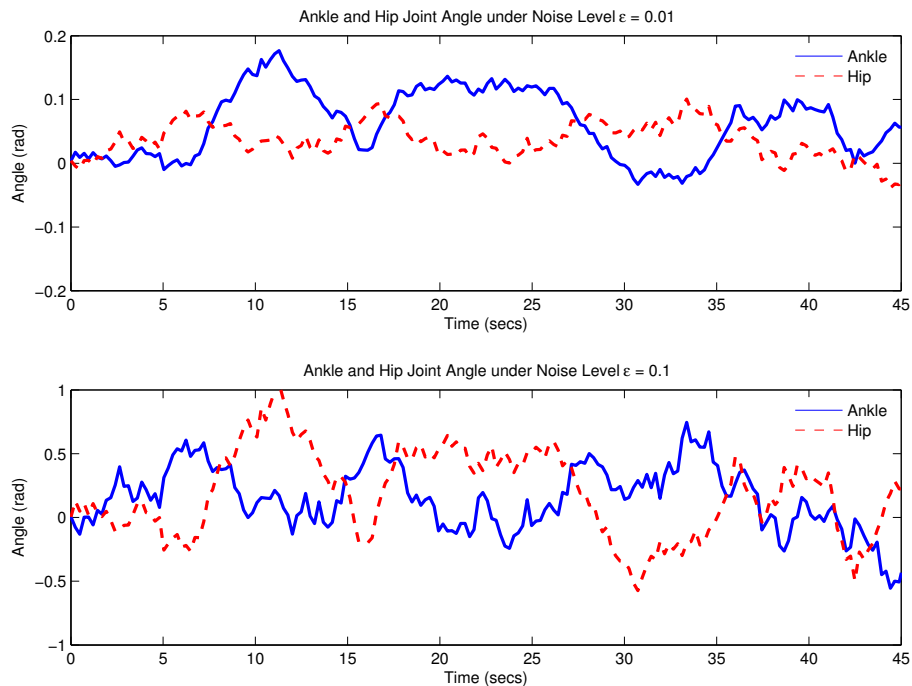


Figure 7.8: Trajectories of ankle and hip angle during steady state response

In Figure 7.9, we compare a single trial of experimental measurement of quiet standing data with the SDF from our model. An adult male subject with 76kg weight

and 1.76 meter height was tested in a quiet standing posture. The mismatch is almost certainly due to the omission of the neural delays from our model.

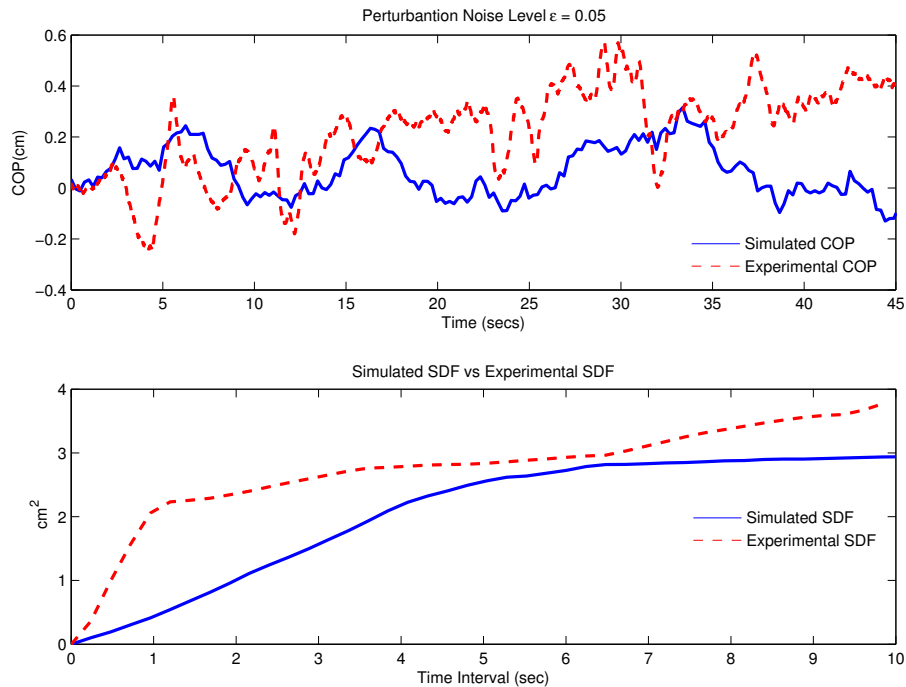


Figure 7.9: SDF of simulation and experimental data

7.3 Summary

In this chapter, we propose an optimal control scheme for regulation of upright posture in the sagittal plane. The three segment inverted pendulum system that approximates the human is controlled by joint torques at the ankle and hip. The proposed optimization criterion is quadratic in the control effort but quartic in the COP , which is a good measurement for assessing the stability of quietly standing. This objective function provides a trade-off between the allowed deviations of the COP from its nominal value

and the neuromuscular energy required to correct for these deviations.

This optimal control problem was solved and the optimally controlled system was simulated for both transient and steady responses. The results are consistent with those observed experimentally. For small perturbations, the ankle angle motion is larger than that of the hip angle. For larger perturbations, this is reversed. The motion at the hip is larger than that at the ankle. Truthfully, the experimental results are more dramatic. That is, the differences between the small and large perturbation cases are larger than in our model. One way that we might achieve a better match would be to better match the size of the perturbations to those in the experiments. We plan to do this soon.

We have ignored the delays in the neuronal control system in this chapter. They can be included easily using the procedure we described in chapter 5. It will not change the basic results of this chapter. The delay will affect the SDF. In fact, it will almost certainly improve the match between the experimental SDF and our theoretical one.

The control mechanism proposed here is a natural one for the human. The large collection of neurons that provide the input signal to the muscles are threshold devices. They can implement any nonlinear gain by just changing their thresholds. In fact, the size principle [?] suggests that the gain of any feedback controller using muscle as the actuator should increase faster than linearly with increasing perturbations. Thus, our nonlinear feedback controller is as easy, if not easier, for the human central nervous system to implement than any linear one.

Chapter 8

Conclusion and Discussion

8.1 Conclusion

We have presented an optimal control model for postural control by a quietly standing human. This model includes a three segment inverted pendulum controlled by joint torques at the ankle and at the hip. It also includes an optimization criterion that is quadratic in the controls but quartic in the states. This optimal control problem was solved for several different values of the weights in the performance criterion. The solution was obtained by first approximating the infinite time performance measure by a finite time performance measure. The entire problem was then discretized in time. The result is a convex programming problem which can be conveniently and reliably solved. Of course, the solution is open loop. By repeatedly solving this problem for different initial conditions and saving the first step of the solution we obtain an approximately optimal feedback solution. This is the basic idea behind MPC.

This means that the solution to the optimal control problem, in the case of full state feedback, would be a nonlinear feedback gain function with 4 inputs and 2 outputs. This is a plausible biological solution. The last stage in the nervous system's controller is a large collection of neurons, each driving a group of muscle fibers. Because neurons are threshold devices, it is easy to achieve almost any nonlinear overall gain by adjusting the thresholds. In fact, the size principle [53] suggests that the gain should increase faster with increasing perturbation than linearly.

In reality, all the states are measured but with significant delays. It is relatively easy to include delays in our model as we have demonstrated for a two segment model with control only at the ankle. Delay adds states to the model. The states associated with sensory delays are unobserved. This implies that a state estimator must be included in the feedback loop. We believe there is considerable biological evidence for the existence of such an estimator. In particular, we believe the existence of a Central Pattern Generator (CPG) [Pearson] provides evidence that such an estimator can be implemented using neurons. This is because a CPG requires much of the same dynamics that a state estimator requires. Furthermore, a state estimator is likely to be a component of a CPG.

Thus, the work reported here suggests a reasonable hypothesis about the fundamentals of motor control. Specifically, it suggests the existence of a state predictor as part of the posture regulation system. We are presently performing additional simulations using our model to more fully understand its implications regarding coordination of muscles in posture regulation. We are also working on neuronal implementations of

Kalman filters and Luenberger observers using realistic models for neurons rather than those in studies of neural networks.

8.2 The Future Work

A remaining question is how a predictor can be constructed using only neurons. It is well accepted that many creatures including cats have a central pattern generator (CPG) that produces the signals to the motor units that then produce the forces that generate repetitive movements. Surprisingly, the CPG seems to require sensor feedback to function. Why? One plausible answer is that the CPG consists of a nominal (open loop—no feedback) signal and a predictor. It is the predictor that needs the feedback.

One might ask why people have not observed a CPG for posture in animal experiments. A possible answer is that the predictor used by the posture regulator needs feedback from vision and the otolith organs. These come from higher in the brain than the sensory feedback needed for pure locomotion. Thus, when one performs the surgery that facilitates the CPG experiments in walking, one destroys the feedback that is essential to the predictor in the posture regulator. At this point this is just speculation. However, it does offer a consistent explanation for the experimental observations and it is very much the way an engineer would design the system. There is other evidence for the existence of a predictor in the CNS. For example, the leg muscles must react to foot strike in running and walking well before the impact could be sensed and processed.

Our work suggests that the posture regulator might be trying to reduce energy

consumption by trading off the muscular energy used against the tightness of regulation. This could possibly be tested experimentally by measuring the energy consumption during perturbed standing. It is important to understand that we are not claiming that posture regulation is achieved by an MPC. Our suggestion is that the human posture regulation is learned and that it continues to adapt throughout life. After all, people are able to maintain their posture even though their weight and strength varies considerably. Constant retuning of the parameters in the controller would be required to achieve this. Such parameter adjustment would permit the controller to be learned assuming the basic framework existed.

Furthermore, the approach developed here can be easily extended to include motion at the knee joint as well as at other locations in the body. The computations do become more difficult. Nonetheless, these extensions will be very worthwhile if it can be shown that the results of this thesis do correspond better to the feasible experiments than other proposed postural regulations.

Finally, performance measures that are quadratic in the controls but higher order in the states have potential uses in other areas than posture regulation. Thus it would be useful to have efficient, fast, and reliable solvers for such problems. We are continuing to work on this.

Bibliography

- [1] A.Hof, M. Gazendam, W. Sinke The condition for dynamic stability. *Journal of Biomechanics* 2004
- [2] Aramaki Y, Nozaki D, Masani K, Sato T, Nakazawa K, and Yano H. Reciprocal angular acceleration of the ankle and hip joints during quiet standing in humans. *Exp Brain Res* 136: 463-473, 2001.
- [3] Accornero N, Capozza M, and Manfredi GW. Clinical multisegmental posturography: age-related changes in stance control. *Electroenceph Clin Neurophysiol* 105: 213-219, 1997.
- [4] Aramaki Y, Nozaki D, Masani K, Sato T, Nakazawa K, and Yano H. Reciprocal angular acceleration of the ankle and hip joints during quiet standing in humans. *Exp Brain Res* 136: 463-473, 2001.
- [5] Athans, M. A. and Falb, P. L., *Optimal Control*, McGraw-Hill, New York, 1966.
- [6] Bellman, R. E. *Dynamic Programming*. Princeton, NJ, 1957.
- [7] Bell F. *Principles of mechanics and biomechanics*. Cheltenham: Stanley Thornes, 1998.
- [8] Bennett DJ, Gorassini M, and Prochazka A. Catching a ball: contributions of intrinsic muscle stiffness, reflexes, and higher order responses. *Can J Physiol Pharmacol* 72: 525-534, 1994.
- [9] Berg K. Balance and its measure in the elderly: a review. *Physiother Can* 1989; 41: 240-46.
- [10] Berg K, Wood-Dauphinee S, Williams J, Gayton D. Measuring balance in the elderly: preliminary development of an instrument. *Physiother Can* 1989; 41: 304-11.
- [11] Braune W, Fischer O. *On the centre of gravity of the human body*. New York: Springer-Verlag, 1985
- [12] Boyd, S.P and L. Vandenberghe. *Convex Optimization*. Cambridge University Press, 2003 Material available at <http://www.stanford.edu/~boyd/cvxbook.html>

- [13] Bryson, A. E and Ho YC. Applied Optimal Control: Optimization, Estimation, and Control. New York: Wiley, 1975.
- [14] Collins JJ and DeLuca CJ. Open-loop and closed-loop control of posture: a random-walk analysis of center-of-pressure trajectories. *Exp Brain Res* 95: 308-318, 1993.
- [15] Collins JJ and DeLuca CJ. Random walking during quiet standing. *Phys Rev Lett* 73: 764-767, 1994.
- [16] Collins JJ and DeLuca CJ. The effects of visual input on open-loop and closed-loop postural control mechanisms. *Exp Brain Res* 103: 151-163, 1995.
- [17] Cutson TM, 1994. Falls in the elderly. *Am Fam Physician*. 49:149-156.
- [18] Day BL, Cauquil AS, Bartolomei L, Pastor MA, and Lyon IN. Human body-segment tilts induced by galvanic stimulation: a vestibularly driven balance protection mechanism. *J Physiol* 500: 661-672, 1997
- [19] Day BL, Steiger MJ, Thompson PD, and Marsden CD. Effect of vision and stance width on human body motion when standing: implications for afferent control of lateral sway. *J Physiol* 469: 479-499, 1993.
- [20] Dietz V. Human neuronal control of automatic functional movements: interaction between central programs and afferent input. *Physiol Rev* 72: 33-69, 1992.
- [21] Dijkstra TM, Schöner G, and Gielen CC. Temporal stability of the action-perception cycle for postural control in a moving visual environment. *Exp Brain Res* 97: 477-486, 1994.
- [22] Dijkstra TM, Schöner G, Giese MA, and Gielen CC. Frequency dependence of the action-perception cycle for postural control in a moving visual environment: relative phase dynamics. *Biol Cybern* 71: 489-501, 1994.
- [23] Fitzpatrick R, Burke D, and Gandevia C. Loop gain of reflexes controlling human standing measured with the use of postural and vestibular disturbances. *J Neurophysiol* 76: 3994-4008, 1996.
- [24] Fitzpatrick R and McCloskey D. Proprioceptive, visual and vestibular thresholds for the perception of sway during standing in humans. *J Physiol* 478: 173-186, 1994a
- [25] Fitzpatrick R, Rogers DK, and McCloskey DI. Stable human standing with lower-limb muscle afferents providing the only sensory input. *J Physiol* 480: 395-403, 1994

- [26] Fitzpatrick R, Taylor JL, and McCloskey DI. Ankle stiffness of standing humans in response to imperceptible perturbation: reflex and task-dependent components. *J Physiol* 454: 533-547, 1992a.
- [27] Fitzpatrick RC, Gorman RB, Burke D, and Gandevia SC. Postural proprioceptive reflexes in standing human subjects: bandwidth of response and transmission characteristics. *J Physiol* 458: 69-83, 1992b.
- [28] Gaebler S, 1993. Predicting which patient will fall again...and again. *J Adv Nurs.* 18:1895-1902.
- [29] Gabor Stepan. Delay effects in the human sensory system during balancing. *Phil. Trans. R. Soc. A* 2009 367, 1195-1212
- [30] Gatev P, Thomas S, Kepple T, and Halett M. Feedforward ankle strategy of balance during quiet stance in adults. *J Physiol* 514: 915-928, 1999
- [31] Ghez, C. & Krakauer, J. (2000) The organization of movement. In: *Principles of neural science*, ed. E. R. Kandel, J. H. Schwartz & T. M. Jessell. McGraw Hill.
- [32] Gurfinkel VS, Ivanenko YP, Levik YS, and Babakova IA. Kinesthetic reference for human orthograde posture. *Neuroscience* 68: 229-243, 1995.
- [33] Hall S. *Basic biomechanics*. St Louis: Mosby Year Book, 1991.
- [34] He J, W.S.Levine, and G. E. Leob, Feedback gains for correcting small perturbations to standing posture. *IEEE Trans. Automat. Contr.* Vol. 36. PP 322-332 1991
- [35] Hill K, Schwarz J, Kalogeropoulos a, et al. Fear of Falling Revisited [J]. *Arch Phys Med Rehabil*, 1996, 77(10): 1025-1029.
- [36] Horak, F. B and Macpherson JM. Postural orientation and equilibrium. In: *Handbook of Physiology. Exercise: Regulation and Integration of Multiple Systems. Control of Respiratory and Cardiovascular Systems*: Bethesda, MD: Am. Physiol. Soc., 1996, sect. 12, pt. II, chapt. 7, p. 255-292.
- [37] Horak, F. B. Clinical measurement of postural control in adults. *Phys Ther* 1987; 67: 1881-85.
- [38] Horak, F. B. Clinical assessment of Balance Disorders. *Gait Posture*, 1997, 6: 762 84.
- [39] Horak, F. B and Nashner LM. Central programming of postural movements: adaptation to altered support-surface configurations. *J Neurophysiol* 55: 1369-1381, 1986.

- [40] Horak FB, Macpherson JM (1996) Postural orientation and equilibrium. In: Rowell L, Sheppard J (eds) Exercise: regulation and integration of multiple systems. Oxford University Press, New York, pp 255-292
- [41] Horak FB, Nashner LM, Diener HC (1990) Postural strategies associated with somatosensory and vestibular loss. *Exp Brain Res* 82:167-177
- [42] Jacks A, Prochazka A, and Trend PSJ. Instability in human forearm movements studied with feed-back-controlled electrical stimulation of muscles. *J Physiol* 402: 443-461, 1988.
- [43] Jeka JJ, Oie KS, and Kiemel T. Multisensory information for human postural control: integrating touch and vision. *Exp Brain Res.* 134(1): 107–125, 2000
- [44] Jeka JJ, Ribeiro P, Oie KS, and Lackner JR. The structure of somatosensory information for human postural control. *Motor Control* 2(1): 13–33, 1998
- [45] Jeka JJ, Schöner G, Dijkstra T, Ribeiro P, and Lackner JR. Coupling of fingertip somatosensory information to head and body sway. *Exp Brain Res* 113(3): 475–483, 1997
- [46] Johansson R, Magnusson M, and Fransson PA. Galvanic vestibular stimulation for analysis of postural adaptation and stability. *IEEE Trans Biomed Eng* 42: 282-292, 1995.
- [47] Joseph J and Nightingale A. Electromyography of muscles of posture: leg muscles in males. *J Physiol* 117: 484-491, 1952
- [48] Kannus P, Parkkari J, Koskinen S, et al. 1999. Fall-induced injuries and deaths among older adults. *JAMA.* 281:1895-1899.
- [49] Karmarkar, Narendra (1984). "A New Polynomial Time Algorithm for Linear Programming", *Combinatorica*, Vol 4, no. 4, pp. 373–395.
- [50] Kiemel T, Oie KS, and Jeka JJ. Multisensory fusion and the stochastic structure of postural sway. *Biol Cybern* 87(4): 262–277, 2002.
- [51] Kuo AD. An optimal control model for analyzing human postural balance. *IEEE Trans Biomed Eng* 42: 87–101, 1995.
- [52] Lacour M, Barthelemy J, Borel L, Magnan J, Xerri C, Chays A, and Ouaknine M. Sensory strategies in human postural control before and after unilateral vestibular neurotomy. *Exp Brain Res* 115: 300-310, 1997.
- [53] G. E. Loeb and C. Ghez, "The motor unit and muscle action," in *Principles of Neural Science*, 4th Edition, edited by E. R. Kandel, J. H. Schwartz, and T. M. Jessell, McGraw-Hill, 2000, p. 676, 686

- [54] Loram ID and Lakie M. Direct measurement of human ankle stiffness during quiet standing: the intrinsic mechanical stiffness is insufficient for stability. *J Physiol* 545(3): 1041–1053, 2002
- [55] Lynn S. Lippert. *Clinical Kinesiology And Anatomy (Clinical Kinesiology for Physical Therapist Assistants)* (Paperback). F. A. Davis Company; 4 edition (May 30, 2006). ISBN-10: 0803612435
- [56] Magnusson M, Enbom H, Johansson R, and Pyykko I. Significance of pressor input from the human feet in anterior–posterior postural control: the effect of hypothermia on vibration-induced body-sway. *Acta Otolaryngol* 110: 182-188, 1990.
- [57] Masani K, Nakazawa K, and Kouzaki M. Two frequency components in ankle extensor activity during human quiet standing. *Soc Neurosci Abstr* 31: 305.2, 2001.
- [58] Masani K, Popovic MR, Nakazawa K. et al. Importance of body sway velocity information in controlling ankle extensor activities during quiet stance. *J Neurophysiol* 2003 ; 90: 3774–82.
- [59] Mauritz KH and Dietz V. Characteristics of postural instability induced by ischemic blocking of leg afferents. *Exp Brain Res* 38: 117-119, 1980
- [60] McCollum, G and Leen, T. K Form and exploration of mechanical stability limits in erect stance. *J. Motor Behav.*, Vol. 21., PP. 225-244. 1989
- [61] Moore T, Martin J, Stone House J. Predicting Falls: Risk assessment tool Versus Clinical Judgment [J]. *Perspectives*. 1996, 20(1) .8-11.
- [62] Morasso P and Schieppati M. Can muscle stiffness alone stabilize upright standing? *J Neurophysiol* 83: 1622–1626, 1999.
- [63] Nashner LM. Adapting reflexes controlling the human posture. *Exp Brain Res* 26: 59-72, 1976.
- [64] Nashner LM. Fixed patterns of rapid postural responses among leg muscles during stance. *Exp Brain Res* 30: 13-24, 1977.
- [65] Neil Campbell and Jane Reece. *Biology* 7th edition. Benjamin Cummings, Publisher, 2005. ISBN 0-8053-7171-0 published by Addison-Wesley-Benjamin Cummings.
- [66] Nijhawan, R. 2008 Visual prediction: psychophysics and neurophysiology of compensation for time delays. *Behav. Brain Sci.* 31, 179–198.
- [67] Nocedal, Jorge; and Stephen Wright (1999). *Numerical Optimization*. New York, NY: Springer. ISBN 0-387-98793-2.

- [68] Panzer VP, Bandinelli S, and Hallett M. Biomechanical assessment of quiet standing and changes associated with aging. *Arch Phys Med Rehabil* 76: 151-157, 1995
- [69] Pavlik AE, Inglis JT, Lauk M, Oddsson L, and Collins JJ. The effects of stochastic galvanic vestibular stimulation on human postural sway. *Exp Brain Res* 124: 273-280, 1999.
- [70] Peterka RJ. Postural control model interpretation of stabilogram diffusion analysis. *Biol Cybern.* 82: 335-343, 2000
- [71] Peterka RJ and Benolken MS. Role of somatosensory and vestibular cues in attenuating visually induced human postural sway. *Exp Brain Res* 105: 101-110, 1995.
- [72] Pontryagin, L. S. *The Mathematical Theory of Optimal Processes* 1962
- [73] Powell L E. Myers a M. The activity-Specific Balance Confidence (abc) Scale [J]. *J Gerontol a Biol Sci Med Sci*, 1995. 50(1), 28-34.
- [74] Rawsky E, 1998. Review of the literature on falls among the elderly. *Image J Nurs Sch.* 30:47-52.
- [75] Rivara FP, Grossman DC, Cummings P, 1997. Medical progress: injury prevention (second of two parts). *N Engl J Med.* 337:613-618.
- [76] Schieppati M, Hugon M, Grasso M, Nardone A, and Galante M. The limits of equilibrium in young and elderly normal subjects and parkinsonians. *Electroenceph Clin Neurophysiol* 93: 286-298, 1994.
- [77] Schieppati M and Nardone A. Medium-latency stretch reflexes of foot and leg muscles analyzed by cooling the lower limb in standing humans. *J Physiol* 503: 691-698, 1997.
- [78] Schöner G. Dynamic theory of action-perception patterns: the "moving room" paradigm. *Biol Cybern* 64: 455-462, 1991.
- [79] Smith JW. The forces operating at the human ankle joint during standing. *J Anat* 91: 545-564, 1957
- [80] Terekhov Y. Stabilometry as a Diagnostic tool in Clinical Medicine. *Can Med assoc J*, 1976, 115:631 - 633.
- [81] Tinetti M E, Richman D, Powell L. Falls Efficacy as a Measure of Fear of Falling[J]. *J Gerontol*, 1990, 45(6):239-243.
- [82] van der Kooij, H., Jacobs, R., Koopman, B., Grootenboer, H., 1999. A multisensory integration model of human stance control. *Biol. Cybern.* 80, 299-308.

- [83] van der Kooij, H., Jacobs, R., Koopman, B., van der Helm, F., 2001. An adaptive model of sensory integration in a dynamic environment applied to human stance control. *Biol. Cybern.* 84, 103–115.
- [84] David A. Winter. *Biomechanics and Motor Control of Human Movement*. Wiley; 3 edition (September 9, 2004). ISBN-10: 047144989X
- [85] Winter DA, Patla AE, Prince F, Ishac M, and Gielo-Perczak K. Stiffness control of balance in quiet standing. *J Neurophysiol* 80: 1211-1221, 1998
- [86] Winter DA, Patla AE, Rietdyk S, and Ishac MG. Ankle muscle stiffness in the control of balance during quiet standing. *J Neurophysiol* 85: 2630-2633, 2001.
- [87] Winter DA, Prince F, Frank JS, Powell C, and Zabjek KF. Unified theory regarding A/P and M/L balance in quiet stance. *J Neurophysiol* 75: 2334-2343, 1996
- [88] Woollacott MH, von Hosten C, and Rosblad B. Relation between muscle response onset and body segmental movements during postural perturbations in humans. *Exp Brain Res* 72: 593-604, 1988.
- [89] Woodworth, R. S. & Schlosberg, H. (1954) *Experimental psychology*.
- [90] Wright, Stephen (1997). *Primal-Dual Interior-Point Methods*. Philadelphia, PA: SIAM. ISBN 0-89871-382-X.
- [91] Yao Li and William S. Levine. An Optimal Control Model for Human Postural Regulation. 2009 American Control Conference, Louis, Missouri, June 10-12, 2009, Page(s): 4705-4710
- [92] Yao Li and William S. Levine. An optimal model predictive control model for human postural regulation. 17th Mediterranean Conference on Control and Automation, June 24-26 2009, Page(s): 1143-1148
- [93] Yao Li and William S. Levine. Models for human postural regulation that include realistic delays and partial observations Proc. of 48th IEEE Conference on Decision and Control Conference. Shanghai, China December 16-18, 2009, Page(s) 4590-4595
- [94] Zatsiorsky VM and Duarte M. Rambling and trembling in quiet standing. *Motor Control* 4: 185-200, 2000.